T H E U N I V E R S I T Y O F M I C H I G A N

COLLEGE OF ENGINEERING
Department of Mechanical Engineering
Heat Transfer Laboratory

Technical Report No. 5

FINITE DIFFERENCE CALCULATION OF PRESSURE RISE IN SATURN S-IVB FUEL TANK

Herman Merte, Jr.
Chai Chin Suh
Edward R. Lady
John A. Clark

ORA Project 07461

under contract with:

NATIONAL AERONAUTICS AND SPACE ADMINISTRATION
GEORGE C. MARSHALL SPACE FLIGHT CENTER
CONTRACT NO. NAS-8-20228
HUNTSVILLE, ALABAMA

administered through:

OFFICE OF RESEARCH ADMINISTRATION ANN ARBOR

April 1969

TABLE OF CONTENTS

TABLE OF CONTENTS (Concluded)

LIST OF TABLES

LIST OF FIGURES

NOMENCLATURE

A - Area, ft^2

a - Cylindrical tank radius, ft; acceleration, ft/sec^2

b - Total tank height, ft

C_p, C_v - Specific heats Btu/lbm-°F

$\frac{Df}{Dt}$ - Substantial derivative of function f

e - Specific internal energy, Btu/lbm

E - Total internal energy, Btu

g - Acceleration due to local gravity, ft/sec^2

h - Heat transfer coefficient, $Btu/hr\text{-}ft^2\text{-}°F$; enthalpy, Btu/lbm

h_{fg} - Latent heat, Btu/lbm

k - Thermal conductivity, Btu/hr-ft-°F

P - Pressure, psia

q - Heat flux, $Btu/hr\text{-}ft^2$

r - Radial distance, ft

Δr - Finite difference of radial distance, ft

R - Gas constant, $\frac{lbf\text{-}ft}{lbm\text{-}°R}$

t - Time, hr

T - Temperature, °R

$\Delta T_w = T_w - T_{sat}$, °R

ΔT_{wmax} - Specified maximum value of ΔT_w, °R

u - Axial component of velocity, ft/sec

U - Dimensionless axial velocity

v - Radial component of velocity, ft/sec

V - Volume, ft^3; dimensionless radial velocity

w - Mass flow rate, lbm/sec

x - Axial distance, ft

X - Liquid height in container, ft

Δx - Finite-difference of vertical distance, ft

Z - Compressibility factor, [1]

Greek Letters

α - Thermal diffusivity, ft^2/hr

β - Coefficient of thermal expansion, $°R^{-1}$

γ - Ratio of specific heats C_p/C_v, [1]

δ - Tank wall thickness, ft

η - Dimensionless radius, [1]

$\Delta\eta$ - Finite difference of dimensionless radius

θ - Dimensionless temperature

ζ - Dimensionless axial distance, [1]

$\Delta\zeta$ - Finite difference of dimensionless axial distance

ψ - Dimensionless stream function

ψ', ψ'' - Liquid and vapor stream functions

τ - Dimensionless time

$\Delta\tau$ - Finite difference of dimensionless time

μ - Kinematic viscosity ft^2/hr

ν - Dynamic viscosity, lbm/ft-hr

ρ - Density, lbm/ft^3

ω' - Vorticity, $[ft\text{-}sec]^{-1}$

ω - Dimensionless vorticity

Subscripts

d - Discharge

f - Liquid or fluid

g - Gas or vapor

i - Liquid-vapor interface

ℓ - Liquid

o - Initial state

p - Pressurization

r - Reduced

s - Saturation

w - Wall

ABSTRACT

The pressure rise of a two-phase system in a closed container subject to an external heat flux is related directly to the temperature of the liquid-vapor interface, which in turn depends on the heat and mass transfer interactions between the liquid, vapor, and container. The problem is formulated here for a cylindrical tank with an axial body force and a symmetrically imposed external heat flux in terms of the transport equations. The temperature and velocity distributions are determined using a finite-difference method, which is coupled with an integral form of the energy equation to determine the pressure rise. The procedure adopted takes into account the possibility of incipient and nucleate boiling.

Numerical computations are carried out for liquid hydrogen in a large, partially filled tank under low gravity. This system models the one orbital experiment conducted to date which provides the only available experimental data. These are the data on pressure rise and system temperatures telemetered from a Saturn LH_2 tank orbiting the earth, the AS-203 low gravity orbital experiment. A discussion of the modeling is included.

The numerical computations are carried out for various distributions of heat flux between the liquid and vapor, and with various container wall properties. The outputs of major interest are the pressure rise, and temperature and velocity distributions. Representative plots of the isotherms and streamlines are included.

The computations indicate that even though the container walls constitute an insignificant portion of the total heat capacity, less than 1% that of the liquid and vapor, variation of the wall heat capacity has a significant influence on the pressure rise rate. During a portion of the process, it is found that radial as well as axial stratification exists, with simultaneous evaporation and condensation occurring at various locations on the liquid-vapor interface.

I. INTRODUCTION

A number of space missions of current interest require the storage of liquid propellents for long periods of time, varying from hours to months. The ultimate goal is to maximize the quantity of useful propellent remaining at the end of this period of time. In the limit this maximum corresponds to the nonvented condition in which the original mass of propellent is retained. Whether nonventing is practical depends on the maximum internal pressure which results from the thermal interaction between the storage container, its contents, and its ambient. The prediction of pressure changes in a nonvented container is thus of major importance for purposes of feasibility determination and optimization.

In Ref. 3 the results of the initial attempt to calculate the pressure rise in a single-component, two-phase system were presented for a two-dimensional case with axial symmetry and an imposed heat flux. The governing equations were placed in finite difference form and solved with an IBM-7090 computer, using the MAD language, for an example case with liquid oxygen.

The measurements of pressure rise in a full size earth orbiting liquid hydrogen container on the Saturn IB vehicle AS-203, as reported in Ref. 17, makes possible a comparison with pressure rise calculated from this model. Certain deviations from the actual physical system are necessary in defining a model owing to the present stage of development of the computational procedures involved. These will be discussed at the appropriate places.

This report presents the results of the computations made on a model simulating the S-IV B stage on the Saturn IB vehicle AS-203, along with comparisons with the measurements. Since the IBM-7090 computer had been replaced by the IBM-360 system at The University of Michigan, it was expedient to transform the source program from MAD to FORTRAN IV, and the computer programs are so presented herein. For the sake of completeness the general formulation presented in Ref. 3 is reproduced here.

The pressure in a tank containing two phases, liquid and vapor, is related directly to the temperature at the liquid-vapor interface for a single component system. For a binary system, the pressure depends not only on the temperature at the interface but the relative liquid-vapor concentration of the two components as well. Pressure changes take place owing to heat and mass transfer interactions between the vapor, liquid, and container walls.

The processes of heat and mass transfer interactions between the gas and liquid phases of a single component in cylinderical containers with axial symmetry are considered in this study. In the general formulation presented first attention is given to the cases of external pressurization with and with-

out liquid discharge as well as to the nonvented case. Solutions are then presented, utilizing numerical finite-difference procedures for the nonvented case.

The initial conditions of the liquid and vapor are considered to be those at equilibrium, with uniform pressure P_o and saturation temperature T_o. From these initial conditions, the walls of the container undergo a thermal perturbation, such as a change in temperature or an exposure to an external heat flux, either of which may be an arbitrary function of time and axial location. The perturbations in the boundary conditions lead to a series of nonequilibrium phenomena within the container. Natural convection currents are set up in the liquid and in the vapor spaces. The liquid-vapor system tends to adjust to the new nonequilibrium conditions within the container by transferring mass and energy across the interface by either evaporation or condensation. The conditions at the liquid-vapor interface couple simultaneous transport processes in the liquid and gas phases. In the case of self-pressurization of nonvented tanks the rate of pressure rise within the tank is governed by the rate of heat and mass transfer from the liquid and the rate of heat transfer from the wall to the gas phase. The interfacial temperature is essentially that of equilibrium (saturation) conditions corresponding to the system pressure. At the same time, the temperature of the liquid-vapor interface affects both the interfacial mass and heat transfer, as well as the convective processes in both phases. These latter processes influence the temperature gradients within both phases and in turn will have an effect on the rate of pressure rise in the ullage space. Indeed, all the processes of heat transfer from the ambient to both phases, the natural convection within the container, the interfacial phenomena and the rate of ullage pressure rise are all mutually coupled. Such interactions have been the subject of many experimental investigations.

Any analytical approach that would adequately describe the phenomena taking place in propellent tanks must take into account these interactions. This requires the calculation of the transient velocity and temperature profiles in both the vapor and liquid phases. Some work has been done along this line.[1-3] The difficulties in solution of this problem is further complicated with the presence of turbulence or boiling of liquid near the tank walls, as their nature is not yet fully understood nor adequately described.[5] Some assumptions are necessary at the present time for the construction of models which reasonably represent the practical situations.

A survey which reviewed much of the available literature in this area, such as pressurization, stratification, and interfacial phenomena in fuel tanks, is given in Ref. 5. Several studies which are pertinent to the present one will be mentioned. Thomas and Morse[6] and Knuth[7] have considered the phase change of suddenly pressurized single-component, liquid-vapor system. Thomas and Morse[6] presented both an exact solution and an approximate solution yielding an explicit expression for the mass transfer at the interface. Yang, et al.,[8-10] have solved the problem of phase change in a suddenly pressurized single-component and binary liquid-vapor system.

Thermodynamic equilibrium is assumed at the interface, i.e., the interfacial temperature is always at the saturation temperature corresponding to the system pressure. Experience shows that this is a reasonable assumption.[5]

Epstein, et al.,[11] used finite-differences for the calculation of the pressurization process. In this model, the axial variation of temperature is considered while the radial variation is neglected. The wall to fluid heat transfer was accounted for by introducing an effective heat transfer coefficient between the fluid and the wall. Also, effective thermal conductivities and mass diffusivities between the adjacent fluid layers were used to simulate the effects of random fluid motion. Provisions for variable tank cross-section as well as variable heat transfer coefficients were made in the program. The effect of boiling near the walls was not considered, and momentum effects were neglected. The principal advantage of this program is its simplicity and the relatively small amount of machine time required to advance the solution to a particular time level. However, the determination of the effective thermal conductivities and heat transfer coefficients and their variation with location require the determination of a large number of empirical constants, which require considerable experimental experience with a particular system.

Although some analytical models have been used to study liquid stratification in self-pressurized propellant containers, with the exception of Ref.[3], none has considered the simultaneous interactions between the liquid and the vapor phases. Most of the available studies of the pressure and temperature transients in the vapor space are experimental in nature and have served to identify some factors influencing the rate of pressure rise within the containers. The studies of Huntley[12] show that liquid stratification causes the pressure to rise at a higher rate than that calculated using the average or mixed mean liquid temperature. These also showed that stirring the liquid causes a smaller rate of pressure rise, while stirring the vapor resulted in a substantial increase in pressure. Higher rates of pressure rise were obtained with smaller ullage volumes. Liebenberg and Edescuty have shown similar results.[13]

II. FORMULATION

A. GENERAL FORMULATION

The formulation of the most general case will be given first. This involves external pressurization, liquid discharge, and the consideration of the vented and nonvented container. The heat capacity of the container side wall is also included in the formulation. The assumptions and limitations will be mentioned as appropriate and the results and problems encountered in the solution of the unvented, nondischarge case will be given.

A cylinderical container of diameter 2a, height b and with wall thickness δ, is partially filled with a liquid as shown in Fig. 1. The initial height of the liquid is X_o, and that of the vapor is $b-X_o$. The origin of the coordinate system is taken at the center of the container base with x-positive in the direction of the liquid. At any time t, the location of the liquid-vapor interface is given by $X = X(t)$. The fluid in both phases is initially at rest in an equilibrium state at a uniform temperature T_o and pressure P_o. From these initial conditions the tank side walls are subjected to an arbitrary heat flux, $q_w(x,t)$. The tank ends are assumed adiabatic with zero heat capacity, but this restriction can be relaxed if desired. The differential equations describing the physical behavior are listed separately below for the various regions.

1. Tank Side Wall

The differential equation describing the temperature-time history of the tank wall, considering the wall to be lumped radially but not axially, is

$$\left(\rho c_p \delta \frac{\partial T}{\partial t}\right)_w = -\left(k \frac{\partial T}{\partial r}\right)_f + \left(\delta k \frac{\partial^2 T}{\partial x^2}\right)_w + q_w(x,t) \quad , \tag{1}$$

where the subscripts w and f refer to the wall and the fluid, respectively. The first term on the right-hand side of Eq. (1) is the rate of heat flow from the wall to the fluid, while the second term accounts for the net axial conduction.

Initial and Boundary Conditions

$$T_w(x,o) = T_o$$

$$\frac{\partial T_w(o,t)}{\partial x} = \frac{\partial T_w(b,t)}{\partial x} = 0 \tag{2}$$

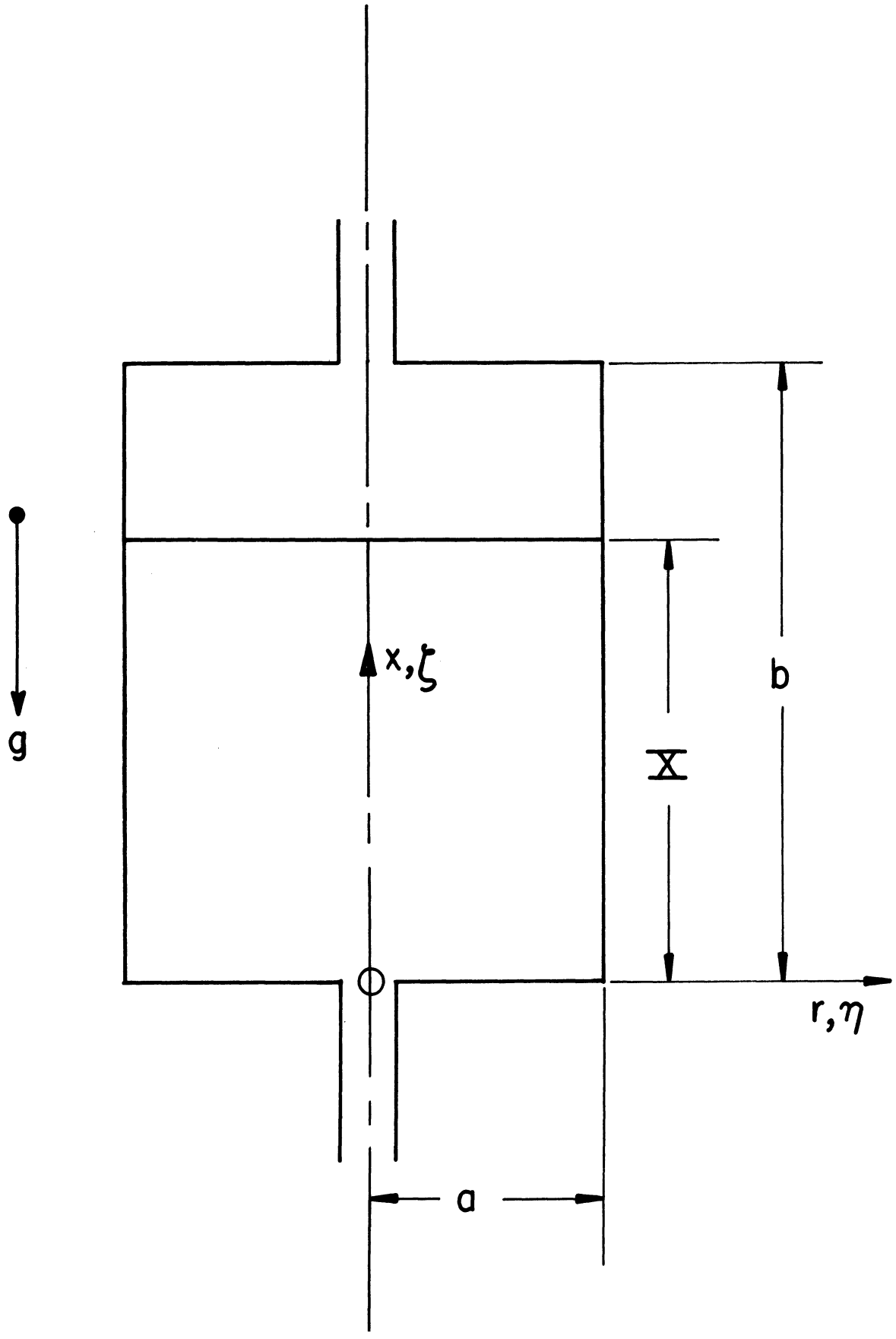

Fig. 1. Container configuration and coordinate system.

2. Liquid Region

The following assumptions are made:

(a) Thermal conductivity and viscosity are constant.

(b) Fluid is incompressible. Density variations are introduced only in the body force term of the momentum equation. These variations are described by

$$\rho = \rho_o[1 + \beta(T_o - T)] \tag{3}$$

(c) The influence of viscous dissipation is neglected.

Governing Equations

(i) axial-momentum

$$\rho \frac{Du}{Dt} = -\rho g - \frac{\partial p}{\partial x} + \mu\left(\frac{\partial^2 u}{\partial x^2} + \frac{1}{r}\frac{\partial u}{\partial r} + \frac{\partial^2 u}{\partial r^2}\right) \tag{4}$$

(ii) radial momentum

$$\rho \frac{Dv}{Dt} = -\frac{\partial P}{\partial r} + \mu\left(\frac{\partial^2 v}{\partial x^2} - \frac{v}{r^2} + \frac{1}{r}\frac{\partial v}{\partial r} + \frac{\partial^2 v}{\partial r^2}\right) \tag{5}$$

(iii) continuity

$$\frac{\partial u}{\partial x} + \frac{\partial v}{\partial r} + \frac{v}{r} = 0 \tag{6}$$

(iv) energy

$$\frac{DT}{Dt} = \alpha\left(\frac{\partial^2 T}{\partial x^2} + \frac{1}{r}\frac{\partial T}{\partial r} + \frac{\partial^2 T}{\partial r^2}\right) \tag{7}$$

Initial Conditions

$$T(x,r,o) = T_o \quad , \quad u(x,r,o) = 0 \quad , \quad v(x,r,o) = 0 \tag{8}$$

Boundary Conditions

Velocity

$$u(o,r,t) = 0 \tag{9}$$

$$u(X_{-o},r,t) = -\frac{w_{\ell d}}{\rho_\ell \pi a^2} \tag{10}$$

where $w_{\ell d}$ is the rate of liquid discharge.

$$u(x,a,t) = 0 \tag{11}$$

$$\frac{\partial u(x,o,t)}{\partial r} = 0 \tag{12}$$

$$v(x,a,t) = 0 \tag{13}$$

$$v(x,o,t) = 0 \tag{14}$$

$$v(o,r,t) = 0 \tag{15}$$

$$\frac{\partial v(X,r,t)}{\partial x} = 0 \tag{16}$$

Temperature

$$T(X,r,t) = T_s(t) \tag{17}$$

$$T(x,a,t) = T_w(x,t) \tag{18}$$

$$\frac{\partial T(o,r,t)}{\partial x} = 0 \tag{19}$$

$$\frac{\partial T(x,o,t)}{\partial r} = 0 \tag{20}$$

where $T_s(t)$ is the saturation temperature corresponding to the system pressure and T_w is the wall temperature, Eq. (1).

3. Vapor Region

The differential equations for the vapor region are obtained assuming negligible changes in the viscosity and thermal conductivity within the vapor phase. The compressibility of the vapor is considered.

Governing Equations

(i) axial momentum

$$\rho \frac{Du}{Dt} = -\rho g - \frac{\partial P}{\partial x} + \mu\left(\frac{\partial^2 u}{\partial x^2} + \frac{1}{r}\frac{\partial u}{\partial r} + \frac{\partial^2 u}{\partial r^2}\right) + \frac{1}{3}\mu\frac{\partial}{\partial x}\left(\frac{\partial u}{\partial x} + \frac{\partial v}{\partial r} + \frac{v}{r}\right) \tag{21}$$

(ii) radial momentum

$$\rho \frac{Dv}{Dt} = -\frac{\partial P}{\partial r} + \mu\left(\frac{\partial^2 v}{\partial x^2} - \frac{v}{r^2} + \frac{1}{r}\frac{\partial v}{\partial r} + \frac{\partial^2 v}{\partial r^2}\right) + \frac{1}{3}\mu\frac{\partial}{\partial r}\left(\frac{\partial u}{\partial x} + \frac{\partial v}{\partial r} + \frac{v}{r}\right) \tag{22}$$

(iii) continuity

$$\frac{D\rho}{Dt} + \rho\left(\frac{\partial u}{\partial x} + \frac{\partial v}{\partial r} + \frac{v}{r}\right) = 0 \quad , \tag{23}$$

(iv) energy

$$\rho c_v \frac{DT}{Dt} + \rho \frac{D(P/\rho)}{Dt} = \frac{DP}{Dt} + k\left(\frac{\partial^2 T}{\partial x^2} + \frac{1}{r}\frac{\partial T}{\partial r} + \frac{\partial^2 T}{\partial r^2}\right) \quad . \tag{24}$$

(v) equation of state

$$P = z\rho RT \tag{25}$$

where z is the compressibility factor which can be evaluated from P, V, T data.

Initial Conditions

$$T(x,r,o) = T_o$$

$$\rho(x,r,o) = \rho_o$$

$$u(x,r,o) = 0$$

$$v(x,r,o) = 0 \qquad (26)$$

Boundary Conditions

Velocity

$$u(b,r,t) = 0 \qquad (27)$$

or

$$u(b,r,t) = u_{gp} = -\frac{w_{gp}}{\rho_{gp}\pi a^2} \quad , \qquad (28)$$

where w_{gp} is the rate of mass flow of the pressurant and ρ_{gp} is its density. Equatio (28) is written for the case of uniform velocity at the inlet diffuser of the tank as in Fig. 2.

$$u(X_{+o},r,t) = u_{gi} \qquad (29)$$

$$\frac{\partial u(x,o,t)}{\partial r} = 0 \qquad (30)$$

$$u(x,a,t) = 0 \qquad (31)$$

$$v(b,r,t) = 0$$

$$v(x,a,t) = 0 \tag{33}$$

$$v(x,o,t) = 0 \tag{34}$$

$$\frac{\partial v(X,r,t)}{\partial x} = 0 \tag{35}$$

where u_{gi} is the velocity of the vapor at the interface caused by simultaneous phase change and liquid discharge, Eq. (45). The boundary conditions given by Eqs. (16) and (35) assume a zero shear stress in both the liquid and vapor at the interface. These are reasonable and are made for the sake of simplification. Another approximation would be to take the vapor velocity at the interface equal to that of the liquid at that point. The interfacial shear stress would then be determined by the analysis. For flows with large radial gas velocities at the interface, this latter boundary condition becomes more realistic.

Temperature

$$T(X,r,t) = T_s(t) \tag{36}$$

$$T(x,a,t) = T_w(x,t) \tag{37}$$

$$\frac{\partial T(x,o,t)}{\partial r} = 0 \tag{38}$$

$$\frac{\partial T(b,r,t)}{\partial x} = 0 \tag{39}$$

or

$$T(b,r,t) = T_{gp}(r,t) \tag{40}$$

Equation (39) applies for the case with no heat transfer across the top surface and no external pressurization, and Eq. (40) for arbitrary external pressurization.

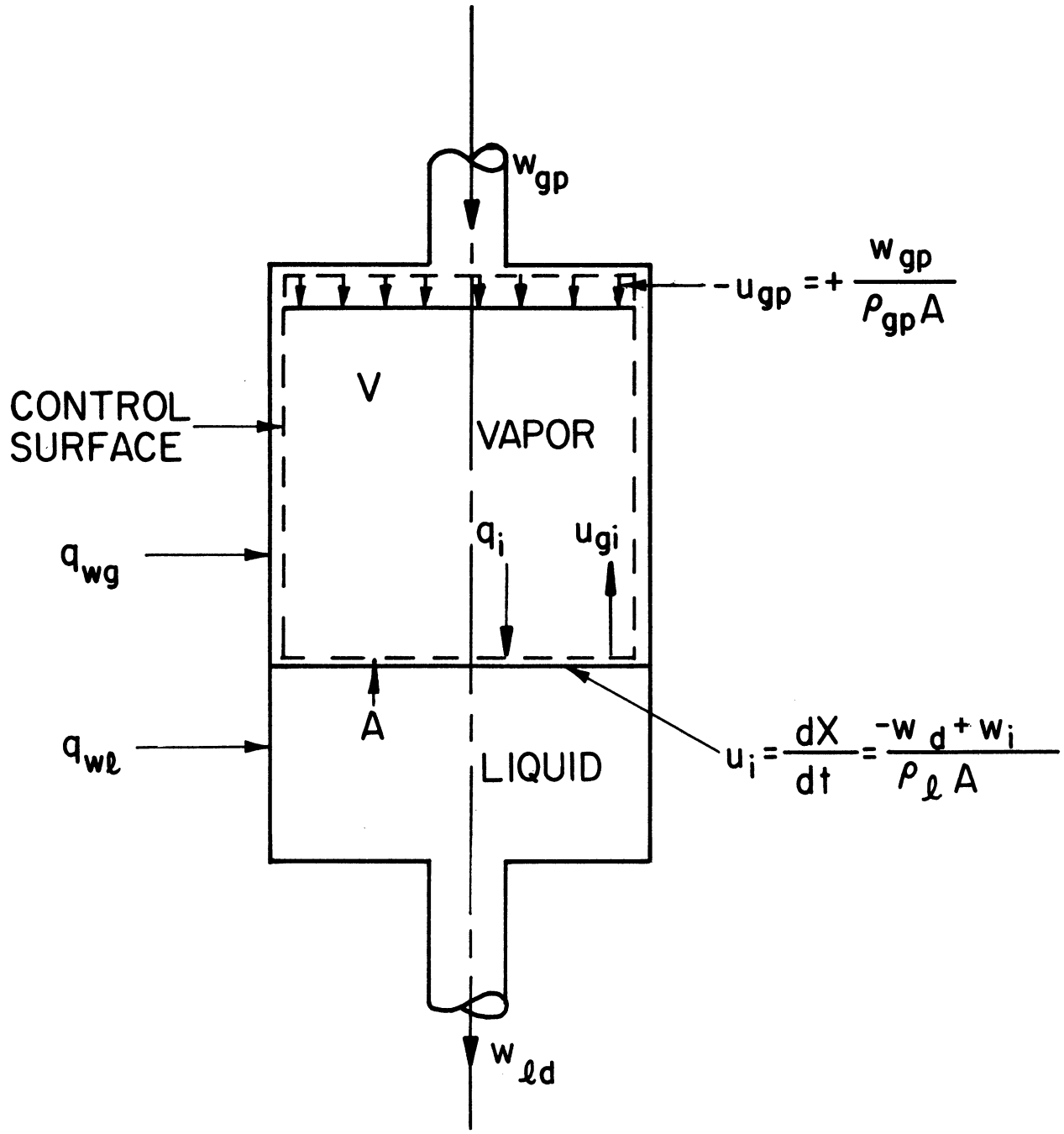

Fig. 2. Control volume of vapor region.

4. Interfacial Heat and Mass Transfer

The processes in the liquid and vapor regions are coupled by T_s in Eqs. (17) and (36) and by u_{gi} in Eq. (29), which is related to the rate of mass transfer at the interface.

The rate of mass transfer by evaporation or condensation across the liquid-vapor interface depends on the relative rates of heat transfer by diffusion from each phase at the interphase. Conservation of energy at the interface determines the rate of phase change as well as the interfacial velocity of displacement, according to;

$$h_{fg} w_i = \int_o^a \left\{ \left[k \frac{\partial T(X,r,t)}{\partial x} \right]_\ell - \left[k \frac{\partial T(X,r,t)}{\partial x} \right]_g \right\} 2\pi r dr \quad , \tag{41}$$

where w_i is the rate of interfacial phase change. According to Eq. (41), w_i will be positive if condensation takes place. The interfacial displacement with no liquid discharge is then given by:

$$\rho_\ell \pi a^2 \frac{dX_i}{dt} = w_i \tag{42}$$

Should it be desirable to include the process of liquid discharge, Eq. (42) would be written

$$\rho_\ell \pi a^2 \frac{dX_d}{dt} = - w_d \tag{43}$$

where w_d is positive for liquid discharge, and

$$u_i = \frac{dX}{dt} = \frac{dX_i}{dt} + \frac{dX_d}{dt} \tag{44}$$

where

$\frac{dX_i}{dt}$ = rate of interfacial displacement due to phase change,

$\frac{dX_d}{dt}$ = rate of interfacial displacement due to liquid discharge,

$\frac{dX}{dt}$ = combined rate of interfacial displacement due to phase change and liquid discharge.

Equation (44) is obtained assuming that the liquid surface remains flat during the discharge process. This is an approximation which neglects the influence of viscosity near the walls and surface tension effects. Such effects are negligible except for very low gravity levels and small Bond numbers.

The vapor velocity u_{gi} at the interface is related to the rate of interfacial displacement due to phase change and discharge by,

$$u_{gi} = -\left(\frac{\rho_\ell - \rho_{gs}}{\rho_{gs}}\right)\frac{dX_i}{dt} + \frac{dX_d}{dt} \tag{45}$$

B. TRANSFORMATION OF THE PARTIAL DIFFERENTIAL EQUATIONS

The momentum and the continuity equations are combined to obtain the vorticity equation and an elliptic equation relating the vorticity and the stream function. This is accomplished in the same manner as described in Refs. 1-3. The x-momentum is differentiated with respect to r, the r-momentum equation is differentiated with respect to x and the two combined to eliminate the pressure terms.

1. Liquid Region

Equations (4) and (5) reduce to:

$$\frac{D\omega'}{Dt} = -\frac{1}{\rho r} g \frac{\partial \rho}{\partial r} + \nu\left[\frac{\partial^2\omega'}{\partial x^2} + \frac{3}{r}\frac{\partial \omega'}{\partial r} + \frac{\partial^2\omega'}{\partial r^2}\right] \tag{46}$$

where ω' is given by:

$$\omega' = \frac{1}{r}\left(\frac{\partial u}{\partial r} - \frac{\partial v}{\partial x}\right) \tag{47}$$

Introducing the stream function ψ', defined by

$$u = \frac{1}{r}\frac{\partial \psi'}{\partial r} \quad ; \quad v = -\frac{1}{r}\frac{\partial \psi'}{\partial x} \tag{48}$$

Equations (7), (46), and (6) are transformed respectively to:

$$\frac{\partial T}{\partial t} + \frac{1}{r}\frac{\partial \psi'}{\partial r}\frac{\partial T}{\partial x} - \frac{1}{r}\frac{\partial \psi'}{\partial x}\frac{\partial T}{\partial r} = \alpha\left(\frac{\partial^2 T}{\partial x^2} + \frac{1}{r}\frac{\partial T}{\partial r} + \frac{\partial^2 T}{\partial r^2}\right) \quad , \tag{49}$$

$$\frac{\partial \omega'}{\partial t} + \frac{1}{r}\frac{\partial \psi'}{\partial r}\frac{\partial \omega'}{\partial x} - \frac{1}{r}\frac{\partial \psi'}{\partial x}\frac{\partial \omega'}{\partial r} = \frac{g\beta}{r}\frac{\partial T}{\partial r} + \nu\left(\frac{\partial^2 \omega'}{\partial x^2} + \frac{3}{r}\frac{\partial \omega'}{\partial r} + \frac{\partial^2 \omega'}{\partial r^2}\right) \quad , \qquad (50)$$

$$\frac{\partial^2 \psi'}{\partial x^2} - \frac{1}{r}\frac{\partial \psi'}{\partial r} + \frac{\partial^2 \psi'}{\partial r^2} = \omega' r^2 \qquad (51)$$

The initial and boundary conditions must also be transformed appropriately. Equations (49), (50), and (51) are solved numerically by finite differences to obtain the temperature, vorticity, and stream function distributions. From Eq. (48) the velocity distributions can then be computed.

2. Vapor Region

Combining the momentum Eqs. (21) and (22) in the manner described above, the following is obtained:

$$\frac{D\omega'}{Dt} = \left[\frac{\omega'}{\rho}\frac{D\rho}{Dt} - \frac{1}{\rho r}\frac{Du}{Dt}\frac{\partial \rho}{\partial r} + \frac{1}{\rho r}\frac{Dv}{Dt}\frac{\partial \rho}{\partial x}\right] - \frac{g}{\rho r}\frac{\partial \rho}{\partial r} + \nu\left[\frac{\partial^2 \omega'}{\partial x^2} + \frac{3}{r}\frac{\partial \omega'}{\partial r}\frac{\partial^2 \omega'}{\partial r^2}\right] \qquad (52)$$

where ω' is given by Eq. (47).

Equation (52) is the vorticity equation for this case. The first terms within the brackets on the right-hand side of this equation account for the compressibility effects due to density variation. Should the compressibility effects be neglected, Eq. (52) will reduce to Eq. (46). It should be noted that the presence of these terms does <u>not</u> introduce any additional difficulties as far as the solution of the vorticity equation is concerned. The difficulty will be in combining the continuity Eq. (23) and Eq. (47), in order to obtain an equation similar to Eq. (51). However, this difficulty can be overcome if the term $\partial\rho/\partial t$ is neglected in combining the continuity Eq. (23) with the definition of vorticity. The rigorous justification for this approximation has not yet been established. In this case Eq. (23) will be rewritten as:

$$\frac{\partial(\rho u)}{\partial x} + \frac{1}{r}\frac{\partial(\rho r v)}{\partial r} = 0 \quad . \qquad (53)$$

The continuity Eq. (53) is combined with Eq. (47) by introducing the stream function ψ'', which satisfies (53). This stream function ψ'' is defined by:

$$u = \frac{1}{\rho r}\frac{\partial \psi''}{\partial r} \quad ; \quad v = -\frac{1}{\rho r}\frac{\partial \psi''}{\partial x} \qquad (54)$$

Substituting (54) and (47) into (53), the following equation which relates ψ'' to ω', is obtained,

$$\frac{\partial^2\psi''}{\partial r^2} - \frac{1}{r}\frac{\partial\psi''}{\partial r} + \frac{\partial^2\psi''}{\partial x^2} = \rho\omega' r^2 + r\left[u\frac{\partial\rho}{\partial r} - v\frac{\partial\rho}{\partial x}\right] \qquad (55)$$

The last terms within the brackets in Eq. (55) account for the density changes in the vapor region. The terms $\partial\rho/\partial r$ and $\partial\rho/\partial x$ are calculated in the finite-difference procedure using the equation of state and the temperature distribution from the previous time step. The coefficients u and v in $u\,\partial\rho/\partial r$ and $v\,\partial\rho/\partial x$ will be taken equal to their values at the previous time step, which is the same procedure used in calculating the nonlinear terms $u\,\partial T/\partial x$, $v\,\partial T/\partial r$, $u\,\partial\omega'/\partial x$, and $v\,\partial\omega'/\partial r$, thus in effect linearizing these terms.

The spatial variation of pressure in the vapor region can be neglected. The density terms in Eqs. (52) and (55) are evaluated using the equation of state (25), and the derivatives given by:

$$\frac{\partial\rho}{\partial r} = -\frac{P}{RZ^2T^2}\left(\frac{\partial(ZT)}{\partial T}\right)_P\frac{\partial T}{\partial r} \qquad (56)$$

$$\frac{\partial\rho}{\partial x} = -\frac{P}{RZ^2T^2}\left(\frac{\partial(ZT)}{\partial T}\right)_P\frac{\partial T}{\partial x} \qquad (57)$$

Substitution in Eq. (52) gives:

$$\frac{D\omega'}{Dt} - \frac{\omega'}{P}\frac{dP}{dt} + \frac{\omega'}{ZT}\left(\frac{\partial(ZT)}{\partial T}\right)_P\frac{DT}{Dt} = -\frac{g}{rZT}\left(\frac{\partial(ZT)}{\partial T}\right)_P\frac{\partial T}{\partial r} + \frac{1}{rZT}\frac{\partial T}{\partial r}\left(\frac{\partial(ZT)}{\partial T}\right)_P \cdot\frac{Du}{Dt} - \frac{1}{rZT}\left(\frac{\partial(ZT)}{\partial T}\right)_P\frac{\partial T}{\partial x}\frac{Dv}{Dt} + \nu\left[\frac{\partial^2\omega'}{\partial x^2} + \frac{3}{r}\frac{\partial\omega'}{\partial r}\frac{\partial^2\omega'}{\partial r^2}\right] \qquad (58)$$

Substitution of Eqs. (25), (56), and (57) into Eq. (55) gives:

$$\frac{\partial^2\psi''}{\partial r^2} - \frac{1}{r}\frac{\partial\psi''}{\partial r} + \frac{\partial^2\psi''}{\partial x^2} = \frac{P}{RZT}\omega' r^2 - \frac{Pr}{RZ^2T^2}\left(\frac{\partial(ZT)}{\partial T}\right)_P\left[u\frac{\partial T}{\partial r} - v\frac{\partial T}{\partial x}\right] \qquad (59)$$

The terms u and v in Eqs. (58) and (59) could also be expressed in terms of ψ'' by Eq. (54). Substitution of the equation of state (25) into the energy Eq. (24) gives:

$$\rho\left[C_v + R\left(\frac{\partial(ZT)}{\partial T}\right)_P\right]\frac{DT}{Dt} = \frac{dP}{dt} + k\nabla^2 T \tag{60}$$

Taking the thermodynamic relation

$$C_p - C_v = T\left(\frac{\partial v}{\partial T}\right)_P\left(\frac{\partial P}{\partial T}\right)_v \tag{61}$$

and the ratio of specific heats

$$\frac{C_p}{C_v} = \gamma \tag{62}$$

and substituting into Eq. (60) and rearranging, another form of the energy equation is:

$$\frac{DT}{Dt} = \frac{1}{1 + \dfrac{(\gamma - 1)Z}{\left(\dfrac{\partial(ZT)}{\partial T}\right)_v}}\cdot\frac{RZT}{C_v P}\frac{dP}{dt} + \frac{\gamma}{1 + \dfrac{(\gamma - 1)Z}{\left(\dfrac{\partial(ZT)}{\partial T}\right)_v}}\alpha\nabla^2 T \tag{63}$$

It might be noted that the body force term in Eq. (58) could also be expressed as:

$$\frac{g}{rZT}\left(\frac{\partial(ZT)}{\partial T}\right)_P\frac{\partial T}{\partial r} = \frac{g}{r}\beta\frac{\partial T}{\partial r} \tag{64}$$

For the case where the behavior of the vapor is approximated adequately by an ideal gas, Eqs. (58), (59), and (63) reduce, respectively, to:

$$\frac{D\omega'}{Dt} - \frac{\omega'}{P}\frac{dP}{dt} + \frac{\omega'}{T}\frac{DT}{Dt} = -\frac{g}{rT}\frac{\partial T}{\partial r} + \frac{1}{rT}\frac{\partial T}{\partial r}\frac{Du}{Dt} - \frac{1}{rT}\frac{\partial T}{\partial x}\frac{Dv}{Dt} + \nu\left[\frac{\partial^2\omega'}{\partial x^2} + \frac{3}{r}\frac{\partial\omega'}{\partial r} + \frac{\partial^2\omega'}{\partial r^2}\right] \tag{65}$$

$$\frac{\partial^2\psi''}{\partial r^2} - \frac{1}{r}\frac{\partial\psi''}{\partial r} + \frac{\partial^2\psi''}{\partial x^2} = \frac{P}{RT}\omega' r^2 - \frac{Pr}{RT^2}\left[u\frac{\partial T}{\partial r} - v\frac{\partial T}{\partial x}\right] \tag{66}$$

$$\frac{DT}{Dt} = \frac{\gamma - 1}{\gamma} \frac{T}{P} \frac{dP}{dt} + \alpha \nabla^2 T \qquad (67)$$

Equations (58), (59) and (63) (or (65)-(67) for ideal gases) together with the transformed boundary conditions constitute a system of 3 equations with 4 unknowns for the vapor space, $\omega'(x,r,t)$, $\psi''(x,r,t)$, $T(x,r,t)$, and $P(t)$. The finite-difference solution of Eqs. (58), (59), and (63) for ω', ψ'', and T requires that a function for dP/dt be available. This is obtained from the First Law of Thermodynamics written as an instantaneous rate equation, taking the vapor space as the control volume. Referring to Fig. 2 this formulation is written:

$$\frac{d}{dt} \int_{V_g(t)} (\rho_g e_g) dV - \int_{A_i} h_{gs} \rho_{gs} (u_{gi} - u_i) dA + \int_{A_p} h_{gp} \rho_{gp} u_{gp} dA = \int_{A_{c.s.}} q dA - P \frac{dV_g}{dt} \qquad (68)$$

This formulation includes the following generalized variation:

$$e_g = e(x,r,t)$$

$$\rho_g = \rho(x,r,t)$$

$$u_{gi} = u(r,t)$$

h_{gs}, ρ_{gs} are uniform over the liquid-vapor interface

u_i is uniform for a flat interface

$h_{gp}, \rho_{gp}, u_{gp}$ are specified by the pressurization process

q is the local heat flux on the control surface, and its integral includes that from the tank wall and through the liquid-vapor interface.

Given property information on $e_g = f_1(P,T)$, $\rho_g = f_2(P,T)$, $h_{gs} = f_3(P)$, $\rho_{gs} = f_4(P)$, the desired term dP/dt can be extracted from the first term of Eq. (68). The necessary properties can come either from specific heat data plus an equation of state, or from tabulated values. It may be anticipated that different computational procedures would be required for each of these.

The procedure will be demonstrated for the case of self-pressurization, that is with no liquid discharge, no external pressurization, and a flat interface. Thus, $w_d = 0$, $w_p = 0$, and $u_{gp} = 0$. Then,

$$\frac{dX}{dt} = u_i = \frac{dX_i}{dt} \tag{69}$$

and from Eq. (45), assuming a uniform vapor velocity across the interface

$$u_{gi} - u_i = \frac{\rho_\ell}{\rho_\ell - \rho_{gs}} u_{gi} \tag{70}$$

For the coordinate frame selected

$$\frac{dV_g}{dt} = - A_i \frac{dX}{dt} = - A_i u_i \tag{71}$$

For brevity

$$q_{tot} = \int_{A_{c.s.}} q dA \tag{72}$$

Substituting Eqs. (70)-(72) into Eq. (68)

$$\frac{d}{dt} \int_{V_g(t)} (\rho_g e_g) dV = q_{tot} + h_{gs} \rho_{gs} \frac{\rho_\ell}{\rho_\ell - \rho_{gs}} u_{gi} A_i + P A_i u_i \tag{73}$$

Using Leibnitz's rule for differentiation of integrals having variable limits the first term of Eq. (73) can be written as

$$\frac{d}{dt} \int_{V_g(t)} (\rho_g e_g) dV = \int_{V_g} \rho_g \frac{\partial e_g}{\partial t} dV + \int_{V_g} e_g \frac{\partial \rho_g}{\partial t} dV - \rho_{gs} e_{gs} u_i A_i \tag{74}$$

Substituting Eq. (74) in Eq. (73) and rearranging with the use of Eq. (45) gives,

$$\int_{V_g} \rho_g \frac{\partial e_g}{\partial t} dV + \int_{V_g} e_g \frac{\partial \rho_g}{\partial t} dV = q_{tot} + h_{gs} A_i u_i (\rho_{gs} - \rho_\ell) \tag{75}$$

For the case in which the use of an equation of state (25) is desired, Eq. (75) can be expressed as the following by means of general thermodynamic property relations:

$$\frac{C_v}{R}\frac{dP}{dt}\int_{V_g}\frac{dV}{\left[\frac{\partial(ZT)}{\partial T}\right]_v}+\int_{V_g}\left\{\frac{PC_v}{R}\frac{1}{\left[\frac{\partial(ZT)}{\partial T}\right]_P}+T\left(\frac{\partial P}{\partial T}\right)_v\right\}\frac{1}{ZT}\left[\frac{\partial(ZT)}{\partial t}\right]dV$$

$$-\frac{P}{R}\int_{V_g}\frac{h_g}{Z^2T^2}\left[\frac{\partial(ZT)}{\partial t}\right]dV=q_{tot}+h_{gs}A_iu_i(\rho_{gs}-\rho_\ell) \qquad (76)$$

The enthalpy terms in Eqs. (75) and (76) can be expressed by:

$$h-h_R=\int_{T_R}^{T}C_{pR}dT+\int_{P_R}^{P}\frac{RT}{P}\left\{Z-\left[\frac{\partial(ZT)}{\partial T}\right]_P\right\}_T dP \qquad (77)$$

where the subscript R refers to a low pressure reference condition.

For an ideal gas with constant specific heat Eq. (76) reduces to:

$$\frac{C_v}{R}\left(\frac{dP}{dt}\right)V_g=q_{tot}+h_{gs}A_iu_i(\rho_{gs}-\rho_\ell) \qquad (78)$$

Expressing the enthalpy in terms of specific heat and rearranging, Eq. (78) reduces to:

$$\frac{dP}{dt}=\frac{R}{C_vV_g}q_{tot}+\frac{RT_s\gamma}{V_g}A_iu_i(\rho_{gs}-\rho_\ell) \qquad (79)$$

For the case far from the region of the critical state, such that $\rho_\ell \gg \rho_{gs}$, Eq. (79) can be written as

$$\frac{dP}{dt}=\frac{R}{C_vV_g}q_{tot}-\frac{w_iR\gamma T_s}{V_g} \qquad (80)$$

where w_i is the rate of interfacial mass transfer (having a negative value for evaporation) and is given by

$$w_i=-\rho_{gs}A_i(u_{gi}-u_i)=-\frac{\rho_\ell\rho_{gs}}{(\rho_\ell-\rho_{gs})}A_iu_{gi} \qquad (81)$$

C. DIMENSIONLESS FORM OF THE EQUATIONS

The governing equations for the wall, liquid, and vapor regions (1), (49), (50), (51), (58), (59), and (63), along with the boundary conditions, are restated in dimensionless forms for convenience.

The substitution used to nondimensionalize these are:

$$\left.\begin{aligned} u &= \frac{\alpha_\ell b}{a^2} U; \qquad v = \frac{\alpha_\ell}{a} V; \qquad T - T_o = \frac{\nu_\ell \alpha_\ell b}{\beta_\ell g a^4} \Theta \\ t &= \frac{a^2}{\alpha_\ell} \tau; \qquad x = b\zeta \ ; \qquad r = a\eta \\ \omega'' &= \frac{\alpha_\ell b}{a^4} \omega; \qquad \psi' = \alpha b \psi \end{aligned}\right\} \tag{82}$$

The resulting dimensionless equations are given below.

1. Tanic Side Wall

The dimensionless equations describing the wall temperature, from Eq. (1), are given by:

(i) $0 \le \zeta \le \zeta_i = \frac{X(t)}{b}$

$$\frac{\partial \Theta_w}{\partial \tau} = - \frac{a}{\delta_w} \cdot \frac{(\rho C_p)_\ell}{(\rho C_p)_w} \left(\frac{\partial \Theta_\ell}{\partial \eta} \right)_{\eta=1} + \frac{a^2}{b^2} \cdot \frac{(\rho C_p)_\ell}{(\rho C_p)_w} \cdot \frac{k_w}{k_\ell} \frac{\partial^2 \Theta_w}{\partial \zeta^2}$$

$$+ \frac{a}{b} \cdot \frac{a}{\delta_w} \cdot \frac{(\rho C_p)_\ell}{(\rho C_p)_w} \cdot Pr_\ell \cdot Gr_w^*(\zeta, t) \tag{83}$$

(ii) $\frac{X(t)}{b} \le \zeta \le 1$

$$\frac{\partial \Theta_w}{\partial \tau} = - \frac{a}{\delta_w} \cdot \frac{(\rho C_p)_\ell}{(\rho C_p)_w} \cdot \frac{k_g}{k_\ell} \left(\frac{\partial \Theta_g}{\partial \eta} \right)_{\eta=1} + \frac{a^2}{b^2} \cdot \frac{(\rho C_p)_\ell}{(\rho C_p)_w} \cdot \frac{k_w}{k_\ell} \cdot \frac{\partial^2 \Theta_w}{\partial \zeta^2}$$

$$+ \frac{a}{b} \cdot \frac{a}{\delta_w} \cdot \frac{(\rho C_p)_\ell}{(\rho C_p)_w} \cdot Pr_\ell \cdot Gr_w^*(\zeta, t) \tag{84}$$

where $Gr_w^*(\zeta,t)$ is the modified Grashof number and is given by:

$$Gr_w^*(\zeta,t) = \frac{g\beta a^4}{k_\ell \nu_\ell^2} q_w(\zeta,t) \tag{85}$$

(iii) Boundary and initial conditions

$$\frac{\partial \theta_w(0,\tau)}{\partial \zeta} = \frac{\partial \theta_w}{\partial \zeta}(1,\tau) = 0 \tag{86}$$

$$\theta(\zeta,0) = 0 \tag{87}$$

2. Liquid Region

(i) The energy equation, Eq. (49)

$$\frac{\partial \theta}{\partial \tau} + \frac{1}{\eta}\cdot\frac{\partial \psi}{\partial \eta}\cdot\frac{\partial \theta}{\partial \zeta} - \frac{1}{\eta}\frac{\partial \psi}{\partial \zeta}\cdot\frac{\partial \theta}{\partial \eta} = \frac{a^2}{b^2}\frac{\partial^2 \theta}{\partial \zeta^2} + \frac{1}{\eta}\frac{\partial \theta}{\partial \eta} + \frac{\partial^2 \theta}{\partial \eta^2} \tag{88}$$

(ii) The vorticity equation, Eq. (50)

$$\frac{\partial \omega}{\partial t} + \frac{1}{\eta}\frac{\partial \psi}{\partial \eta}\frac{\partial \omega}{\partial \zeta} - \frac{1}{\eta}\frac{\partial \psi}{\partial \zeta}\frac{\partial \omega}{\partial \eta} = Pr_\ell\left[\frac{1}{\eta}\frac{\partial \theta}{\partial \eta} + \frac{a^2}{b^2}\frac{\partial^2 \omega}{\partial \zeta^2} + \frac{3}{\eta}\frac{\partial \omega}{\partial \eta} + \frac{\partial^2 \omega}{\partial \eta^2}\right] \tag{89}$$

(iii) The vorticity-stream function equation, Eq. (51)

$$\frac{1}{\eta^2}\left(\frac{a^2}{b^2}\frac{\partial^2 \psi}{\partial \zeta^2} - \frac{1}{\eta}\frac{\partial \psi}{\partial \eta} + \frac{\partial^2 \psi}{\partial \eta^2}\right) = \omega \tag{90}$$

$$U = \frac{1}{\eta}\frac{\partial \psi}{\partial \eta} \quad ; \quad V = -\frac{1}{\eta}\frac{\partial \psi}{\partial \zeta} \tag{91}$$

(iv) The boundary conditions

(1) Stream function boundary conditions

$$\psi(0,\eta,\tau) = \frac{\partial \psi(0,\eta,\tau)}{\partial \zeta} = 0 \tag{92}$$

$$\psi(\zeta_i,\eta,\tau) = \frac{\partial^2 \psi(\zeta_i,\eta,\tau)}{\partial \zeta^2} = 0 \tag{93}$$

$$\psi(\zeta,0,\tau) = \frac{\partial}{\partial\eta}\left[\frac{1}{\eta}\frac{\partial\psi(\zeta,0,\tau)}{\partial\eta}\right] = 0 \tag{94}$$

$$\psi(\zeta,1,\tau) = \frac{\partial\psi(\zeta,1,\tau)}{\partial\eta} = 0 \tag{95}$$

(2) Vorticity boundary conditions

$$\omega(1,\eta,\tau) = 0 \tag{96}$$

$$\omega(\zeta,0,\tau) = 0 \tag{97}$$

Two additional vorticity boundary conditions are required at the tank wall and bottom. An explicit expression for the vorticity at any of these locations is difficult to obtain. The method of solution used in this work, which follows that of Refs. 1-3, overcomes this difficulty.

(3) Thermal boundary conditions

$$\Theta(\zeta,1,\tau) = \Theta_w(\zeta,\tau) \tag{98}$$

$$\Theta(\zeta_i,\eta,\tau) = \Theta_s(\tau) \tag{99}$$

$$\frac{\partial\Theta(0,\eta,\tau)}{\partial\zeta} = 0 \tag{100}$$

$$\frac{\partial\Theta(\zeta,0,\tau)}{\partial\eta} = 0 \tag{101}$$

where Θ_s is given by:

$$\Theta_s(\tau) = \frac{a}{b}\,Pr_\ell\left[T_s(t) - T_o\right]\frac{g\beta_\ell a^3}{\nu_\ell^2} \tag{102}$$

(4) Initial conditions

$$\Theta(\zeta,\eta,0) = U(\zeta,\eta,0) = V(\zeta,\eta,0) = \omega(\zeta,\eta,0) = \psi(\zeta,\eta,0) = 0 \tag{103}$$

3. Vapor Region

(i) The energy equation, Eq. (63)

$$\frac{\partial\theta}{\partial\tau} + \frac{1}{\rho\eta}\frac{\partial\psi}{\partial\eta}\frac{\partial\theta}{\partial\zeta} - \frac{1}{\rho\eta}\frac{\partial\psi}{\partial\zeta}\frac{\partial\theta}{\partial\eta} = \frac{1}{1 + (\gamma - 1)Z/\left(\frac{\partial(ZT)}{\partial T}\right)_v}\cdot\frac{RZ}{C_v}\cdot\frac{(\theta + \theta_o)}{P}\cdot\frac{dP}{d\tau}$$

$$+ \frac{\gamma}{1 + (\gamma - 1)Z/\left(\frac{\partial(ZT)}{\partial T}\right)_v}\frac{\alpha_g}{\alpha_\ell}\left[\frac{a^2}{b^2}\frac{\partial^2\theta}{\partial\zeta^2} + \frac{1}{\eta}\frac{\partial\theta}{\partial\eta} + \frac{\partial^2\theta}{\partial\eta^2}\right] \tag{104}$$

where

$$\theta_o = \frac{g\beta_\ell a^4}{\nu_\ell \alpha_\ell b}\,T_o \tag{105}$$

(ii) The vorticity equation, Eq. (58)

$$\frac{\partial\omega}{\partial\tau} + \frac{1}{\rho\eta}\cdot\frac{\partial\psi}{\partial\eta}\cdot\frac{\partial\omega}{\partial\zeta} - \frac{1}{\rho\eta}\cdot\frac{\partial\psi}{\partial\zeta}\cdot\frac{\partial\omega}{\partial\eta} = Pr_\ell\,\frac{\nu_g}{\nu_\ell}\left[\frac{a^2}{b^2}\frac{\partial^2\omega}{\partial\zeta^2} + \frac{3}{\eta}\frac{\partial\omega}{\partial\eta} + \frac{\partial^2\omega}{\partial\eta^2}\right] + \frac{ga^4}{\alpha_\ell^2 bZ\eta(\theta + \theta_o)}\left(\frac{\partial(ZT)}{\partial T}\right)_P\frac{\partial\theta}{\partial\eta}$$

$$+ \frac{1}{\eta Z(\theta + \theta_o)}\left(\frac{\partial(ZT)}{\partial T}\right)_P\frac{\partial\theta}{\partial\eta}\frac{DU}{D\tau} - \frac{1}{\eta Z(\theta + \theta_o)}\left(\frac{\partial(ZT)}{\partial T}\right)_P\frac{\partial\theta}{\partial\zeta}\frac{DV}{D\tau} + \frac{\omega}{P}\left(\frac{dP}{d\tau}\right) \tag{106}$$

where β has been replaced by the term:

$$\beta_g = \frac{1}{ZT}\left(\frac{\partial(ZT)}{\partial T}\right)_P \tag{107}$$

as in Eq. (64).

(iii) The vorticity-stream function equation, Eq. (59)

$$\frac{a^2}{b^2}\frac{\partial^2\psi}{\partial\zeta^2} - \frac{1}{\eta}\frac{\partial\psi}{\partial\eta} + \frac{\partial^2\psi}{\partial\eta^2} = \frac{P}{ZR(\theta + \theta_o)}\left(\frac{g\beta_\ell a^4}{\nu_\ell \alpha_\ell b}\right)\omega\eta^2$$

$$- \left(\frac{g\beta_\ell a^4}{\nu_\ell \alpha_\ell b}\right)\frac{P}{Z^2R(\theta + \theta_o)}\left(\frac{\partial(ZT)}{\partial T}\right)_P \eta\left[U\frac{\partial\theta}{\partial\eta} - \frac{a^2}{b^2}V\frac{\partial\theta}{\partial\zeta}\right] \qquad (108)$$

(iv) Boundary conditions

(1) Stream-function boundary conditions

$$\psi(1,\eta,\tau) = \frac{\partial\psi(1,\eta,\tau)}{\partial\zeta} = 0 \qquad (109)$$

$$\psi(\zeta_i,\eta,\tau) = \frac{\rho_{gs}U_{gi}\eta^2}{2} = (\rho_\ell - \rho_{gs})\frac{w_i}{\rho_\ell\alpha_\ell}\cdot\frac{\eta^2}{2\pi b} \qquad (110)$$

$$\psi(\zeta,0,\tau) = \frac{\partial}{\partial\eta}\left(\frac{1}{\rho_{gi}\eta}\frac{\partial\psi(\zeta,0,\tau)}{\partial\eta}\right) = 0 \qquad (111)$$

$$\psi(\zeta,1,\tau) = \frac{\partial\psi(\zeta,1,\tau)}{\partial\eta} = 0 \qquad (112)$$

(2) Vorticity boundary conditions

$$\omega(\zeta,0,\tau) = 0 \qquad (113a)$$

$$\omega(\zeta_i,\eta,\tau) = 0 \qquad (113b)$$

(3) Temperature boundary conditions

$$\theta(\zeta_i,\eta,\tau) = \theta_s(\tau) \qquad (114)$$

$$\frac{\partial\theta(1,\eta,\tau)}{\partial\zeta} = 0 \qquad (115)$$

$$\theta(\zeta,1,\tau) = \theta_w(\zeta,\tau) \tag{116}$$

$$\frac{\partial\theta(\zeta,0,\tau)}{\partial\eta} = 0 \tag{117}$$

(4) Initial conditions

$$\theta(\zeta,\eta,0) = U(\zeta,\eta,0) = V(\zeta,\eta,0) = \psi(\zeta,\eta,0) = \omega(\zeta,\eta,0) = 0 \tag{118}$$

From the above results, it is clear that the temperature, pressure, and velocity within the container are functions of the parameters Gr_w^*, Pr, $(\rho C_p)_\ell/(\rho C_p)_w$, (k_w/k_ℓ), (α_g/α_ℓ), (ν_g/ν_ℓ), (β_g/β_ℓ), (a/b), and (a/δ). Gr_w^* is defined in Eq. (85).

III. METHOD OF SOLUTION

A. FINITE-DIFFERENCE FORMS

The finite-difference method of solution used in Refs. 1-2 is adopted here. A complete discussion of the application of difference methods for the solution of the energy and vorticity equations is given in these references, along with the problem of stability of the difference equations. A brief discussion of the method of solution will be made here.

The basic technique in the application of finite-difference methods for the solution of partial differential equations is the use of Taylor Series Expansion to approximate the derivatives at a point in terms of the value of the function at that point and/or at its neighboring points. This may be demonstrated as follows:

1. The time derivative is represented by

$$\frac{\partial f}{\partial \tau} = \frac{f(\tau + \Delta\tau) - f(\tau)}{\Delta\tau} + O(\Delta\tau) \tag{119}$$

2. The first order derivatives $\partial f/\partial \zeta$ and $\partial f/\partial \eta$ can be approximated by

$$\text{(i)} \quad \frac{\partial f}{\partial \zeta} = \frac{f(\zeta + \Delta\zeta, \eta, \tau) - f(\zeta, \eta, \tau)}{\Delta\zeta} + O(\Delta\zeta) \text{ (forward differences)} \tag{120}$$

or

$$\text{(ii)} \quad \frac{\partial f}{\partial \zeta} = \frac{f(\zeta, \eta, \tau) - f(\zeta - \Delta\zeta, \eta, \tau)}{\Delta\zeta} + O(\Delta\zeta) \quad \text{(backward differences)} \tag{121}$$

or

$$\text{(iii)} \quad \frac{\partial f}{\partial \zeta} = \frac{f(\zeta + \Delta\zeta, \eta, \tau) - f(\zeta - \Delta\zeta, \eta, \tau)}{2\Delta\zeta} + O(\Delta\zeta)^2 \quad \text{(central differences)} \tag{122}$$

3. The second order derivatives are replaced by finite-differences according to the formula.

$$\frac{\partial^2 f}{\partial \zeta^2} = \frac{f(\zeta + \Delta\zeta, \eta, \tau) - 2f(\zeta, \eta, \tau) + f(\zeta - \Delta\zeta, \eta, \tau)}{(\Delta\zeta)^2} + O(\Delta\zeta)^2 \tag{123}$$

The function f represents either θ or ω, and $\Delta\zeta$ is the spatial increment in the ζ-direction. The last term on the righthand side of Eqs. (119) through (123) indicates the order of the truncation error involved in replacing the derivatives by finite-differences. It is clear that the central differences offer a better representation of the first order derivative $\partial f/\partial\zeta$ than the forward or backward differences. However, the form used to approximate the first order derivatives is usually determined by stability considerations. Similar formulations can be written for the derivatives $\partial f/\partial\eta$ and $\partial^2 f/\partial\eta^2$.

The substitution of the above formulae in the energy and vorticity equations produces a set of explicit difference equations. However, if the values of the function f in Eqs. (120) through (123) are taken at the time level $\tau + \Delta\tau$ instead of being taken at time level τ, the resulting finite-difference methods may require the use of small time increments and consequently large machine time. Certain implicit formulations may permit the use of large increments. The application of both explicit and implicit methods to the present problem has been extensively investigated in Ref. 2. It was concluded that the lack of explicit boundary conditions for the vorticity at the solid boundaries prevent the use of large time increments, i.e., implicit methods. Other than that, it was decided to employ explicit methods.

It is clear from Eqs. (120) through (122) that more than one explicit finite-difference formulation can be constructed for each of the vorticity and energy equations. The finite-difference formulation chosen for the solution of the present problem is dictated by stability, as well as practical considerations, which will be shown below in studying the stability of the finite-difference equations.

The method of solution used in the present problem can be summarized as follows:

1. The time derivatives $\partial\theta/\partial\tau$ and $\partial\omega/\partial\tau$ are approximated by Eq. (119).

2. The nonlinear terms $U\,\partial\theta/\partial\zeta$, $V\,\partial\theta/\partial\eta$, $U\,\partial\omega/\partial\zeta$, and $V\,\partial\omega/\partial\eta$ are linearized by considering the velocity components U and V to be known and are taken equal to their values at time level τ. The order of the error introduced by this linearization can be obtained from Taylor Series Expansion. If U_o and U are the values of the axial velocity component at time levels τ_o and $\tau_o + \Delta\tau$, respectively, then

$$U\frac{\partial\theta}{\partial\zeta} = U_o\frac{\partial\theta}{\partial\zeta} + \left[\frac{\partial U}{\partial\tau}\Delta\tau + O(\Delta\tau)^2\right]\frac{\partial\theta}{\partial\zeta} = U_o\frac{\partial\theta}{\partial\zeta} + O(\Delta\tau)\frac{\partial\theta}{\partial\zeta} \qquad (124)$$

The second term of the right side of Eq. (124) represents the linearization error.

3. The nonlinear terms $U\ \partial\theta/\partial\zeta$ and $U\ \partial\omega/\partial\zeta$ are approximated by backward differences, Eq. (121), if the coefficient velocity U is positive and by forward differences, Eq. (120), if U is negative. The same procedure is followed for approximating the terms $V\ \partial\theta/\partial\eta$ and $V\ \partial\omega/\partial\eta$ according to the sign of the velocity component V.

4. Central differences are used to approximate the first order terms $1/\eta\ \partial\theta/\partial\eta$, $3/\eta\ \partial\omega/\partial\eta$, and $1/\eta\ \partial\psi/\partial\eta$. No stability problems will be encountered in this case. At the centerline where both η and $\partial\theta/\partial\eta$ are zero, $1/\eta\ \partial\theta/\partial\eta$ is replaced by its limit according to L'Hospital's rule

$$\lim_{\eta\to 0} \frac{1}{\eta}\frac{\partial\theta}{\partial\eta} = \frac{\partial^2\theta}{\partial\eta^2}\Big|_{\eta=0} \tag{125}$$

5. The second order term $\partial^2\theta/\partial\zeta^2$, $\partial^2\theta/\partial\eta^2$, $\partial^2\omega/\partial\zeta^2$, $\partial^2\omega/\partial\eta^2$, $\partial^2\psi/\partial\zeta^2$, and $\partial^2\psi/\partial\eta^2$ are represented by Eq. (123).

6. Although the first order derivative $\partial\theta/\partial\eta\big|_{\eta=1}$ in Eqs. (83) and (84) can be represented by any of Eqs. (120), (121), or (122), the following formula, which has a higher order truncation error, is used,

$$\frac{\partial\theta}{\partial\eta}\Big|_{\eta=1} = \frac{11\theta(\zeta,1) - 18\theta(\zeta,\eta-\Delta\eta) + 9\theta(\zeta,\eta-2\Delta\eta) - 2\theta(\zeta,\eta-3\Delta\eta)}{6\Delta\eta} \tag{126}$$

Similarly

$$\frac{\partial\theta_\ell}{\partial\zeta}\Big|_{\zeta=\zeta_i} = \frac{11\theta(\zeta_i,\eta) - 18\theta(\zeta_i-\Delta\zeta,\eta) + 9\theta(\zeta_i-2\Delta\zeta,\eta) - 2\theta(\zeta_i-3\Delta\zeta,\eta)}{6\Delta\zeta} \tag{127}$$

In determining the side wall temperature at the location of the interface by the finite-difference procedure, a special difference equation must be used in order to take proper physical account of the possible axial variation of heat flux imposed on the wall, the difference in thermal conductivity between the liquid and vapor, and the possible difference in axial grid spacing in the liquid and vapor regions.

The energy equation for the nodal point in the wall at the liquid-vapor interface is:

$$\frac{\theta_{wi}(\tau+\Delta\tau) - \theta_{wi}(\tau)}{\Delta\tau}\left(\frac{\Delta\zeta_\ell + \Delta\zeta_g}{2}\right) = -\left(\frac{a(k_\ell \Delta\zeta_\ell + k_g \Delta\zeta_g)}{2\,\rho_w\, C_{pw}\,\delta\,\alpha_\ell}\right)$$

$$\frac{11\theta(\zeta_i,\eta_w) - 18\theta(\zeta_i,\eta_w-\Delta\eta) + 9\theta(\zeta_i,\eta_w-2\Delta\eta) - 2\theta(\zeta_i,\eta_w-3\Delta\eta)}{6\Delta\eta}$$

$$+\left(\frac{a^2}{b^2}\frac{\alpha_w}{\alpha_\ell}\right)(\Delta\zeta_\ell+\Delta\zeta_g)\,\frac{\theta(\zeta_i+\Delta\zeta,\eta_w) - \left(1+\frac{\Delta\zeta_g}{\Delta\zeta_\ell}\right)\theta(\zeta_i,\eta_w) + \frac{\Delta\zeta_g}{\Delta\zeta_\ell}\,\theta(\zeta_i-\Delta\zeta,\eta_w)}{\frac{\Delta\zeta_\ell\,\Delta\zeta_g}{2}\left(1+\frac{\Delta\zeta_g}{\Delta\zeta_\ell}\right)}$$

$$+ (q_{w\ell}\Delta\zeta_\ell + q_{wg}\Delta\zeta_g)\left(\frac{\beta_\ell g\, a^6}{2\,\nu_\ell \alpha_\ell^2\, b\rho_w C_{pw}\,\delta}\right) \qquad (128)$$

7. As mentioned earlier, two vorticity boundary conditions each are required in the liquid and vapor regions in addition to those given by Eqs. (96) and (97) for the liquid and Eqs. (113a) and (113b) for the vapor. An explicit expression is difficult to find, but the procedure followed in the numerical computations is described here. The step-by-step explicit computations of vorticity allow progressing from one vorticity distribution to the next at all grid points except those on the boundary, using the values of the vorticity from the previous time step. The new values of the vorticity are used to determine the stream function, which in turn are used to compute the vorticity at the solid boundaries.

Using the Taylor series expansion together with the stream function boundary conditions, the following expressions are obtained for the vorticity at the solid boundaries:

Sidewall

$$\omega(\zeta,\eta_w) = \frac{8\psi(\zeta,\eta_w-\Delta\eta) - \psi(\zeta,\eta_w-2\Delta\eta)}{2(\Delta\eta)^2} \qquad (129)$$

Bottom (or top)

$$\omega(o,\eta) = \frac{a^2}{2b^2} \frac{8\psi(o+\Delta\xi,\eta) - \psi(o+2\Delta\xi,\eta)}{\eta^2(\Delta\xi)^2} \tag{130}$$

B. STABILITY CRITERIA

The stability of the finite-difference equations is an important consideration in establishing the size of the grid and the time steps, and the form of difference. The details are given in Ref. 2. As might be anticipated, the size of the grid and time steps will also be governed by the storage capacity of the machine and limitations of time and cost. The necessary requirements for stability are given by the following:

$$\Delta\tau\left(\frac{2a^2}{b^2(\Delta\zeta)^2} + \frac{2}{(\Delta\eta)^2} + \frac{|U_{i,j}|}{\Delta\zeta} + \frac{|V_{i,j}|}{\Delta\eta}\right) \leq 1 \tag{131}$$

$$\Delta\tau\left(\frac{2a^2Pr}{b^2(\Delta\zeta)^2} + \frac{2\ Pr}{(\Delta\eta)^2} + \frac{|U_{i,j}|}{\Delta\zeta} + \frac{|V_{i,j}|}{\Delta\eta}\right) \leq 1 \tag{132}$$

For the centerline, where V = 0,

$$\Delta\tau\left(\frac{2a^2}{b^2(\Delta\zeta)^2} + \frac{4}{(\Delta\eta)^2} + \frac{|U_{i,1}|}{\Delta\zeta}\right) \leq 1 \tag{133}$$

$$\Delta\tau\left(\frac{2a^2Pr}{b^2(\Delta\zeta)^2} + \frac{4\ Pr}{(\Delta\eta)^2} + \frac{|U_{i,1}|}{\Delta\zeta}\right) \leq 1 \tag{134}$$

whichever one of the above is the most restrictive must be used in calculating the maximum value of $\Delta\tau$ permitted.

C. COMPUTATIONAL PROCEDURES

The sequence of steps in establishing the numerical calculation is as follows:

(1) A convenient grid size is selected, limited by the machine storage capacity.

(2) A suitable time increment is chosen. This may be adjusted during the process of computation as necessary to maintain numerical stability.

(3) The temperature distribution is computed using velocities, temperatures, and pressure from the previous time step.

(4) These temperatures are used to compute the vorticity at the interior nodal points at the current time step.

(5) The stream function is computed at the interior nodal points.

(6) The vorticities at the solid boundaries are calculated using computed stream functions.

(7) The velocity components are calculated.

(8) The rate of phase change at the interface is determined using the computed temperature distribution, with Eq. (41).

(9) The pressure rise is computed with an equation such as (80) using the parameters from the previous time step.

(10) The above procedures are repeated successively.

A problem inherent in the use of numerical methods is the accurate determination of temperature gradients. In the present application temperature gradients are computed in the liquid and vapor at the liquid-vapor interface to determine the rate of phase change, from Eq. (41), and in the liquid and vapor at the wall to determine the heat transfer to the bulk liquid and vapor, respectively.

The general problem of the effect of grid size on the interfacial heat and mass transfer is presented in some detail here.

The formulation with Eq. (41) was used by a number of investigators[6-11] to determine the rate of interfacial phase change for the case of a suddenly pressurized one-dimensional model. However, the determination of the temperature gradients by numerical representation of the calculated temperature distribution in the case of self-pressurized containers may be difficult for two-dimensional cases because of the increased machine storage requirements combined with large temperature gradients near the interface, which cause the phase changes. These large temperature gradients exist in a very thin layer near the interface, as has been shown by experimental measurements.[14,15] This requires the use of a very small grid size in order to obtain an acceptable approximation for the temperature gradients near the interface.

In the case of the temperature gradients in the fluid adjacent to the wall two aspects must be considered when either the heat flux or the wall temperatures are imposed. One is similar to the liquid-vapor interface problem in that the grid spacing should again be small enough to permit sufficiently accurate representation of the temperature distribution in the fluid, either liquid or vapor, and in general dictates that the grid spacing be as small as possible. The degree of being sufficiently small will depend upon the magnitude of the imposed heat flux or the imposed temperature, and the response of the transient convective process to these disturbances under the prevailing effective gravity level. The only true test available is to vary the grid size for given conditions and compare the coupled results.

The other aspect to be considered is a physical one involving only the liquid, but is also related to the problem of grid spacing. If the temperature of the solid wall in contact with the liquid exceeds the saturation temperature by some amount, dependent upon various parameters including liquid and solid properties and the configuration, nucleate boiling will be initiated. This particular heating surface superheat might be called the incipient boiling point. If information on the incipient boiling point is available for the prevailing conditions, an imposed wall temperature below this point then represents no additional problem beyond that of having sufficiently small grid sizes, as discussed above. For the case of a heat flux imposed on the outer surface of the container, however, the resulting wall temperature is a variable dependent upon a number of parameters such as wall thickness and heat capacity, fluid properties, acceleration level, and container geometry. Whether the wall temperature will exceed the incipient boiling point will not be known a priori, since the wall temperature is computed during the course of the computations.

The procedure by which the possibility of nucleate boiling is taken into account is based on the following physical assumptions:

(1) should nucleate boiling begin, further increases in heat flux generally result in relatively small increases in surface temperature as compared to non-boiling convection. This has been observed widely (e.g., Ref. 16).

(2) The vapor bubbles formed are transported by buoyant forces to the ullage volume quite rapidly. The extent to which this may occur is as yet uncertain, but may be anticipated to depend upon the degree of subcooling present, the pressure and the effective gravity level. These are implemented in the computational procedure by considering that should the tank wall temperature, and hence the liquid adjacent to the wall, exceed the existing saturation temperature by some arbitrary amount, this excess is eliminated by the evaporation of the appropriate amount of liquid directly into the ullage space. In effect, then, a portion of the vapor bypasses the liquid-vapor interface. The arbitrary amount referred to above, the symbol for which is given as ΔT_{wmax} might be considered as the incipient boiling point, and no longer will be arbitrary when sufficient information on its behavior is available.

The physical phenomena described above is simulated in the computer program as follows:

(1) The container wall temperature is calculated using Eq. (1).

(2) The liquid temperature is obtained using Eq. (49).

(3) The calculated wall temperature in the liquid region is examined. If it exceeds the saturation temperature by more than the prescribed temperature difference ΔT_{wmax}, it then is reduced such that it equals the saturation temperature plus the prescribed temperature difference.

(4) Part of the heat added to the liquid region appears as enthalpy in the wall and liquid and the rest is used for evaporating some of the liquid. The portion of the heat transferred to the liquid and resulting in evaporation is determined by setting an energy balance according to

$$\int_0^x 2\pi a q_w(x,t)\, dxdt + \int_0^a 2\pi r q_{i\ell} dr = \int_0^a \int_0^X 2\rho_\ell c_{p\ell} \pi r \frac{\partial T_\ell}{\partial t} dxdr + \int_0^X 2\pi a \delta \rho_w c_{pw} \frac{\partial T_w}{\partial t} dx + w_i h_{fg} \tag{135}$$

where $q_{i\ell}$ is the rate of heat flow from the interface to the liquid and is given by,

$$q_{i\ell} = k_\ell \left(\frac{\partial T_\ell}{\partial x}\right)_{x=X} \tag{136}$$

Equations (135) and (136) are used to determine the rate of evaporation from the interface, w_i.

If the difference between the wall temperature and the saturation temperature is less than the specified maximum, ΔT_{wmax}, then the procedure above is bypassed and computations proceed as described earlier. An implicit assumption in the use of this procedure is that the laminar flow conditions described by the momentum and energy equations are not affected. This may be reasonable if the container is relatively large compared to the "bubble boundary layer" region next to the wall. In other words, if the vapor bubbles remain in the vicinity of the wall, the major bulk laminar motion of the liquid will not be influenced by their movement to the ullage space. An accurate physical description of this behavior requires additional analytical and experimental investigation in incipient boiling and the departure and motion of vapor bubbles

under low gravity fields with various patterns of subcooling.

D. COMPUTER PROGRAM

The simplified computer program flow chart based on the formulation presented is given in Appendix A.

Appendix B shows the computer program statement list for the case with liquid hydrogen and with the assumption of ideal gas behavior for the vapor. FORTRAN IV language is used here. In Appendix C are listed the meanings and units of the computer symbols employed. Appendix D lists the inputs (variables) required for the program, along with the units, and Appendix E presents a typical output. The compiled results for a number of computer runs covering several variables are presented and discussed in Section IV for liquid hydrogen.

IV. RESULTS

Computations were carried out with the program listing of Appendix B, using values of inputs calculated from the telemetered flight data of the Saturn IB vehicle AS-203, as reported in Ref. 17, so as to compare the calculated pressure rise with the measurements. Not only do differences exist between the actual physical system and the model which serves as the basis for the computer solution, but uncertainties exist in the accuracy of the necessary computer inputs given in Ref. 17, thus making a realistic comparison between the measured and predicted pressure rises difficult at this time. In order to indicate the possible influence of the more significant uncertain inputs, these are treated as variables in several cases.

A. GENERAL ASSUMPTIONS

The general assumptions incorporated into the particular program of Appendix B are listed below:

1. The tank is cylindrical with flat ends.

2. Acceleration or body forces act along the axis.

3. Two-dimensional conditions prevail, with variations only along the axis and radially.

4. Flow conditions are laminar within the entire container.

5. The vapor behaves as an ideal gas.

6. The liquid has constant properties except in the body force terms.

7. The tank side wall is uniform in thickness and has constant properties. The wall is lumped in the radial direction but axial conduction is taken into consideration.

8. The imposed heat flux on the outside of the tank wall is uniform, but differs in those portions in contact with the liquid and vapor.

9. The ends of the tank are adiabatic, and the heat capacity of the ends is neglected.

10. The grid size varies in the liquid and vapor region as liquid fraction changes, in order that a nodal point always exist at the liquid-vapor interface.

11. Initial conditions of uniform temperature and zero velocity exists within the container.

12. The Bond number is sufficiently large that a reasonable approximation to a flat liquid-vapor interface exists.

B. VARIATIONS POSSIBLE IN PROGRAM

By relatively minor modifications to the program, some of the above listed general assumptions can be relaxed, providing additional flexibility. In any case, however, axial symmetry must be maintained in order that the problem be two-dimensional.

1. The imposed heat flux can be varied axially and with time.

2. Specified initial conditions of temperature and velocity can be utilized.

3. Specified heat flux to the tank ends, including variations with radius and time, and including heat capacity can be incorporated.

4. If the description of the physical process warrants, imposed temperatures of the container walls can be utilized, with variation axially and with time.

5. Axial variation of tank side wall thickness and variation of specific heat with temperature can be accounted for.

6. Radial variations in the tank wall temperature can be taken into consideration. This may be particularly desirable if the wall is of composite construction.

Although the influence of variations in liquid properties with temperature and pressure can be incorporated with minor changes, the use of real gas properties in the vapor space will require major modifications to the program. This would be necessary should the pressure variation be large or should the pressure approach the critical state.

Major modifications also are necessary to handle the spacewise variation of grid size in either the liquid or vapor domains.

C. INPUT PARAMETERS

Appendix D lists the input requirements for the program as presented in Appendix B. For purposes of presentation and discussion the inputs are subdivided by categories of geometry, heat flux, acceleration level (for body

forces), fluid properties, and miscellaneous.

1. Geometry

The S-IVB LH_2 tank is cylindrical with hemispherical ends outward at the upper end and inward at the lower end. The computer model here consists of a cylindrical tank with flat ends. For purposes of simulation it was decided to maintain the diameter, total volume, and ullage volume approximately the same between the physical system and the model. This makes the wetted area of the model considerably less than in the physical system, and cognizance of this should be taken in interpreting the results. The significant geometrical comparisons are shown in Table I.

TABLE I

COMPARISON OF GEOMETRY FOR LH_2 TANKS

	S-IVB	Computer Model
Diameter	21.6 ft	22.0 ft
Total volume	10,500 ft^3	11,050 ft^3
Ullage fraction	0.66	0.677
LH_2 mass (initial)	16,000 lbm	15,700 lbm
Gas H_2 mass (initial)	≈ 500 lbm	≈ 500 lbm
Liquid volume	3,570 ft^3	3,570 ft^3
Height of tank	36.4 ft	29.2 ft
Wetted side wall area	952 ft^2	651 ft^2
Wetted bottom area	505 ft^2	379 ft^2
Total wetted area	1,457 ft^2	1,030 ft^2
Unwetted side wall area	1,528 ft^2	1,365 ft^2
Unwetted top area	430 ft^2	379 ft^2
Total unwetted area	1,958 ft^2	1,744 ft^2
Total skin area	3,415 ft^2	2,774 ft^2

The tank side wall of the S-IVB consists (Ref. 22) of a lamination of polyurethane foam (with glass fibers and glass cloth on inside) and 0.134 in. thick aluminum on the outside, with reinforcing ribs 0.10 in. thick by 0.650 in. high on a 9.5 $in.^2$ waffle pattern. Since the model as presently constituted considers only a radially lumped (thermally) wall, the composite properties of the physical system cannot properly be taken into account, and requires a modification of the program. For purposes of this study, a radially lumped wall was assumed, using in one case the properties of the insulating layer of polyurethane foam alone, and in the other case the uninsulated aluminum skin alone, giving due regard for the axial conductance path contribution of the

reinforcing ribs. The effect of each of these models is to make the wall temperature more nonuniform in the axial direction than would be the case with a composite wall model, and results in a different distribution of energy input rate between the liquid and vapor. The relevant properties used are listed in Table II. As a further test of the influence of wall material, one computation was conducted for stainless steel with the same thickness as the aluminum.

TABLE II

TANK WALL PROPERTIES

Material	Polyurethane	Aluminum	Stainless Steel
Thickness, δ	0.71 in.	0.140 in.	0.140 in.
Density, ρ_w	10 lbm/ft^3	169 lbm/ft^3	488 lbm/ft^3
Specific heat, C_{pw}	0.35 Btu/lbm-°R	0.20 Btu/lbm-°R	0.11 Btu/lbm-°R
Thermal conductivity, k_w	0.025 Btu/hr-ft-°R	219.5 Btu/hr-ft-°R	8.0 Btu/hr-ft-°R
Thermal diffusivity, α_w	0.1985×10^{-5} ft^2/sec	1.675×10^{-2} ft^2/sec	4.16×10^{-5} ft^2/sec
Total heat capacity, $\rho C_p \delta$	0.207 Btu/°F-ft^2	0.394 Btu/°F-ft^2	0.626 Btu/°F-ft^2

The properties listed above apply for near room temperature, which is valid if a polyurethane layer of insulation lies between the cryogenic liquid and the outer metal skin.

A number of computer runs were also conducted with the aluminum wall case, but using a heat capacity equal to 1/10 of that tabulated above. This in effect makes the heat transfer rate to the tank contents more nearly equal to that on the exterior surface of the tank, but retains the axial conduction effects of the tank side walls. The desirability of minimizing the tank wall heat capacity arises because the heating rate is given to the tank contents, excluding the tank walls.

2. Heat Flux

In Section VII of Ref. 17, the mean rates of energy input to the liquid and gaseous contents of the fuel tank are computed from the physical measurements by four different procedures. These heating rates are summarized in Table III and the computation procedures discussed are below.

The values by procedure A are based on an energy balance using the temperature measurements in the liquid and vapor during the closed tank experiment. In this procedure it was assumed that all of the energy required for evaporation during this period comes from the liquid alone.

TABLE III

S-IVB FUEL TANK HEATING RATES

Procedure	Liquid, Btu/sec	Ullage, Btu/sec	Total, Btu/sec
A	29.9	5.9	35.8
B	23.5	11.5	35.0
C	21.0	6.6	27.6
D	13.5	17.0	30.5

Procedure B is based on the continuous vent data, using the mean values from Figs. VII-2 and VII-3 in Ref. 17. It might be anticipated that some difference in the pressure rise would arise between using a mean value and a periodic heating rate as in Fig. VII-2 owing to the nonlinearity of the system.

Procedure C is based on a combination of the continuous vent data and the fluid temperatures measured during a transient period between the first and second blowdown.

The heating rates with procedure D are computed by using the temperature measurements across the tank walls to calculate the wall heat flux, using previously determined values of the thermal conductivity of the wall material.

It is noted that these different procedures give results ranging from approximately equal energy input rates to the liquid and vapor, to liquid rate five times that to the vapor. If the primary source of energy is solar radiation, the heat flux should be distributed almost uniformly on the tank exterior, in the axial direction. The higher heating rate to the liquid might then be considered as due to axial conduction from the vapor region to the liquid region, as a result of the lower heat transfer rate between the inner tank wall and the vapor compared to that between the tank wall and the liquid.

In the computer model the total energy input rate of 35.8 Btu/sec, corresponding to procedure A in Table III was used. In one case this is distributed between the liquid and vapor as in procedure A, and in the other case it is distributed such that the heat flux is uniform over the entire exterior of the container wall. Using the side wall areas of Table I, these result in the distributions as shown in Table IV. The heat fluxes listed are exterior to the surface, and owing to the heat capacity of the tank walls it can be expected that the energy input rate to the contents of the tank will be much lower than that of the actual case which this model simulates, with a lower pressure rise.

TABLE IV

COMPUTER MODEL HEAT FLUX DISTRIBUTION

Case	Heating Rate, Btu/sec			Heat Flux, Btu/hr-ft^2	
	Liquid	Ullage	Total	Liquid	Ullage
A	29.9	5.9	35.8	165.5	15.6
E	11.6	24.3	35.8	64.0	64.0

3. Acceleration

From Fig. IV-13 of Ref. 17 it is noted that during the closed tank experiment, the vehicle acceleration decreased approximately exponentially from $a/g_o = 3.7 \times 10^{-4}$ at the beginning to $a/g_o = 0.8 \times 10^{-4}$ at the end. For determining the influence of other parameters an approximate average value of $a/g_o = 1.7 \times 10^{-4}$ was used. However, to provide an indication of the significance of the body forces, computations were made with values of a/g_o above and below this level at 2.5×10^{-4} and 1.0×10^{-4}.

4. Fluid Properties

The properties of hydrogen used in the computer model were obtained in Refs. 17-19. Those listed here are taken as constant, corresponding to the saturation temperature at the initial pressure of 12.4 lbf/in.^{2}.

Liquid Hydrogen:

Thermal conductivity, $k_\ell = 1.89 \times 10^{-5}$ Btu/sec-ft-°R

Coefficient of expansion, $\beta_\ell = 0.862 \times 10^{-2}$ °R^{-1}

Kinematic viscosity, $\nu_\ell = 2.065 \times 10^{-6}$ ft^2/sec

Specific heat, $C_{p\ell} = 2.6$ Btu/lbm-°R

Thermal diffusivity, $\alpha_\ell = 16.6 \times 10^{-7}$ ft^2/sec

Density, $\rho_\ell = 4.39$ lbm/ft^3

Gaseous Hydrogen:

Thermal conductivity, $k_v = 2.5 \times 10^{-6}$ Btu/sec-ft-°R

Kinematic viscosity, $\nu_v = 0.85 \times 10^{-5}$ ft^2/sec

Specific heat, $C_{pv} = 2.85$ Btu/lbm-°R

Specific heat, $C_{vv} = 1.492$ Btu/lbm-°R

Thermal diffusivity, $\alpha_v = 1.06 \times 10^{-5}$ ft^2/sec

Gas constant, R = 766.4 ft-lbf/lbm-°R

To evaluate the saturation temperature corresponding to the system pressure the following correlation and constants (Ref. 20) are used.

$$\log_{10} P = A + \frac{B}{C + T} + DT \qquad (137)$$

where

P = vapor pressure in atm
T = temperature in °K
A = 2.000620
B = -50.09708
C = 1.0044
D = 1.74849×10^{-2}

Data on the latent heat of vaporization in the range of interest are read in tabular form.[21]

5. Miscellaneous

Within the limitations on the total number of nodal points, dictated by the machine storage capacity and other economic aspects of the computational process, one can adjust the distribution of nodal points between the liquid and vapor region somewhat arbitrarily. For most effective use, including an optimum accuracy, the nodal points should be more concentrated in regions of greater velocity and/or temperature gradients. In the present case, with 31 axial nodes present, and on ullage fraction of 2/3, the axial grid spacing was selected which gave a spacing in the liquid region 1/4 that in the vapor region, since it was felt that the largest changes would take place in the liquid region. In one case a run was repeated with equal axial grid spacing to test the influence of this parameter alone. The resulting differences were negligibly small.

An additional parameter, which must be specified is the value of $\Delta T_{w\,max}$, the arbitrary amount by which the side wall temperature cannot exceed the saturation temperature. This can be considered as the incipient boiling point.

Coeling[4] studied incipient pool boiling for cryogenic fluids, and reported that the initial vapor formation in liquid hydrogen and liquid nitrogen is primarily a function of the surface superheat, for a given surface—fluid combination, and is not a strong function of orientation or heat flux. The results of the measurements for 14 surface-orientation combinations were plotted and it was found that the heat flux and surface superheat of each individual observation was generally located along the natural convection correlations, $Nu = 0.14\ (Gr\ Pr)^{1/3}$, for all horizontal surface-liquid combinations. From this correlation, surface superheat is calculated as 2.3°R at 166 Btu/hr-ft^2 for LH_2.

Due to the uncertainty, $\Delta T_{w\,max}$ was assigned 1°R for the present work. On a surface consisting of a glass fiber material coated with an epoxy cement, similar to the inner lining of the LH_2 tank on the S-IVB stage, it was reported[4] that the surface became active at approximately 0.5°R superheat.

D. RESULTS OF COMPUTATIONS

In Table V are listed the various computational runs made, with a listing of the different independent variables used, and the significant dependent variables, or outputs, at different values of real time. These latter are the system pressure and the total mass of liquid evaporated. Reference to these runs in the following comparisons will be made in terms of the B-H numbers listed. Most of the column headings in Table V are self-explanatory. The Max. Real Time gives the maximum time for which a run was made, but is not the computer time. The Max. Time Steps gives the maximum number of time steps used in the numerical marching procedure, and gives an indication of the computer time used.

1. Typical Plots of Streamlines and Isotherms

In Figs. 3a, b, and c are shown computer output plots of the non-dimensional isotherms in the liquid and vapor regions at three different times during the transient heating process in Run B-H 47. These dimensionless temperatures can be converted to real temperatures by means of Eq. (82). Although the computer grid contained 21 x 31 nodal points, for these graphical presentations these were increased by a factor of three in each direction by linear interpolation of the results such as shown in Appendix E.

Each digit in the body of the plot corresponds to a range of temperatures within which the temperature at that point lies. The key for the ranges is given in the table at the bottom of each figure. Except for the digits 1 and 9,

TABLE V

INDEX OF COMPUTER RUNS

Run No.	B-H No.	No. of Vertical Divisions in Liquid	a/g	$(q/A)_V$ Btu/hr-ft^2	$(q/A)_I$ Btu/hr-ft^2	Wall Material	C_{pw}, Btu/lbm-°F	Total Wall Heat Capacity, $\rho C_p t$, Btu/°F-ft^2	K_w, Btu/hr-ft-°F	α_w, ft^2/sec	Max. Real Time, sec	Max. No. of Time Steps	Max. Press., lbf/in.^{2}	Max. Total Evap., lbm	Time, sec: 100 Press., lbf/in.^{2}	100 Total Evap., lbm	600 Press., lbf/in.^{2}	600 Total Evap., lbm	2000 Press., lbf/in.^{2}	2000 Total Evap., lbm	4600 Press., lbf/in.^{2}	4600 Total Evap., lbm	5000 Press., lbf/in.^{2}	5000 Total Evap., lbm	5360 Press., lbf/in.^{2}	5360 Total Evap., lbm
I-1	47	20	$1.7(10)^{-4}$	15.55	165.5	Poly.	.35	.207	.025	$.1985(10)^{-5}$	4712.2	1644	18.57	106.95	---	---	12.76	7.03	14.27	34.77	18.38	103.9				
I-2	53	10	$1.7(10)^{-4}$	15.55	165.5	Poly.	.35	.207	.025	$.1985(10)^{-5}$	5002.4	1183	19.5	123.	---	---	12.86	9.05	14.48	39.2	18.7	111.2	19.5	123.		
I-3	59	20	$1.7(10)^{-4}$	15.55	165.5	Al	.02	.0394	219.5	.018	5361.5	2586	21.16	62.75	---	---	12.57	.79	14.63	25.9	19.5	54.4	20.4	58.8	21.16	62.95
I-4	63	20	$1.7(10)^{-4}$	15.55	165.5	Al	.002	.00394	219.5	.18	670.1	1156	13.44	.0353	12.45	.00131	13.29	.0482								
V-1	52	20	$1.7(10)^{-4}$	64.	64.	Poly.	.35	.207	.025	$.1985(10)^{-5}$	5003.	1093	16.5	.62	---	---	12.49	.207	13.08	.330	15.87	.579	16.5	.62		
V-2	55	20	$1.7(10)^{-4}$	64.	64.	S.S.	.11	.626	8.0	$.416(10)^{-4}$	5360.7	777	14.8	19.3	---	---	12.6	3.65	12.86	4.96	14.3	17.5	14.6	18.6	14.8	19.3
V-3	56	20	$1.7(10)^{-4}$	64.	64.	Al	.0215	.0425	219.5	.01675	2000.1	1023	15.5	6.8	---	---	13.04	6.68	15.5	6.81						
V-4	57	20	$1.7(10)^{-4}$	64.	64.	Al	.2	.394	219.5	.0018	5360.	955	15.1	8.45	---	---	12.56	2.5	12.94	4.12	14.54	8.37	14.8	8.4	15.1	8.45
V-5	62	20	$1.7(10)^{-4}$	64.	64.	Al	.002	.00394	219.5	.18	100.	851	25.28	263.1	25.28	263.1										
V-6*	71	20	$1.7(10)^{-4}$	64.	64.	Al	.02	.0394	219.5	.018	2000.5	1551	18.47	64.3	12.42	.0113	12.97	4.80	18.47	64.3						
II-1	64	20	$(10)^{-4}$	15.55	165.5	Al	.02	.0394	219.5	.018	2501.7	814	15.65	32.7	12.41	.137	12.80	5.53	14.79	26.4						
II-2	65	20	$2.5(10)^{-4}$	15.55	165.5	Al	.02	.0394	219.5	.018	3500.1	1937	17.37	43.6	12.41	.137	12.56	.855	14.66	26.9						
III-1**	66	20	$1.7(10)^{-4}$	64.	64.	Al	.0215	.0425	219.5	.01675	3402.	1881	20.52	1.468	---	---	12.82	1.24	15.41	1.31						

*No liquid wall temperature suppressing.
**This run only has ullage fraction of .333, but all others have .667.

each digit, and the blank spaces between, represent equal ranges of temperature. To provide the maximum information it was necessary to change ranges between Figs. 3a and b. Thus, the digit 7 in Fig. 3a corresponds to the same range of temperatures as the digit 6 in Figs. 3b and c.

In the liquid regions of Figs. 3a and b one can note the motion of the heated liquid adjacent to the wall as it rises toward the interface, and then turns inward, and then downward. As a result "stratification" can exist not only in the axial direction but radially as well, owing to the very low level of axial body force used. In the vapor region one notes the formation of one and then two vortices. From Fig. 3c, it is possible to have quite large temperature differences in the vapor at a given axial level, depending on the radius.

These figures indicate that the liquid is superheated to some extent almost throughout the entire domain, and axial stratification is almost nonexistent for these conditions. The pressure rise rate, which is related to the temperature of the liquid-vapor interface, is thus much lower than if axial stratification were present, since the heat capacity of the liquid is being effectively utilized. It is felt that the lack of axial stratification in the present case is a consequence of the larger initial ullage fraction used. This was demonstrated in results presented in Ref. 3, which showed a large stratification for small ullage fractions, even with a lower level of a/g.

In Figs. 4a, b, and c the dimensionless stream functions corresponding to the isotherms of Figs. 3a-c are plotted. Lines of constant stream function correspond to streamlines and shows the flow patterns, and the succession of the three figures indicate the transient development of the flow patterns. The table at the bottom of the figures show the range of stream functions corresponding to each digit, and are the same in the three figures.

The real velocity components at each location can be calculated by Eqs. (82) and (91) for the liquid region, and by Eq. (82) and the dimensionless form of Eq. (54) for the vapor region. Increasing gradients in the stream function correspond to increasing velocities in the direction perpendicular to the gradients. It is thus noted in Figs. 4a-c that the velocities are increasing with time, and that the velocities in the liquid and vapor regions adjacent to the interface are in opposite directions. Regions of uniform stream functions completely enclosed indicate the existence of vortices, and are noted in all cases in both the liquid and vapor regions, while Fig. 4c shows a double vortex in the vapor region. Dimensional stream functions (units in ft^3/sec) are plotted in Figs. 5a-d for the same conditions but at slightly different times as those in Figs. 4a-c.

2. Influence of Change of Grid Size

In one case the grid size in the axial direction was changed between the liquid and vapor region, indicated in B-H 47 and B-H 53 in Table V. The sig-

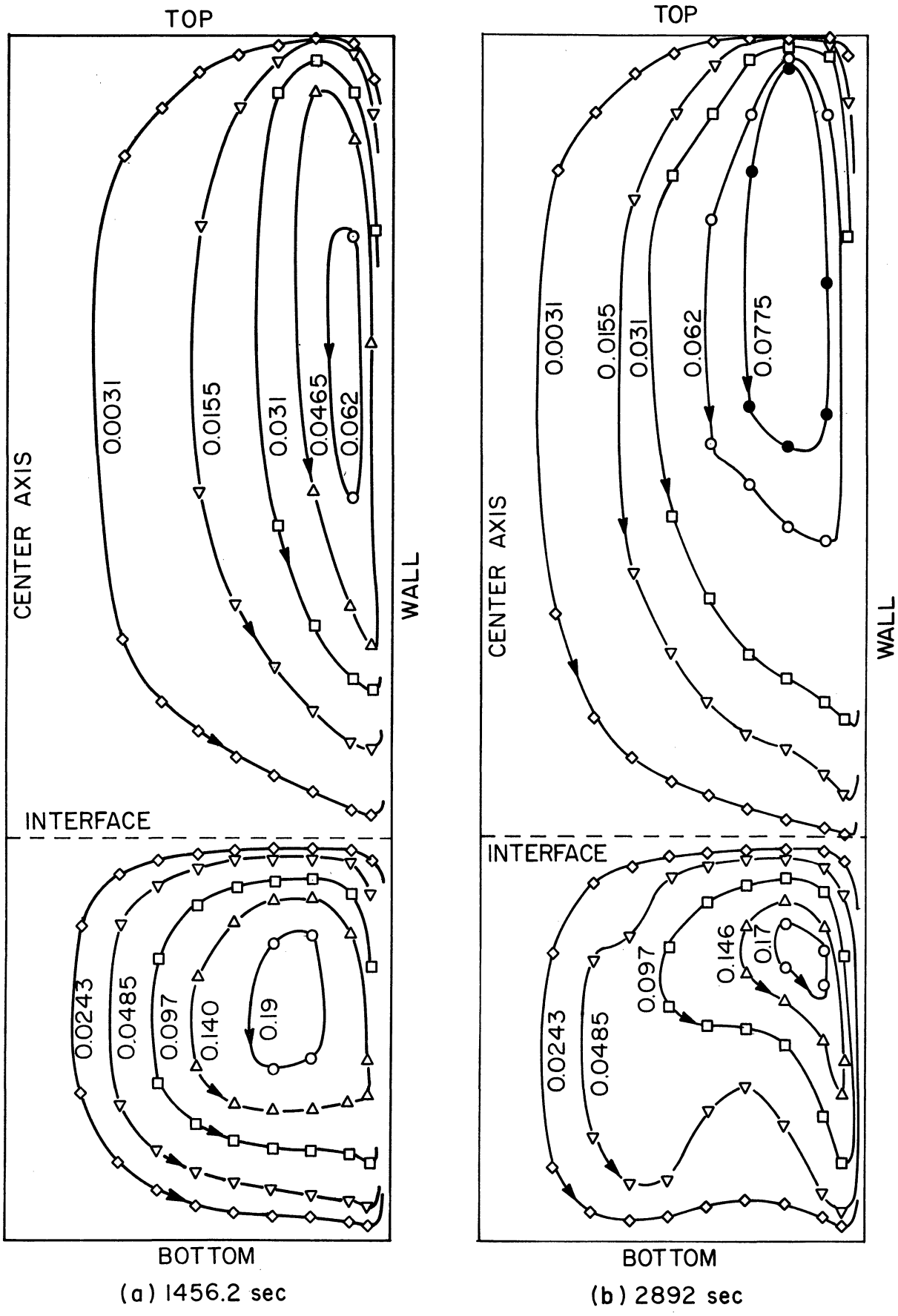

Fig. 5. Streamlines—Run B-H 47.

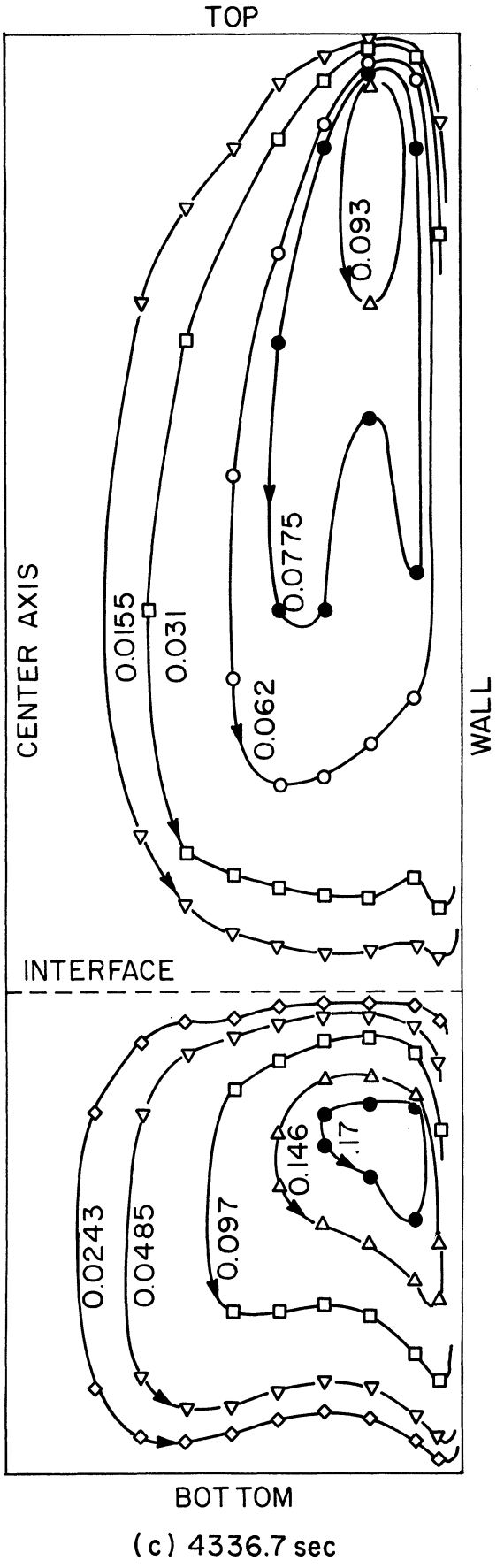

(c) 4336.7 sec

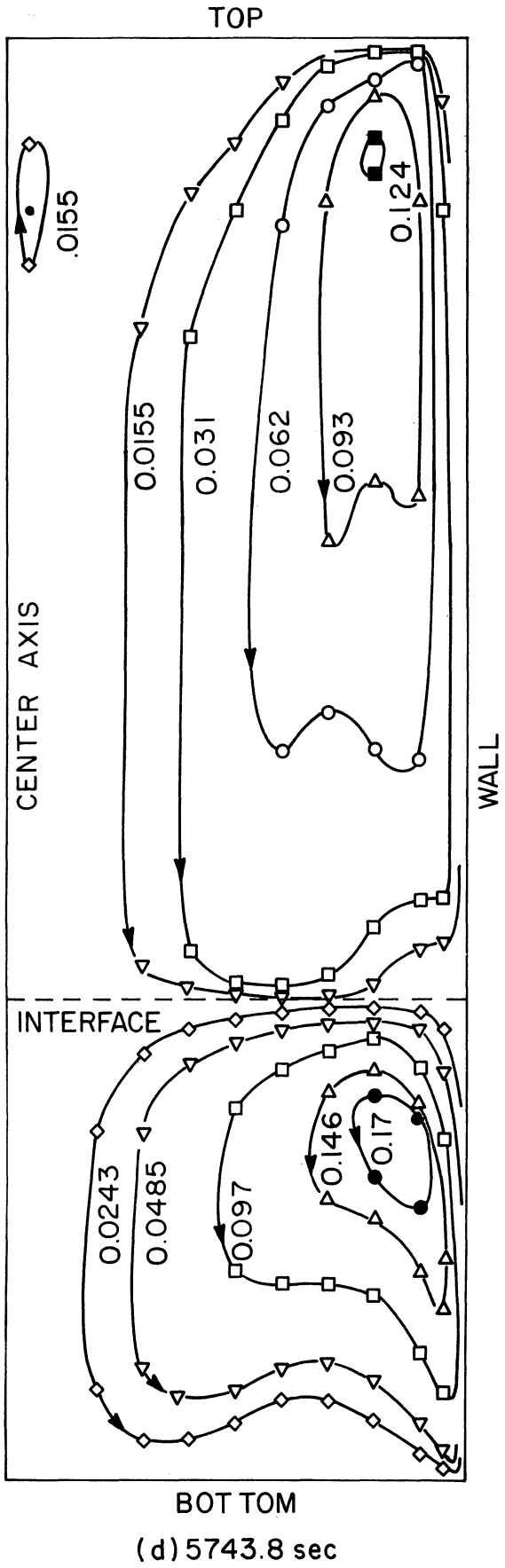

(d) 5743.8 sec

Fig. 5. (Concluded)

nificant differences are summarized in Table VI below. The tank height is 29.2 ft, and the liquid depth is 9.4 ft. The difference in pressure rise amounts to 5% of the computed pressure rise and may be neglected in light of other present uncertainties. One difference that can be significant is in the number of computational steps required, which is related to the computer operating time. Smaller nodal spacing results in smaller time steps because of computational stability requirements, and an increase in running time of almost 50% is noted above. This may be unwarranted in terms of justifiable benefits.

TABLE VI

EFFECT OF AXIAL GRID SIZE

B-H No.	No. of Nodes		Nodal Spacing, ft		System Pressure After 4600 sec, lbf/in.^{2}	Maximum Number of Time Steps
	Liquid	Vapor	Liquid	Vapor		
47	20	10	0.47	1.98	18.38	1644
53	10	20	0.94	0.99	18.70	1183

3. Influence of Heat Flux Distribution

The influence of the distribution of the heat flux on the pressure rise is shown in Fig. 6 for two materials, where the total heat capacities of the wall differ by a factor of 5. For a given material, the slopes of the pressure-time curve, giving the rate of pressure rise, become asymptotically the same, regardless of the heat flux distribution. This might be expected since for a given material the total heat capacities are the same, and the total energy input rate is also the same. Also, the slopes for the wall with higher heat capacity are somewhat less than for the aluminum. This is also what one might expect, unless one examines the relative heat capacities of the walls and the fluids. The heat capacity of the liquid in the tank is 40,800 Btu/°F, and that of the vapor is 1400 Btu/°F. The ratio of the wall to the total fluid heat capacity is tabulated in Table VII for the different cases. From Table VII, the highest wall heat capacity, with polyurethane, is only 1% of that of the fluid contents, and only 0.2% with the aluminum used (C_p = .02). This being the case, one would hardly expect a difference in behavior to be evident, for a given heat flux. Such is not the case, as is seen in Fig. 6, where a distinct difference in slope between the two materials is seen. The explanation lies in that not all of the heat capacity of the liquid is brought into effective use, because of the time lag associated with the dynamics of the fluid motion taking place from the walls to the interior.

Symbol	B-H No.	Btu/ft²-hr $(q/A)_L$	Btu/ft²-hr $(q/A)_v$	MTL	C_p Btu/lbm-°F	$\rho C_p \varepsilon$ Btu/°F-ft²
○	52	64.	64.	Poly.	.35	.200
●	47	165.5	15.55	Poly.	.35	.200
△	56	64.	64.	Al	.02	.040
▲	59	165.5	15.55	Al	.02	.040

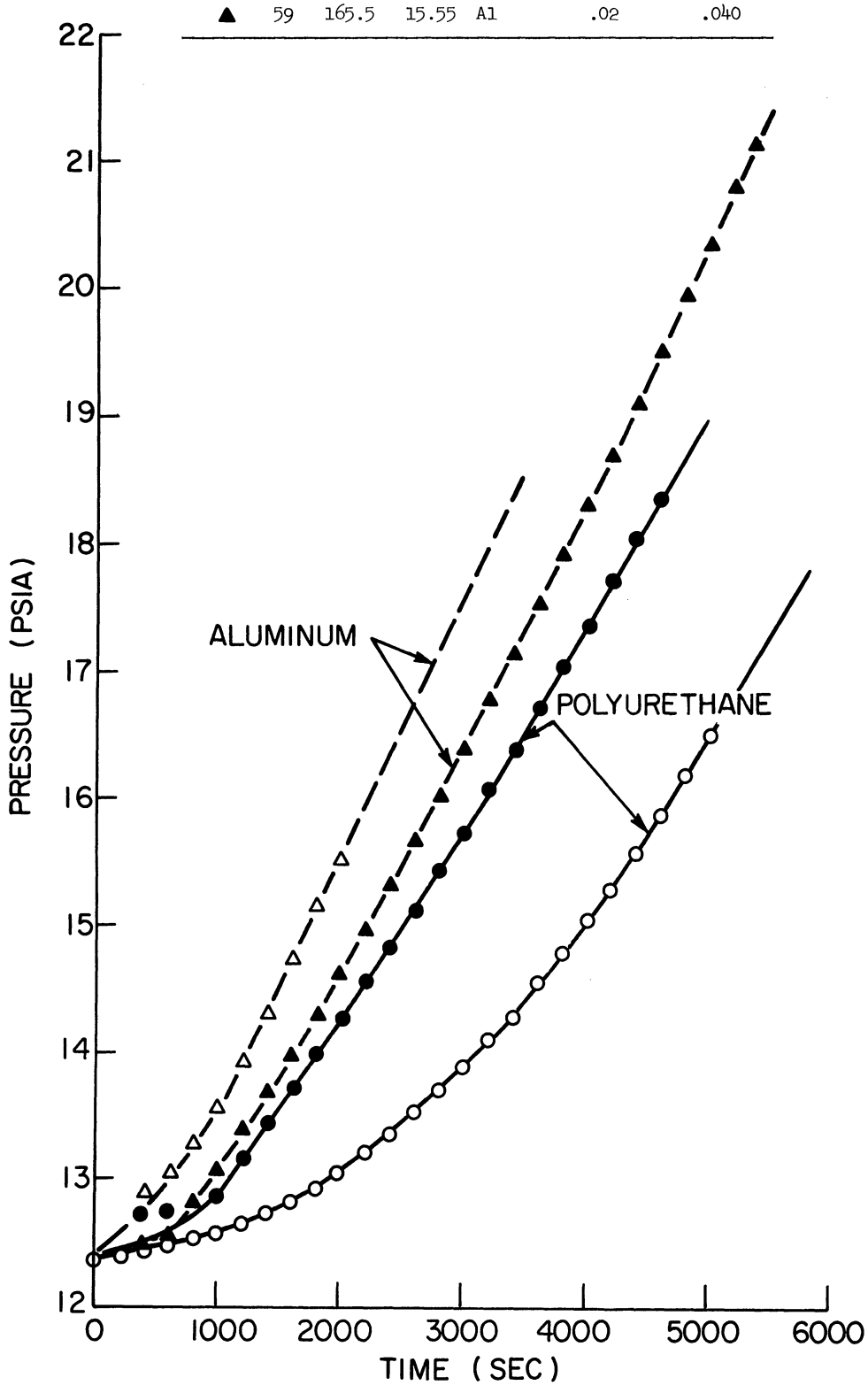

Fig. 6. Effect of heat flux distribution on pressure rise.

TABLE VII

COMPARISON OF HEAT CAPACITIES OF TANK AND CONTENTS—COMPUTER MODEL

Material	Polyurethane	Aluminum		
Specific heat, C_p, Btu/lbm-°F	.35	.2	.02	.002
Wall heat capacity, $\rho C_p \delta$, Btu/°F-ft^2	.200	.400	.040	.004
Total wall heat capacity, Btu/°F	400	800	80	8
Ratio—total wall to fluid heat capacity	0.95%	1.9%	0.19%	0.019%

With the polyurethane, the pressure rise rate is more rapid, initially, with the higher heat flux to the liquid. Since the total energy input rate is the same in both cases, it appears that heat transfer to the liquid has the primary influence on the pressure rise. This is reasonable on physical grounds. The system pressure is directly related to the liquid-vapor interface temperature, and the pressure rise rate is greatest when the transport rate of energy from the container walls to the interface is the greatest. In light of the existing axial body forces, this is the case with greater heat transfer to the liquid region. Examination of the computed temperature distributions shows that the liquid temperatures are greater for B-H 47 than for B-H 52 throughout.

With the aluminum walls of low heat capacity, the initial pressure rise rate is more rapid with the low heat flux to the liquid, opposite to that noted above, although the difference between the two heat fluxes is not so great. Detailed examination of the computer output results shows that this apparent reversal of the effect of the heat flux distribution is a consequence of the very low heat capacity of the aluminum wall coupled with the provision in the program to limit the superheat of the wall, as designated by the "incipient boiling point," ΔT_{wmax}. With the high heat flux to the liquid, the wall temperature rises very rapidly to this point. Any further rise above this level (which is imposed as constant above the instantaneous saturation temperature) is suppressed by evaporation of the appropriate amount of liquid from the vicinity of the wall directly into the ullage space. Because of the large ullage fraction this in itself has negligible effect on the pressure in the ullage space. Because of the continual transport of this excess energy to the ullage, by way of the latent heat, the energy available for heating the bulk liquid is less, even though the heat flux to the outside of the walls in the liquid region is greater. Hence the pressure rise is less. In a real situation, the vapor generated by boiling at the wall would pass to the ullage space by motion through the liquid, and in so doing would be transferring part of the latent heat energy to the liquid, and stir the liquid additionally. This would serve to increase the rate of pressure rise for a given heat flux. Insofar as the present model does not take into account the transfer of heat between the vapor bubbles and the bulk liquid, nor the stirring action near the wall induced by the bubbles, the model

must be considered incomplete.

4. Influence of Wall Material

For the same total energy input rate, the influence of the container wall on the pressure rise is indicated in Fig. 7. For convenience, the wall properties of specific heat and total heat capacity are included.

The stainless steel wall has the largest total wall heat capacity and the lowest pressure rise rate. One notes in Fig. 7 that for the same heat flux distribution, equal in the liquid and vapor regions, that the pressure rise rate increases directly as the total wall heat capacity decreases successively with Runs B-H 55, 57, 52, and 56. A zero wall heat capacity would correspond to the case where the imposed heat flux is applied directly to the fluid contents. In these four runs the wall thickness and material vary, hence the possible compound influence of axial conduction is present.

For the same material, wall thickness, and equal heat flux, one can observe the effect of the specific heat of the wall, C_p, alone in Runs B-H 56 and 57, with the same axial conduction in both cases. A very large increase in pressure rise rate occurs, and were the heat capacity decreased further, further increases in pressure rise would take place. This was done for one case with the heat flux being higher to the liquid than to the vapor, Runs B-H 59 and 63 in Fig. 7.

An operational difficulty arises as the wall heat capacity decreases, which in effect increases the net heat flux to the fluid. Owing to the larger temperature differences in the fluid the velocity increases, requiring smaller computational time steps because of the stability limitations imposed by Eqs. (131)-(134). The result is an increase in the ratio of computer time to real time. As an example, in Fig. 7, Run B-H 63 required approximately 20 min of computer time to cover 10 min of real time, while Run B-H 59 required 20 min of computer time for 100 min of real time.

5. Influence of Body Forces

The influence of changing the axial body force on the pressure rise is shown in the lower part of Fig. 8, for one set of conditions of high liquid heat flux with the aluminum walls. The effect of the different body forces is almost negligible for this case, and arises because of the predominant role that the process of bulk boiling plays in suppressing the wall temperature rise for the particular conditions selected. The vapor generation taking place at the liquid vapor interface is negligibly small compared to that associated with bulk boiling. Changing the body forces should have no direct effect on the vapor generation of bulk boiling, but should influence the phase change taking place at the liquid-vapor interface since body forces affect the natural convec-

Symbol	B-H No.	Btu/ft^2-hr $(q/A)_L$	Btu/ft^2-hr $(q/A)_v$	MTL	C_p Btu/lbm-°F	$\rho C_p \xi$ Btu/°F-ft^2
●	56	64.	64.	Al	.02	.04
○	57	64.	64.	Al	.2	.4
□	52	64.	64.	Poly.	.35	.2
△	55	64.	64.	S.S.	.11	.63
+	59	165.5	15.55	Al	.02	.04
×	63	165.5	15.55	Al	.002	.004

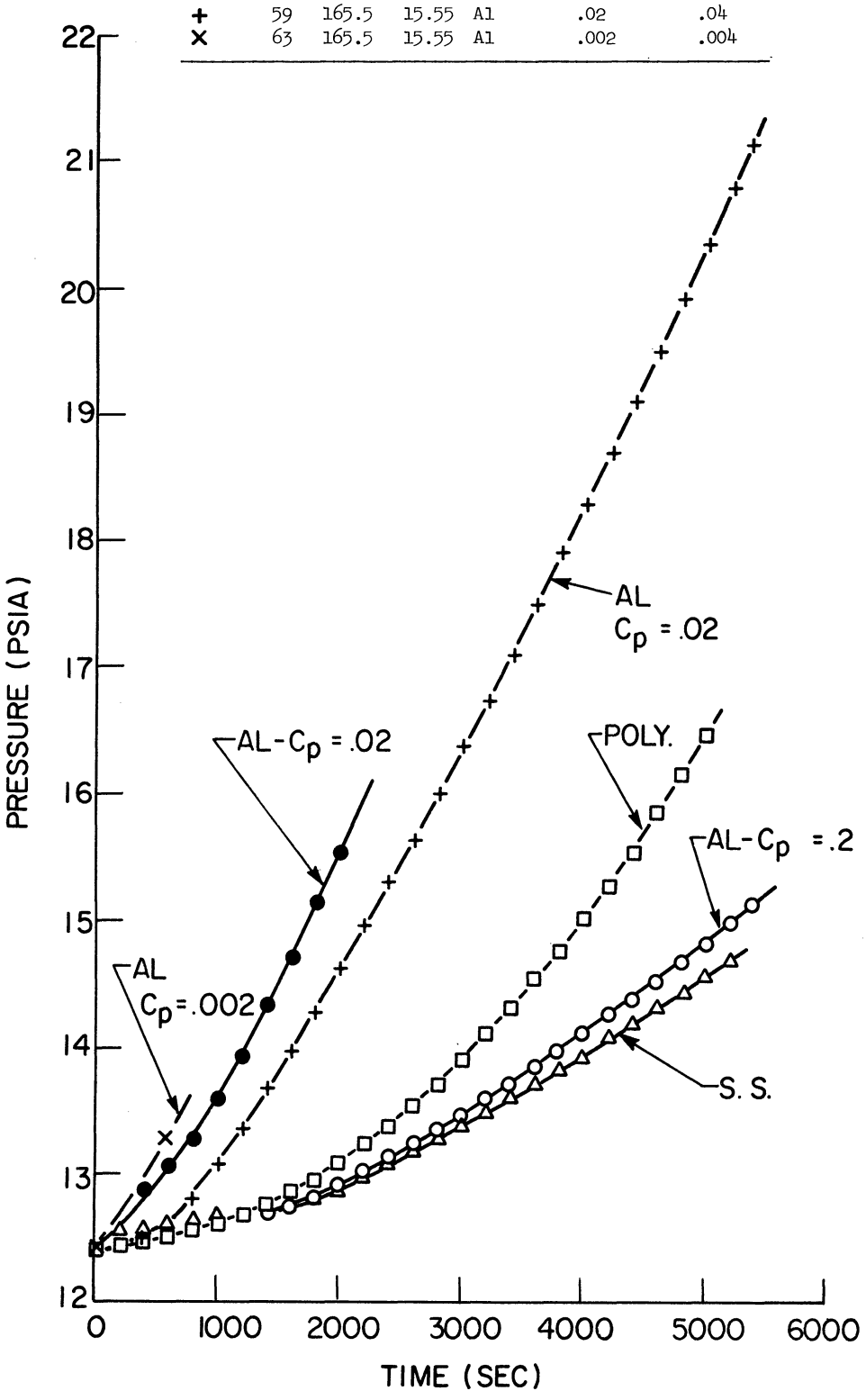

Fig. 7. Effect of wall material on pressure rise.

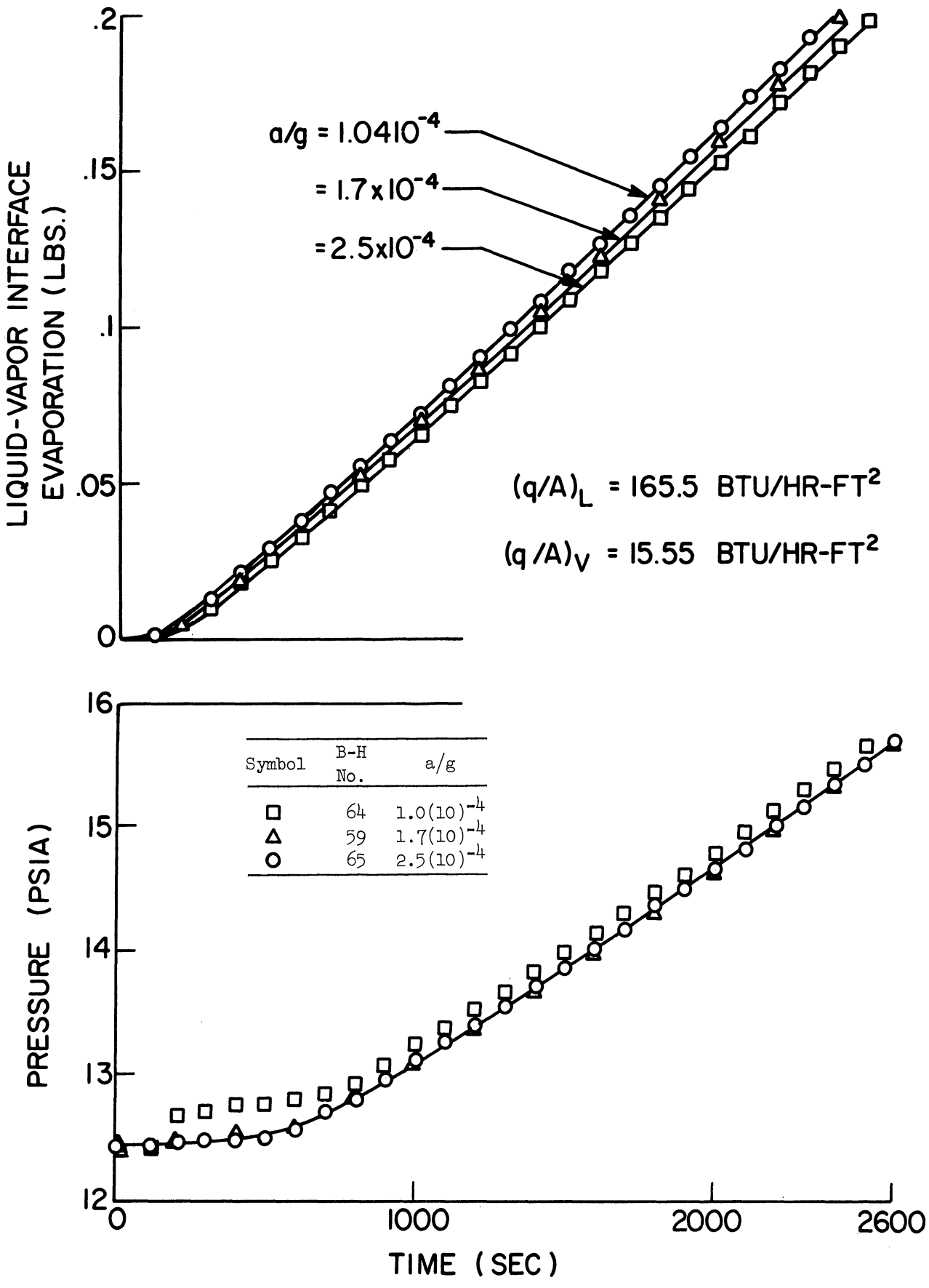

Fig. 8. Effect of body force on pressure rise.

tive process by which heated liquid is brought to the vicinity of the interface. That this is indeed the case is noted from the upper part of Fig. 8, which shows that increasing the body force increases the rate of evaporation of the liquid. Were the proper combination of parameters selected such that bulk boiling did not occur, it could then be expected that a more pronounced effect of a/g on the pressure rise would be present.

6. Influence of Ullage Fraction

Figure 9 indicates that changing the ullage fraction from a value of 2/3 to 1/3 has negligible influence on the pressure rise. The flux to the liquid and vapor regions are made equal in order that the total energy input rate be the same for both cases. Even though the pressure is changed negligibly, a significant difference in the mass evaporated exists, with a larger mass evaporated associated with the larger ullage fraction. The trends observed are similar to that obtained with liquid oxygen (Ref. 3). Were the heat flux to the liquid to be different from that to the vapor, then differences in pressure rise rate would occur with different values of ullage fraction, since the total energy input rates would also differ. Also, differences in behavior can be expected if the ullage fractions are very large or very small, for the same heat flux. The physical explanation as to why the pressures do not change for the present case in Fig. 9 lie in counteracting effects. As the ullage fraction decreases, less vapor is needed for a given pressure rise, hence less energy is stored as latent heat. However, the increased heat capacity associated with increased amounts of liquid compensates approximately for this.

E. DISCUSSION

The pressure and total mass evaporated from computer Run B-H 47 are repeated in Fig. 10 as a function of time. The program listing in Appendix B incorporates the ability to sotre and/or punch intermediate results for reinsertion at a later time to continue the computations. In the case where the results are punched, only distributions of the stream functions and temperature are retained, along with the system pressure (i.e., the U and V velocity components are discarded). To observe the influence of not using the velocities at the start of each section, computer Run B-H 47 was repeated by starting and stopping the computational process a number of times, as indicated at the bottom of Fig. 10. The general overall trend is affected only in a minor way if one neglects the "starting transients," and the comparison with the continuous run is quite good.

Included in Fig. 10 is the final measured pressure in the LH_2 tank on the AS-203 flight, as taken from Ref. 17, and is considerably higher than the results predicted by the particular computer model included. A number of factors which contribute to this difference have already been discussed, and the more significant of these will be reviewed here.

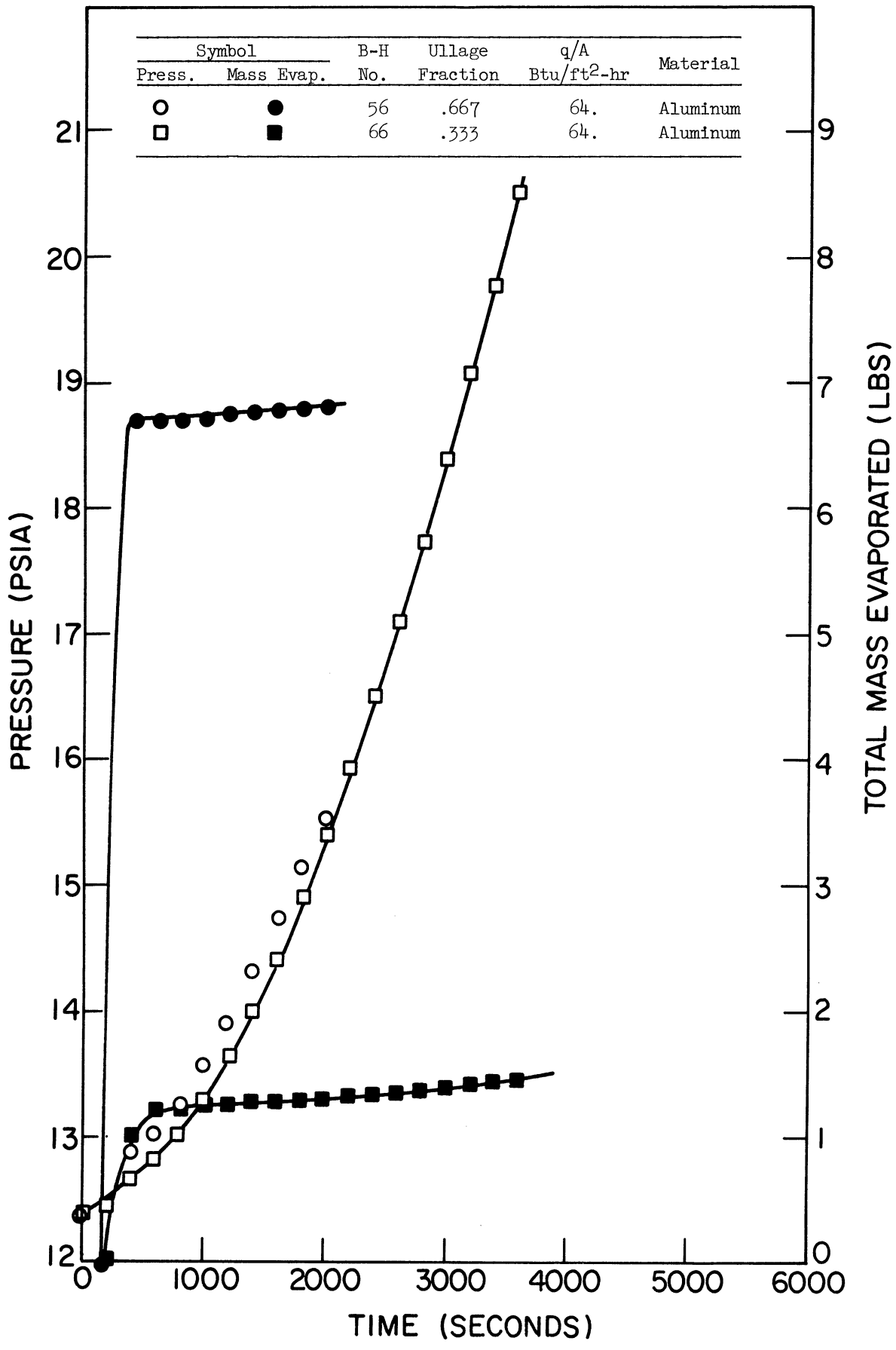

Fig. 9. Effect of ullage fraction on pressure rise.

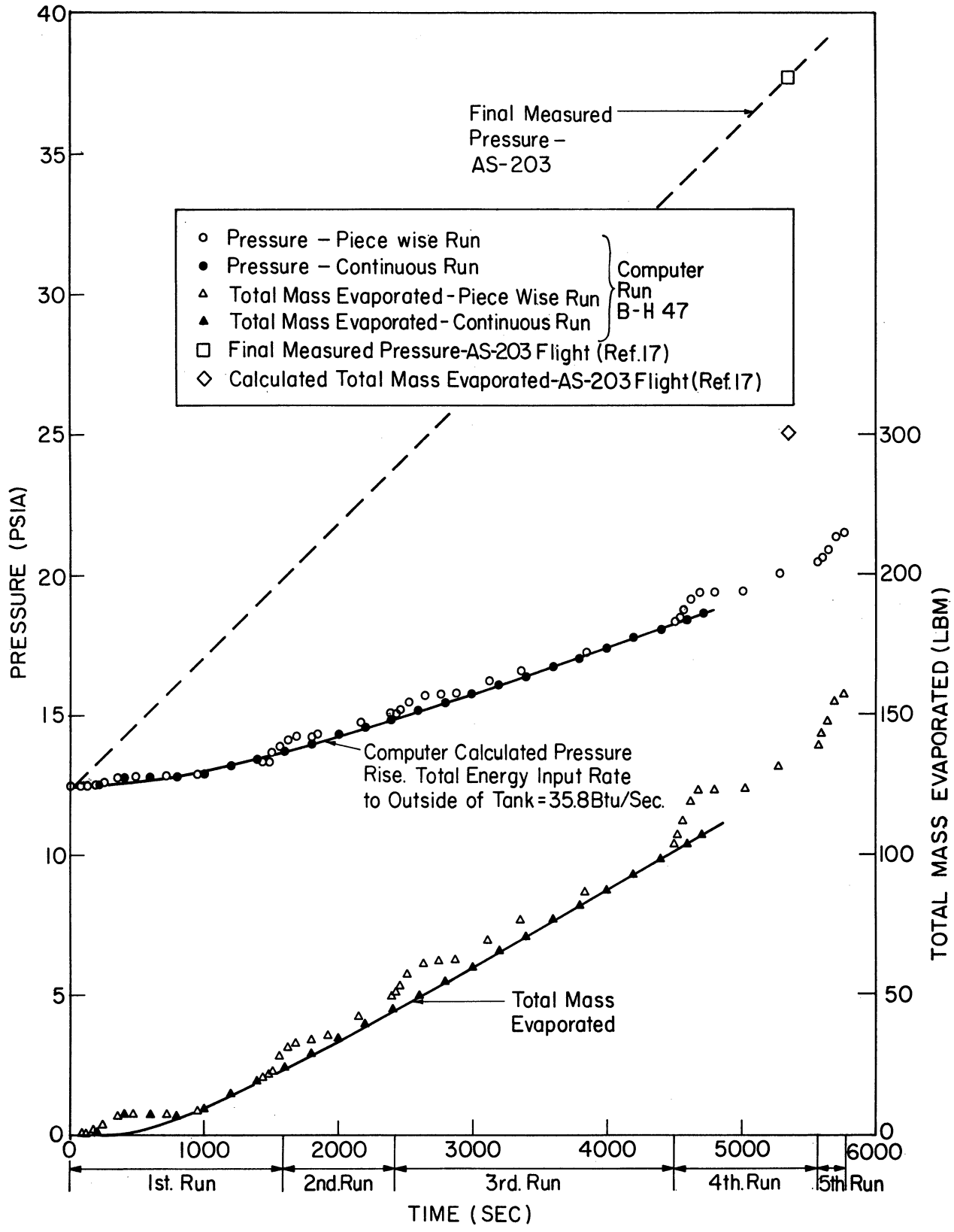

Fig. 10. Composite computed pressure rise.

The geometrical difference between the actual system and the model is obvious. Although the total volumes and total energy input rates were maintained the same, the wall heat flux could not be modeled simultaneously because of the geometrical differences in wetted and nonwetted heat transfer surface areas. These differences are shown in Table VIII. Cases A and E correspond to the heat fluxes for the actual and computer models listed in Table IV, each case having the same respective energy input rates to the liquid and vapor regions. For case F, the heat flux is considered uniform over the entire actual tank surface area. The heat flux for this case is almost one-half that of the smallest used for the computer model. In all cases the total energy input rate is 35.8 Btu/sec. If the heat flux for the computer model were maintained the same as that based on the actual geometry, then the total energy input rates would differ between the two cases.

TABLE VIII

COMPARISONS BETWEEN ACTUAL AND COMPUTER MODEL HEAT FLUXES

Case	Computer Model, Btu/hr-ft^2		Based on Actual Geometry, Btu/hr-ft^2	
	$(q/A)_L$	$(q/A)_v$	$(q/A)_L$ Wetted	$(q/A)_v$ Unwetted
A	165.5	15.6	74	10.9
E	64	64	28.7	44.7
F			37.8	37.8

The greater heat flux to the wall in the liquid region, in the computer model, results in a large rate of increase in wall temperature. The combination of conduction and convection in the liquid is not sufficient to transport the energy away from the wall, and the incipient boiling point is quickly reached. In the results presented thus far, the incipient boiling point was included as an input parameter. Since in the physical process of nucleate boiling changes in the wall temperatures are relatively small, this was simulated by suppressing the wall temperature with an appropriate release of vapor to the ullage space, computed with Eq. (135). The generation of this vapor in effect reduces the rate of temperature rise of the bulk liquid that might otherwise take place, and with a large ullage fraction the pressure rise rate would also be smaller.

For one case only, a computer run was made in which the suppression of the liquid wall temperatures did not take place (i.e., no nucleate boiling was permitted). The resulting system pressure behavior is plotted in Fig. 11 as B-H 71. Included for reference purposes, as a basis for comparison is the otherwise identical case B-H 56. Computations were carried out for only 2000 sec, which corresponds to 20 min of computer time. However, if the pressure behavior in Run B-H 71 were extrapolated linearly to 5500 sec, the predicted

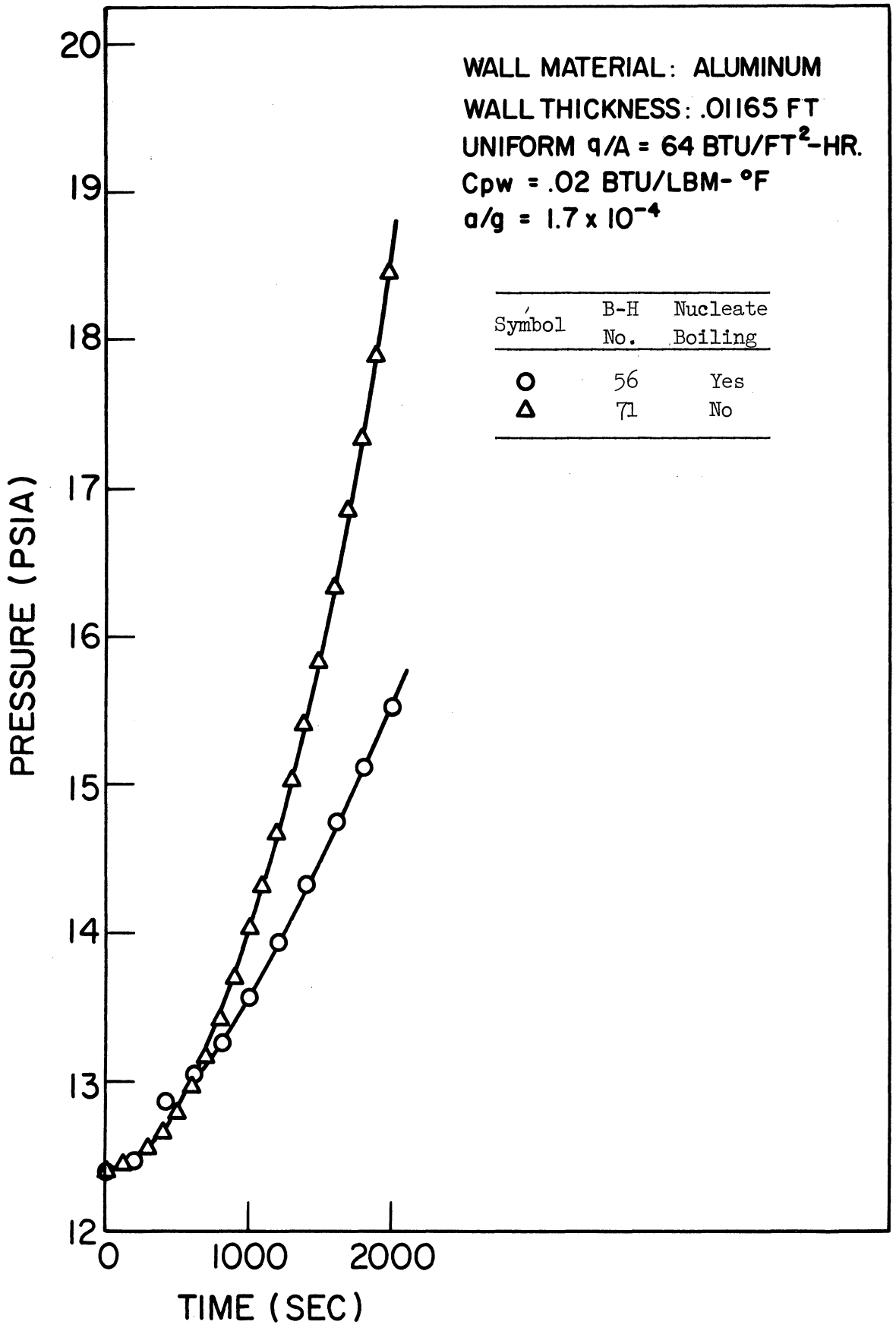

Fig. 11. Effect of nucleate boiling on pressure rise.

pressure would be 38.6 lbf/in.^{2}, as compared with 37.7 lbf/in.^{2} in the actual case (Fig. 10).

Although the pressure comparison is quite good, the computed bulk liquid temperatures become unrealistically high. For Run B-H 56, with nucleate boiling, at the end of 2000 sec the saturation temperature was 38.2°R with a mean bulk temperature of 38.8°R, whereas for Run B-H 71 the saturation temperature was 39.4°R with a mean bulk temperature of 387.9°R. This is a result of the high heat flux to the liquid, case E in Table VIII, and in effect states that, in a real system patterned after this computer model, nucleate boiling would most certainly occur at the wall. In Section VII-A of Ref. 17, statements are made that nucleate boiling indeed occurred on the AS-203 flight, with the vapor apparently recondensing in the bulk liquid.

The computer model used here considers that the vapor generated by nucleate boiling at the wall passes directly to the ullage space. Vapor bubbles traveling from the vicinity of the wall to the ullage space would in fact introduce two effects, both of which must be included in the computer model in order to have a more complete description. The motion of the bubbles would tend to increase the velocity of the liquid, and also would tend to heat the liquid as it travels toward the liquid-vapor interface, if collapse takes place. The effect of each of these would be to increase further the rate of pressure rise.

In the course of the transient processes occurring in the closed container, both with and without simulated nucleate boiling, it was observed that simultaneous evaporation and condensation occurs at the liquid-vapor interface during certain early intervals. This is demonstrated in Fig. 12, which includes the same two cases presented in Fig. 11. The ordinate is the local relative mass flux, either evaporation or condensation, at the liquid-vapor interface as a function of radius and time. The logarithmic ordinate scale increases in both the evaporation and condensation directions.

With nucleate boiling, Run B-H 56, condensation near the centerline persists for a considerable period. Since the boiling adds a great deal of vapor to the ullage and the bulk liquid temperature rise is relatively slow, the compression of the ullage vapor tends to increase the condensation and reduces the tendency for boiling as the system pressure increases, which is related to the temperature at the liquid-vapor interface. The evaporation rate near the side wall of the tank quickly reaches a steady value, which indicates that the temperature gradients in the liquid and vapor in that region remain constant.

With no nucleate boiling permitted, Run B-H 71, condensation also occurs near the centerline, but for a short period only. The evaporation rate becomes quite large, due to the establishment of large temperature gradients in the liquid, which is possible when no restriction on the level of wall temperature is present.

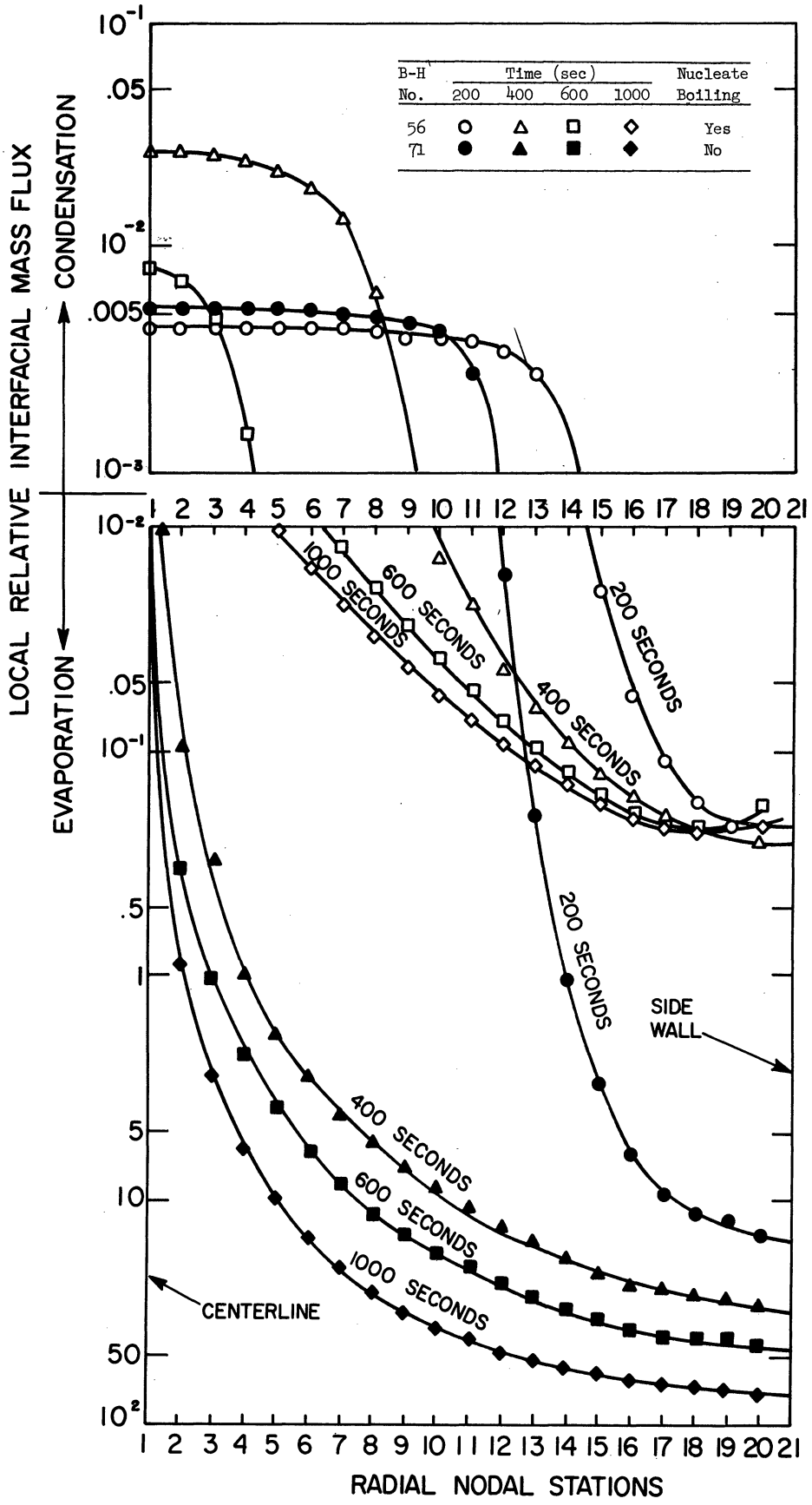

Fig. 12. Effect of nucleate boiling on local liquid-vapor interface mass transfer.

An additional improvement in the computer model could be made by the use of nonlumped walls, as discussed earlier in Sections C.1 and C.2. In the actual case, aluminum is on the outer side with an insulating material on the inner side. This tends to make the temperature on the outer side more uniform because of axial conduction. The boundary condition of an imposed heat flux can result in somewhat artificial results if the axial conduction is not included, and is particularly important in the vicinity of the liquid-vapor interface where the axial gradients in the wall can become large.

One additional observation on the numerical procedure should be made. On beginning the computational process, the changes take place from the region where the disturbance takes place, and progress one node per computational time step. This means that one must not attribute undue significance to the results until sufficient computational steps have taken place to influence all of the nodes. This is particularly important when one is attempting to model a physical system which itself is not stagnant at the outset by a system initially at a uniformly stationary condition.

APPENDIX A

COMPUTER PROGRAM FLOW CHART

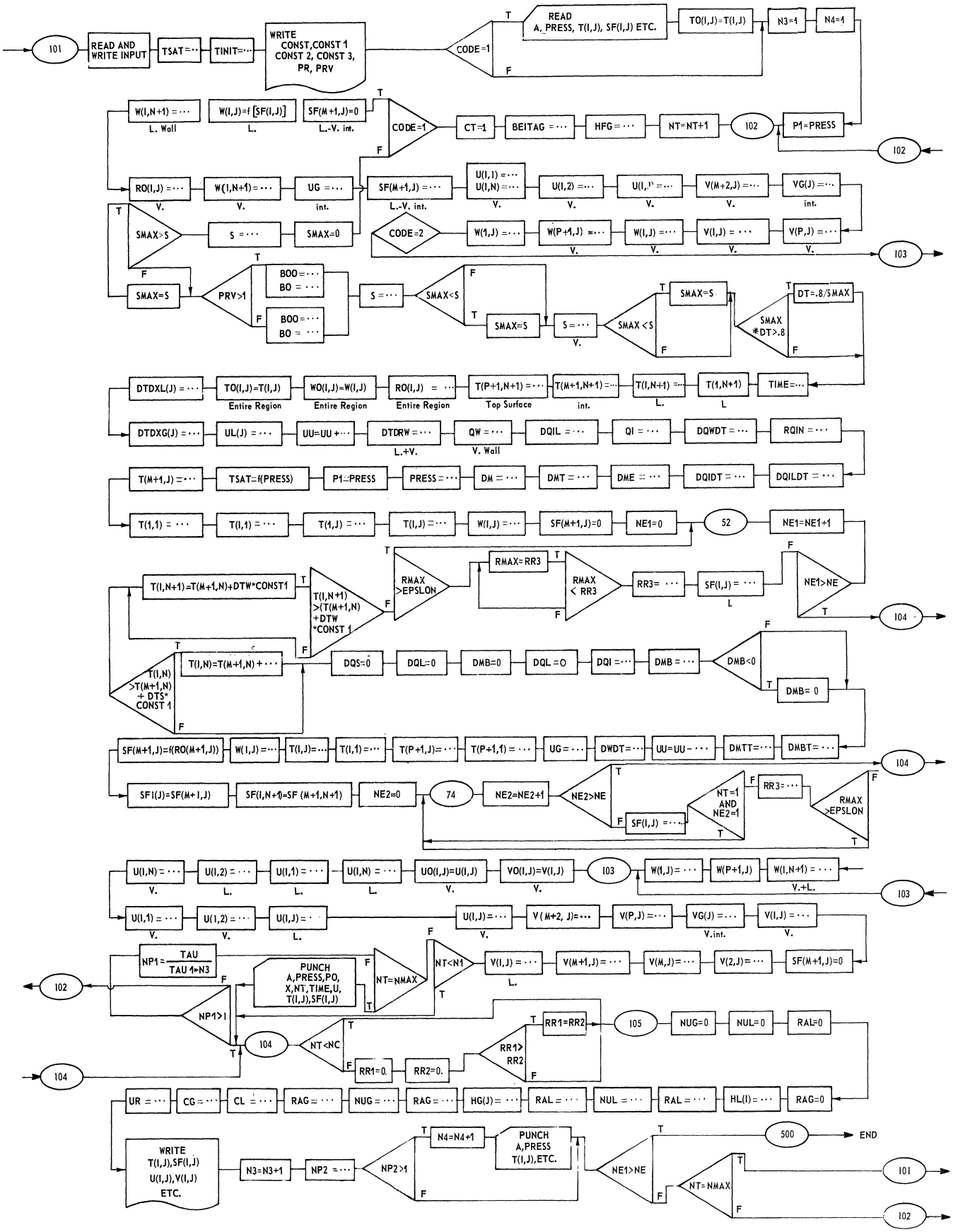
101
READ AND WRITE INPUT
TSAT=···
TINIT=···
WRITE CONST,CONST 1 CONST 2, CONST 3, PR, PRV
CODE=1
READ A, PRESS, T(I,J), SF(I,J) ETC.
TO(I,J)=T(I,J)
N3=1
N4=1
W(I,N+1)=···
L. Wall
W(I,J)=f[SF(I,J)]
L.
SF(M+1,J)=0
L.-V. int.
CODE=1
CT=1
BEITAG=···
HFG=···
NT=NT+1
102
P1=PRESS
RO(I,J)=···
V.
W(I,N+1)=···
V.
UG=···
int.
SF(M+1,J)=···
L.-V. int.
U(I,1)=···
U(I,N)=···
V.
U(I,2)=···
V.
U(I,N-1)=···
V.
V(M+2,J)=···
V.
VG(J)=···
int.
SMAX>S
S=···
SMAX=0
CODE=2
W(1,J)=···
W(P+1,J)=···
V.
W(I,J)=···
V.
V(I,J)=···
V.
V(P,J)=···
V.
103
SMAX=S
PRV>1
BOO=···
BO=···
BOO=···
BO=···
S=···
SMAX<S
SMAX=S
S=···
V.
SMAX<S
SMAX=S
SMAX *DT>.8
DT=.8/SMAX
DTDXL(J)=···
TO(I,J)=T(I,J)
Entire Region
WO(I,J)=W(I,J)
Entire Region
RO(I,J)=···
Entire Region
T(P+1,N+1)=···
Top Surface
T(M+1,N+1)=···
int.
T(1,N+1)=···
L.
T(1,N+1)
L
TIME=···
DTDXG(J)=···
UL(J)=···
UU=UU+···
DTDRW=···
L.+V.
QW=···
V. Wall
DQIL=···
QI=···
DQWDT=···
RQIN=···
T(M+1,J)=···
TSAT=f(PRESS)
P1=PRESS
PRESS=···
DM=···
DMT=···
DME=···
DQIDT=···
DQILDT=···
T(1,1)=···
T(I,1)=···
T(1,J)=···
T(I,J)=···
W(I,J)=···
SF(M+1,J)=0
NE1=0
52
NE1=NE1+1
T(I,N+1)=T(M+1,N)+DTW*CONST1
T(I,N+1)>(T(M+1,N)+DTW*CONST 1
RMAX>EPSLON
RMAX=RR3
RMAX<RR3
RR3=···
SF(I,J)=···
L
NE1>NE
104
T(I,N)>T(M+1,N)+DTS*CONST 1
T(I,N)=T(M+1,N)+···
DQS=0
DQL=0
DMB=0
DQL=0
DQI=···
DMB=···
DMB<0
DMB=0
SF(M+1,J)=f(RO(M+1,J))
W(I,J)=···
T(I,J)=···
T(I,1)=···
T(P+1,J)=···
T(P+1,1)=···
UG=···
DWDT=···
UU=UU-···
DMTT=···
DMBT=···
104
SF1(J)=SF(M+1,J)
SF(I,N+1)=SF(M+1,N+1)
NE2=0
74
NE2=NE2+1
NE2>NE
SF(I,J)=···
NT=1 AND NE2=1
RR3=···
RMAX>EPSLON
U(I,N)=···
V.
U(I,2)=···
L.
U(I,1)=···
L.
U(I,N)=···
L.
UO(I,J)=U(I,J)
V.
VO(I,J)=V(I,J)
V.
103
W(1,J)=···
W(P+1,J)
W(I,N+1)=···
V.+L.
103
U(I,1)=···
V.
U(1,2)=···
V.
U(I,J)=···
L.
U(I,J)=···
V.
V(M+2,J)=···
V(P,J)=···
VG(J)=···
V.int.
V(I,J)=···
V.
NP1=TAU/(TAU 1*N3)
PUNCH A,PRESS,PO, X,NT,TIME,U, T(I,J),SF(I,J)
NT=NMAX
NT<N1
V(I,J)=···
L.
V(M+1,J)=···
V(M,J)=···
V(2,J)=···
SF(M+1,J)=0
102
NP1>1
104
NT<NC
RR1=0.
RR2=0.
RR1>RR2
RR1=RR2
105
NUG=0
NUL=0
RAL=0
104
UR=···
CG=···
CL=···
RAG=···
NUG=···
RAG=···
HG(J)=···
RAL=···
NUL=···
RAL=···
HL(I)=···
RAG=0
WRITE T(I,J),SF(I,J) U(I,J),V(I,J) ETC.
N3=N3+1
NP2=···
NP2>1
N4=N4+1
PUNCH A,PRESS T(I,J),ETC.
NE1>NE
NT=NMAX
500
END
101
102

APPENDIX B

LH_2 COMPUTER PROGRAM LISTING

```
                C     PROGRAM FOR CYLINDRICAL CONTAINER FOR IDEAL GAS-HYDROGEN
0001                  DIMENSION U(31,21),V(31,21),T(31,21),SF(31,21),W(31,21),TO(31,21),
                     1WO(31,21),SFI(31),EJ(31),F(31),DI(31),DR1(31),DR2(31),DR3(31),
                     2DR4(31),R1(31),R2(31),R3(31),R4(31),R5(31),A1(31),A2(31),A3(31),
                     3C2(31),C1(31,21),C3(31,21),EJ1(31),D1(31),D2(31),R6(31),DR6(31),
                     4UL(31),DR5(31),        DR7(31),DR8(31),        A4(31),VG(31),
                     5RO(31,21),DTDRW(31),DTDXG(31),UO(31,21),VO(31,21),DTDXL(31),HL(31)
                     6,HG(31),C4(31,21),RT(31,21),ZTT(12),FHHFG(12),TT(12),HHFG(12)
0002                  INTEGER CODE,H,P,TAU1,TAU2
0003                  REAL KG,KL,M1,M2,M3,M4,M5,M6,M7,NP1,NEW,NEWV,NUG,NUL,M11,M23,NP2
0004            204   FORMAT(3F12.4,F12.8,I4,F12.8,E16.8/2E13.6/(5E16.8))
0005                  NAMELIST/DATA1/A,AOVERB,P,M,N,X,CODE,DT,NMAX,PO,G,QSURFG,QSURFL,
                     1DTW,DTS,       ALPHA,NEW,KL,BEITA,ROL,CP,ALPHAV,NEWV,KG,CPV,CV,
                     2RGAS,ALPHAW,CPW,ROW,DELTA,TAU1,N1,NE,EPSLON,NC,NR,B1,B2,B3,B4,Z,
                     3ZTT,FHHFG,NDIM,TAU2
                     4/DATA2/CONST,CONST2,CONST1,CONST3,PR,PRV
0006            101   READ(5,DATA1,END=500)
0007                  WRITE(6,DATA1)
0008                       K1=M+1
0009                       K2=N+1
0010                       K3=P+1
0011                  K4=M+2
0012                  K5=N-1
0013                  K6=M+3
0014                  K7=P-1
0015                  K8=M-1
0016                  DATA A1,A2,A3,A4,C2,D1,D2,DI,DR1,DR2,DR3,DR4,DR5,DR6,DR7,DR8,
                     1DTDRW,DTDXG,DTDXL,EJ,EJ1,F,HG,HL,R1,R2,R3,R4,R5,R6,SFI,UL,VG/
                     21023*0.0/,C1,C3,C4,RO,SF,T,TO,U,UO,V,VO,W,WO,RT/9114*0.0/,
                     3BO,F1,F2,F3,E1,TIME,RR1,E2,E3, UU,TAU,P1,DMT,DMBT,DM,A6,M6,NP1,
                     4DMB,DMTT/20*0.0/,NT,NE1,NE2,N2/4*0/
0017                       I1=M/2.+1
0018                       Y=AOVERB
0019                  B=A/AOVERB
0020                       PR=NEW/ALPHA
0021                       PRV=NEWV/ALPHAV
0022                        RNEW=NEWV/NEW
0023                       RALPHA=ALPHAV/ALPHA
0024                       DR=1.0/N
0025                       ER2=DR*DR
0026                       GAM=CPV/CV
0027                       DYY=2.0*ER2
0028                       ER6=ER2/2.0
0029                       PRESS=PO
0030                      BB=(B3*B4-ALOG10(PRESS)+B1)
0031                       C=(B2-B3*ALOG10(PRESS)+B1*B3)
0032                       D=BB*BB -4.*B4*C
0033                        TSAT=(-BB+SQRT(D))/(2.*B4)
0034                  TINIT=TSAT
0035                       CONST = A*A/ALPHA
0036                       CONST1=Y*PR*G*BEITA*(A** 3)/NEW/NEW
0037                       CONST2=1.0/CONST
0038                       CONST3=1.0/CONST1
0039                  WRITE(6,DATA2)
0040                       M1=AOVERB*QSURFL*(A** 5)*BEITA*G/ALPHA/ALPHA/NEW/ROW/CPW
```

```
                1      /DELTA
0041                   M2=KL*A/ALPHA/ROW/CPW/DELTA
0042                   M3=KG*A/ALPHA/ROW/CPW/DELTA
0043                   M7=ACVERB*QSURFG*(A** 5)*BEITA*G/ALPHA/ALPHA/NEW/ROW/CPW
                1      /DELTA
0044                   M5=CONST1*TINIT
0045                   D2R=DR/2.0
0046                   AOVRB2=AOVERB*AOVERB
0047                DO 11 J=2,K2
0048                   A1(J)=ER2*ER2*(J-1.)*(J-1.)
0049                   C2(J)=1.+1./(2.*(J-1.))
0050                   A4(J)=1.0/(J-1.0)/DR/4.0
0051          11       R1(J)=12*(J-1.0)*ER2
0052                IF(CODE.NE.1) GO TO 14
0053                READ (5, 204)A,PRESS,PO,X,NT,TIME,UU,DMBT,DMTT,((T(I,J),J=1,K2),
               1I=1,K3),((SF(I,J),J=1,K2),I=1,K3)
0054                DO 13 I=1,K3
0055                DO 13 J=1,K2
0056          13       TO(I,J)=T(I,J)
0057          14    N3=1
0058                N4=1
0059                   P1=PRESS
0060         102        NT=NT+1
0061                TSATK=TSAT/1.8
0062                CALL ATSM(TSATK,ZTT,FHHFG,12,1,TT,HHFG,NDIM)
0063                CALL ALI(TSATK,TT,HHFG,HFGJ,NDIM,0.1,IER)
0064                   HFG=0.215*HFGJ
0065                   RP=PRESS/PO
0066                I=(P+M)/2.+1
0067                J=N/2.+1
0068                   BEITAG = 1./(TINIT+T(I,J)/CONST1)
0069                   M4=(GAM-1)/GAM
0070                   CT=1.
0071                   DX=X/M
0072                   DX2=DX*DX
0073                   DZ=(1.0-X)/(P-M)
0074                DZX=DZ/DX
0075                DZX1=DZX+1.
0076                DZX2=.5*DX*DZ*DZX1
0077                DZXH=2./(DZ+DX)
0078                   DZ2=DZ*DZ
0079                   DRZ=ER2/DZ2
0080                   F3=DRZ*Y*Y
0081                   BJ1=2.*(1+F3)
0082                   DXR=DX2/ER2
0083                   DRX=ER2/DX2
0084                   F1=DRX*Y*Y
0085                   F2=DXR/Y/Y
0086                D2Z=DZ/2.
0087                   ZOVR2=Z/2.0
0088                    BJ=2.*(1.+F1)
0089                BO=2.*PR*Y*Y/DX2+2.*PR/ER2
0090                   EJ(1)=0.
0091                   EJ1(1)=0.
0092                DO 15 J=2,K2
```

```
0093                    A2(J)=DX2*ER2*(J-1.)*(J-1.)/Y/Y
0094                     A3(J)=DX2/Y/Y/(J-1.)/ER2/2.
0095                     D1(J)=BJ-C2(J)*EJ(J-1)
0096                    R2(J)=12*(J-1.)*DR*DX
0097                    D2(J)=BJ1-C2(J)*EJ1(J-1)
0098                    EJ1(J)=(1-1/(2.0*(J-1.0)))/D2(J)
0099                    R4(J)=Y*Y/(J-1.)/(J-1.)/ER2/DX2/2.
0100                    R5(J)=Y*Y/(J-1.)/(J-1.)/ER2/DZ2/2.
0101                    R6(J)=12*(J-1.)*DR*DZ
0102          15        EJ(J)=(1-1/(2.0*(J-1.0)))/D1(J)
0103              IF(CODE.NE.1) GO TO 107
0104              DO 16 J=2,N
0105          16        SF(M+I,J)=0.
0106              DO 17 I=2,M
0107              DO 17 J=2,N
0108          17        W(I,J)=((SF(I+1,J)-2 *SF(I,J)+SF(I-1,J))*Y*Y/DX2-(SF(I,J+1)-
                     1      SF(I,J-1))/ER2/(J-1.0)/2+(SF(I,J+1)-2.0*SF(I,J)+SF(I,J-1))/
                     2      ER2)/ER2/(J-1.0)/(J-1.0)
0109              DO 18 I=2,M
0110          18        W(I,N+1)= (8.*SF(I,N)-SF(I,N-1)-7.*SF(I,N+1))/DYY
0111              DO 19 I=K1,K3
0112              DO 19 J=1,K2
0113          19        RO(I,J)=CONST1*PRESS*144./RGAS/(T(I,J)+M5)
0114              DO 20 I=K4,P
0115          20        W(I,N+1)=(8*SF(I,N)-SF(I,N-1)-7*SF(I,N+1))/DYY/RO(I,N+1)
0116                    UG=-UU*(ROL/RO(M+1,1)-1.0)
0117              DO 21 J=2,K2
0118          21        SF(M+1,J)=RO(M+1,J)*UG*ER2*(J-1.0)*(J-1.0)/2.0
0119              DO 22 I=K1,P
0120                    U(I,N)=2.*(3*SF(I,N)-6*SF(I,N-1)+SF(I,N-2))/R1(N)/RO(I,N)
0121                    U(I,1)=SF(I,2)/ER6/RO(I,1)
0122          22        U(I,2)=2.*(6.*SF(I,3)-SF(I,4)-3.*SF(I,2))/R1(2)/RO(I,2)
0123              DO 23 I=K1,P
0124              DO 23 J=3,K5
0125          23        U(I,J)=(SF(I,J-2)-8*SF(I,J-1)+8*SF(I,J+1)-SF(I,J-2))/R1(J)
                     1      /RO(I,J)
0126              DO 24 J=2,N
0127                    V(M+2,J)=2.*(3.*SF(M+2,J)+SF(M+4,J)-6.*SF(M+3,J)+2.*SF(M+1,J)
                     1      )/R6(J)/RO(M+2,J)
0128                    VG(J)=2.*(SF(M+3,J)-8.*SF(M+2,J)+7.*SF(M+1,J))/R6(J)/RO(M+1,J
                     1      )
0129          24        V(P,J)=2.*(6.*SF(P-1,J)-3.*SF(P,J)-SF(P-2,J))/R6(J)/RO(P,J)
0130              DO 25 J=2,N
0131              DO 25 I=K6,P
0132          25        V(I,J)=(SF(I+2,J)-8*SF(I+1,J)+8*SF(I-1,J)-SF(I-2,J))/R1(J)/RO
                     1      (I,J)
0133              DO 26 I=K4,P
0134              DO 26 J=2,N
0135          26        W(I,J)=((SF(I+1,J)-2.*SF(I,J)+SF(I-1,J))*Y*Y/DZ2-(SF(I,J+1)-
                     1      SF(I,J-1))/ER2/(J-1.)/2+(SF(I,J+1)-2*SF(I,J)+SF(I,J-1))/ER2)/
                     2      ER2/(J-1.)/(J-1.)/RO(I,J)-(U(I,J)*(RO(I,J+1)-
                     3      RO(I,J-1))/D2R-V(I,J)*(RO(I+1,J)-RO(I-1,J))/D2Z)*A4(J)/RO(I,J
                     4      )
0136              DO 260 J=2,N
0137                    W(P+1,J)=(-SF(P-1,J)+8.*SF(P,J)-7.*SF(P+1,J))
```

```
                1      *R5(J)/RO(P+1,J)
0138          260      W(1,J)=(-SF(3,J)+8.*SF(2,J))*R4(J)
0139                   CODE=2
0140                 GO TO 103
0141          107      SMAX=0.
0142                 DO 27 I=2,K1
0143                 DO 27 J=1,N
0144                 S=BO+ABS(U(I,J))/DX+ABS(V(I,J))/DR
0145           27    IF(SMAX.LT.S) SMAX=S
0146                 IF(PRV.LE.1.) GO TO 28
0147                      BOO=4.*PRV/ER2+2.*PRV*Y*Y/DZ2
0148                      BO=2.*PRV*(Y*Y/DZ2+1./ER2)
0149                 GO TO 301
0150           28        BOO=4./ER2+2.*Y*Y/DZ2
0151                      BO=2.*(Y*Y/DZ2+1./ER2)
0152          301    DO 29 I=K4,P
0153                 DO 29 J=2,N
0154                 S=BO+ABS(U(I,J))/DZ+ABS(V(I,J))/DR
0155           29    IF(SMAX.LT.S) SMAX=S
0156                 DO 30 I=K4,P
0157                 S=BOO+ABS(U(I,1))/DZ
0158           30    IF(SMAX.LT.S) SMAX=S
0159                 IF((SMAX*DT).GT.0.8) DT=0.8/SMAX
0160                      TIME=TIME+DT
0161                      TAU=TIME * CONST
0162                 X=X+UU*DT
0163                      DX1=DT/DX
0164                      DZ1=DT/DZ
0165                      DZ3=CT*DT*Y*Y*RALPHA/DZ2
0166                      DZ5=2.*DZ3
0167                      DZ7 = DT *Y * Y * PR * RNEW / DZ2
0168                      DZ8=DT*Y*Y*ALPHAW/ALPHA/DZ2
0169                 DZ88=DT*Y*Y*ALPHAW/ALPHA/DZX2
0170                 M11=DT*.5*BEITA*G*(A**6)/(ALPHA*ALPHA*NEW*ROW*CPW*DELTA*B)
0171                 M23=.5*DT*A/(ALPHA*ROW*CPW*DELTA)
0172                      DY3=CT*DT*RALPHA/ER2
0173                      DY1=2.*DY3
0174                      DY7 = DT * RNEW * PR / ER2
0175                      DY5=4.*DY3
0176                      DX3=DT*Y*Y/DX2
0177                      ER3=N*N*DT
0178                      ER4=N*DT
0179                      ER5=4.*ER3
0180                      DX5=2.*DX3
0181                      ER1=2*ER3
0182                      DX7=DX3*PR
0183                      DX8=DT*Y*Y*ALPHAW/ALPHA/DX2
0184                      ER7=ER3*PR
0185                      E1=1.0-DX5-ER5
0186                      E2=1.0-DX5-ER1
0187                      E3=1.0-2.0*DX7-2.0*ER7
0188                 DO 31 J=2,K2
0189                      FI=0.5/(J-1.0)
0190                      EI=1.5/(J-1.0)
0191                      DR1(J)=ER3*(1.0-FI)
```

```
0192                    DR2(J)=ER3*(1.0+FI)
0193                    DR3(J)=ER3*(1.0-EI)
0194                    DR4(J)=ER3*(1.0+EI)
0195                    R3(J)=PR*ER3/(J-1.0)/2.0
0196                    DR5(J)=CT*RALPHA*DR1(J)
0197                    DR6(J)=CT*RALPHA*DR2(J)
0198                    DR7(J) = DR3(J) * PR * RNEW
0199          31        DR8(J) = DR4(J) * PR * RNEW
0200                  DO 32 I=2,M
0201                  DO 32 J=1,N
0202                    C1(I,J)=U(I,J)*DX1
0203          32        C3(I,J)=V(I,J)*ER4
0204                  T(1,N+1)=TO(1,N+1)+DT*M1-DT*M2*(11.*TO(1,N+1)-18.*TO(1,N)+9.*
                     1TO(1,N-1)-2.*TO(1,N-2))/6./DR +2.*DX8*(TO(2,N+1)-TO(1,N+1))
0205                  DO 33 I=2,M
0206          33      T(I,N+1)=TO(I,N+1)+DT*M1-DT*M2*(11.*TO(I,N+1)-18.*TO(I,N)+9.*TO(I,
                     1N-1)-2.*TO(I,N-2))/6./DR+DX8*(TO(I+1,N+1)-2.*TO(I,N+1)+TO(I-1,N+1
                     2))
0207                  T(M+1,N+1)=TO(M+1,N+1)+DZXH*((QSURFL*DX+QSURFG*DZ)*M11-(KL*DX+KG*
                     1DZ)*M23*(11.*TO(M+1,N+1)-18.*TO(M+1,N)+9.*TO(M+1,N-1)-2.*TO(M+1,
                     2N-2))/6./DR+DZ88*(TO(M+2,N+1)-DZX1*TO(M+1,N+1)+DZX*TO(M,N+1))*(DX
                     3+DZ))
0208                  DO 34 I=K4,P
0209          34      T(I,N+1)=TO(I,N+1)+DT*M7-DT*M3*(11.*TO(I,N+1)-18.*TO(I,N)+9.*TO(I,
                     1N-1)-2.*TO(I,N-2))/6./DR+DZ8*(TO(I+1,N+1)-2.*TO(I,N+1)+TO(I-1,N+1
                     2))
0210                  T(P+1,N+1)=TO(P+1,N+1)+DT*M7-DT*M3*(11.*TO(P+1,N+1)-18.*TO(P+1,N)+
                     19.*TO(P+1,N-1)-2.*TO(P+1,N-2))/6./DR+2.*DZ8*(TO(P,N+1)-TO(P+1,N+1)
                     2)
0211                  DO 35 I=1,K3
0212                  DO 35 J=1,K2
0213                    WO(I,J)=W(I,J)
0214          35        TO(I,J)=T(I,J)
0215                  DO 402 I=K1,K3
0216                  DO 402 J=1,K2
0217        402       RO(I,J)=CONST1*PRESS*144.0/RGAS  /(T(I,J)+M5)
0218                  DO 36 J=1,N
0219                    DTDXL(J)=(11*T(M+1,J)-18*T(M,J)+9*T(M-1,J)-2*T(M-2,J))/6/DX
0220                    DTDXG(J)=(-11*T(M+1,J)+18*T(M+2,J)-9*T(M+3,J)+2*T(M+4,J))/DZ/
                       1    6
0221          36        UL(J)=(DTDXL(J)-DTDXG(J)*KG/KL)*CP*NEW*NEW*AOVERB/PR/
                       1    BEITA/G/HFG/(A** 3)
0222                  UU=0.
0223                  DO 37 J=1,N
0224          37      UU=UU+(UL(J+1)+UL(J))*(2.0*J-1.0)*ER2/2.0
0225                  DO 38 I=1,K3
0226          38        DTDRW(I)=(11*T(I,N+1)-18* T(I,N)+9*T(I,N-1)-2*T(I,N-2))/6/DR
0227                    QW=0.
0228                  DO 39 I=K1,P
0229          39        QW=QW+(DTDRW(I)+DTDRW(I+1))*DZ/2.
0230                    QI=0.
0231                    DQIL = 0.
0232                  DO 40 J=1,N
0233                    DQIL = DQIL+(DTDXL(J)+DTDXL(J+1))*(2.0*J-1.0)*ER2/2.0
0234          40        QI=QI+(DTDXG(J)+DTDXG(J+1))*(2.0*J-1.0)*ER2/2.0
```

```
0235                    DQWDT=QW*KG*6.28*NEW*ALPHA/BEITA/G/A/A/AOVERB/AOVERB
0236                    RQIN=DQWDT*AOVERB/6.28/A/A/QSURFG/(1-X)
0237                    DQILDT = 3.14*DQIL*KL*NEW*ALPHA/BEITA/G/A/A
0238                    DQIDT=3.14*QI*KG*NEW*ALPHA/BEITA/G/A/A
0239                DME=DT*UU*ROL*(A**3)*3.14/AOVERB
0240                    DMT=DMT+DME
0241                    DM=-DMB+DME
0242                    PRESS=PRESS+RGAS*AOVERB/(3.14*144.*(A**3)*  (1.-X))*((DQWDT-
                   1    DQIDT)*DT*A** 2 /(CV*ALPHA)-DM*GAM*TSAT)
0243                    A6=(PRESS-P1)/PRESS
0244                    M6=(PRESS-P1)/P1
0245                    P1=PRESS
0246                   BB=(B3*B4-ALOG10(PRESS)+B1)
0247                    C=(B2-B3*ALOG10(PRESS)+B1*B3)
0248                    D=BB*BB -4.*B4*C
0249                     TSAT=(-BB+SQRT(D))/(2.*B4)
0250                    A5=2.*DT*AOVERB*G*(A** 3 )/ALPHA/ALPHA
0251                DO 41 J=1,N
0252             41     T(M+1,J)=(TSAT-TINIT)*CONST1
0253                    T(1,1)=TO(1,1)*E1+TO(1,2)*DX5+TO(2,1)*ER5
0254                DO 43 I=2,M
0255                IF(U(I,1).LE.0.) GO TO 42
0256                    C=(TO(I-1,1)-TO(I,1))*C1(I,1)
0257                GO TO 43
0258             42     C=(TO(I,1)-TO(I+1,1))*C1(I,1)
0259             43     T(I,1)=TO(I,1)*E1+TO(I,2)*ER5+(TO(I+1,1)+TO(I-1,1))*DX3 +C
0260                DO 44 J=2,N
0261             44     T(1,J)=TO(1,J)*E2+TO(2,J)*DX5+TO(1,J-1)*DR1(J)
                   1    +TO(1,J+1)*DR2(J)
0262                DO 47 J=2,N
0263                DO 47 I=2,M
0264                IF(U(I,J).LE.0.) GO TO 45
0265                    C=(TO(I-1,J)-TO(I,J))*C1(I,J)
0266                GO TO 303
0267             45     C=(TO(I,J)-TO(I+1,J))*C1(I,J)
0268            303  IF(V(I,J).LE.0.) GO TO 46
0269                    D=(TO(I,J-1)-TO(I,J))*C3(I,J)
0270                GO TO 47
0271             46     D=(TO(I,J)-TO(I,J+1))*C3(I,J)
0272             47     T(I,J)= TO(I,J)*E2+(TO(I+1,J)+TO(I-1,J))*DX3+
                   1    TO(I,J-1)*DR1(J)+TO(I,J+1)*DR2(J)+C+D
0273                DO 50 I=2,M
0274                DO 50 J=2,N
0275                    FI=R3(J)*(T(I,J+1)-T(I,J-1))
0276                IF(U(I,J).LE.0.) GO TO 48
0277                    C=(WO(I-1,J)-WO(I,J))*C1(I,J)
0278                GO TO 305
0279             48     C=(WO(I,J)-WO(I+1,J))*C1(I,J)
0280            305  IF(V(I,J).LE.0.) GO TO 49
0281                    D=(WO(I,J-1)-WO(I,J))*C3(I,J)
0282                GO TO 50
0283             49     D=(WO(I,J)-WO(I,J+1))*C3(I,J)
0284             50     W(I,J)=WO(I,J)*E3+(WO(I+1,J)+WO(I-1,J))*DX7+C+D+
                   1    WO(I,J-1)*DR3(J)+WO(I,J+1)*DR4(J)+FI
0285                DO 51 J=2,K2
```

```
0286          51        SF(M+1,J)=0.
0287                    NE1=0
0288          52        NE1=NE1+1
0289              IF(NE1.GT.NE) GO TO 104
0290              DO 53 I=1,K1
0291              DO 53 J=1, K2
0292          53        C3 (I,J)=SF(I,J)
0293                    I=1
0294          54         I=I+1
0295                    F(1)=0.
0296              DO 55 J=2,N
0297                    DI(J)=(C3(I+1,J)+C3(I-1,J))*F1-W(I,J)*A1(J)
0298          55         F(J)=(DI(J)+F(J-1)*C2(J))/D1(J)
0299              DO 56 J=1,K5
0300                   H=N+1-J
0301          56        SF(I,H)=EJ(H)*SF(I,H+1)+F(H)
0302              IF(I.LT.M) GO TO 54
0303                   RMAX=0.
0304              DO 57 I=2,M,NR
0305              DO 57 J=2,N,NR
0306              RR3=ABS((SF(I,J)-C3(I,J))/(C3(I,J)+1.0E-20))
0307          57  IF(RMAX.LT.RR3) RMAX=RR3
0308              IF(RMAX.GT.EPSLON) GO TO 52
0309              DO 58 I=1,K1
0310              IF(T(I,N+1).GT.(T(M+1,N)+DTW*CONST1)) T(I,N+1)=T(M+1,N)+DTW*CONST1
0311          58  IF(T(I,N).GT.(T(M+1,N)+DTS*CONST1)) T(I,N)=T(M+1,N)+DTS*CONST1
0312                   DQS = 0.
0313                   DQL = 0.
0314                   DMB=0.
0315                   CT2=6.28*A*A*DX*ROW*CPW*DELTA/AOVERB/2.0/CONST1
0316              DO 59 I=1,M
0317                   C=T(I,N+1)+T(I+1,N+1)
0318                   DQS=DQS+(C-C4(I,N+1))*CT2
0319          59       C4(I,N+1)=C
0320              DO 60 J=1,K2
0321          60       DR1(J)=3.14*ROL*CP*(A** 3)*DX*ER2*(2.0*J-1.0)/AOVERB
0322              DO 61 I=1,M
0323              DO 61 J=1,N
0324                   C = (T(I,J)+T(I,J+1)+T(I+1,J)+T(I+1,J+1))/4.0/CONST1
0325                   DQL = DQL +(C-C4(I,J))*DR1(J)
0326          61       C4(I,J) = C
0327                   DQI=(6.28*A*A*X*QSURFL/AOVERB+DQILDT)*DT*CONST
0328                   DMB = (DQI-DQL-DQS)/HFG
0329              IF(DMB.LT.0.) DMB=0.
0330                   DMBT=DMBT+DMB
0331                   DMTT=DMT-DMBT
0332              UU=UU-AOVERB*DMB/3.14/(A**3)/ROL/DT
0333                   DWDT=-.581*PRESS*ALPHA*A*UU/AOVERB
0334              UG=-UU*(ROL/RO(M+1,1)-1.0)
0335                   E1=1-DZ5-DY5
0336                   E2=1-DZ5-DY1
0337                   E3=1-2*DZ7-2*DY7
0338              DO 62 I=K4,P
0339              DO 62 J=1,N
0340                   C1(I,J)=DZ1*U(I,J)
```

```
0341          62        C3(I,J)=V(I,J)*ER4
0342                    T(P+1,1)=TO(P+1,1)*E1+TO(P,1)*DZ5+TO(P+1,2)*DY5
                     1     +M4*M6*(M5+TO(P+1,1))
0343                   DO 63 J=2,N
0344          63        T(P+1,J)=TO(P+1,J)*E2+TO(P,J)*DZ5+TO(P+1,J-1)*DR5(J)+TO(P+1,J
                     1     +1)*DR6(J)+M4*M6*(M5+TO(P+1,J))
0345                   DO 65 I=K4,P
0346                   IF(U(I,1).LE.0.) GO TO 64
0347                        C=(TO(I-1,1)-TO(I,1))*C1(I,1)
0348                   GO TO 65
0349          64        C=(TO(I,1)-TO(I+1,1))*C1(I,1)
0350          65        T(I,1)=TO(I,1)*E1+TO(I,2)*DY5+(TO(I+1,1)+TO(I-1,1))*DZ3 +C
                     1      +M4*M6*(M5+TO(I,1))
0351                   DO 68 I=K4,P
0352                   DO 68 J=2,N
0353                   IF(U(I,J).LE.0.) GO TO 66
0354                        C=(TO(I-1,J)-TO(I,J))*C1(I,J)
0355                   GO TO 308
0356          66        C=(TO(I,J)-TO(I+1,J))*C1(I,J)
0357         308     IF(V(I,J).LE.0.) GO TO 67
0358                        D=(TO(I,J-1)-TO(I,J))*C3(I,J)
0359                   GO TO 68
0360          67        D=(TO(I,J)-TO(I,J+1))*C3(I,J)
0361          68        T(I,J)= TO(I,J)*E2+(TO(I+1,J)+TO(I-1,J))*DZ3+
                     1     TO(I,J-1)*DR5(J)+TO(I,J+1)*DR6(J)+C+D +M4*M6*(M5+TO(I,J))
0362                   DO 71 I=K4,P
0363                   DO 71 J=2,N
0364                        FI=A4(J)*(-(2*(U(I,J)-UO(I,J))+C1(I,J)*(U(I+1,J)-U(I-1,J))+
                     1     C3(I,J)*(U(I,J+1)-U(I,J-1)))*(RO(I,J+1)-RO(I,J-1))+AOVRB2*(2.
                     2    *(V(I,J)-VO(I,J))+C1(I,J)*(V(I+1,J)-V(I-1,J))+C3(I,J)*(V(I,J+1
                     3     )-V(I,J-1)))*(RO(I+1,J)-RO(I-1,J)))/RO(I,J)-W(I,J)*(2*(T(I,J)
                     4     -TO(I,J))+C1(I,J)*(T(I+1,J)-T(I-1,J))+C3(I,J)*(T(I,J+1)-T(I,J
                     5     -1)))/ZOVR2/(T(I,J)+M5)+A6*W(I,J)
0365                   IF(U(I,J).LE.0.) GO TO 69
0366                        C=(WO(I-1,J)-WO(I,J))*C1(I,J)
0367                   GO TO 310
0368          69        C=(WO(I,J)-WO(I+1,J))*C1(I,J)
0369         310     IF(V(I,J).LE.0.) GO TO 70
0370                        D=(WO(I,J-1)-WO(I,J))*C3(I,J)
0371                   GO TO 71
0372          70        D=(WO(I,J)-WO(I,J+1))*C3(I,J)
0373          71        W(I,J)=WO(I,J)*E3+(WO(I+1,J)+WO(I-1,J))*DZ7 +C+D +
                     1     WO(I,J-1)*DR7(J)+WO(I,J+1)*DR8(J)+FI
                     2     +A5*A4(J)*(T(I,J+1)-T(I,J-1))/(T(I,J)+M5)
0374                   DO 72 J=2,N
0375                        SF(M+1,J)=RO(M+1,J)*UG*ER2*(J-1.0)*(J-1.0)/2.0
0376          72        SFI(J)=SF(M+1,J)
0377                   DO 73 I=K4,P
0378          73        SF(I,N+1)=SF(M+1,N+1)
0379                        NE2=0
0380          74        NE2=NE2+1
0381                   IF(NE2.GT.NE) GO TO 104
0382                   DO 75 I=K1,K3
0383                   DO 75 J=1,K2
0384          75        C3(I,J)=SF(I,J)
```

```
0385                    I=M+1
0386          76        I=I+1
0387                DO 77 J=2,N
0388                    DI(J)=(C3(I+1,J)+C3(I-1,J))*F3-(W(I,J)*RO(I,J)+A4(J)*(U(I,J)*
                     1  (RO(I,J+1)-RO(I,J-1))/D2R-V(I,J)*(RO(I+1,J)-RO(I-1,J))/D2Z))*
                     2  A1(J)
0389          77        F(J)=(DI(J)+F(J-1)*C2(J))/D2(J)
0390                DO 78 J=2,N
0391                K=N+2-J
0392          78        SF(I,K)=EJ1(K)*SF(I,K+1)+F(K)
0393                IF(I.LT.P) GO TO 76
0394                IF(NT.EQ.1.AND.NE2.EQ.1) GO TO 74
0395                    RMAXX=0.
0396                DO 79 I=K4,P,NR
0397                DO 79 J=2,N,NR
0398                    RR3= ABS ((SF(I,J)-C3(I,J))/(C3(I,J)+1.0E-20))
0399          79    IF(RMAXX.LT.RR3) RMAXX=RR3
0400                IF(RMAXX.GT.EPSLON) GO TO 74
0401                DO 80 I=2,M
0402          80        W(I,N+1)=(8.*SF(I,N)-SF(I,N-1)-7.*SF(I,N+1))/DYY
0403                DO 81 I=K4,P
0404          81        W(I,N+1)=(8*SF(I,N)-SF(I,N-1)-7*SF(I,N+1))/DYY/RO(I,N+1)
0405                DO 82 J=2,N
0406                    W(P+1,J)=(-SF(P-1,J)+8.*SF(P,J)-7.*SF(P+1,J))*R5(J)/RO(P+1,J)
0407          82        W(1,J)=(-SF(3,J)+8.0*SF(2,J))*R4(J)
0408         103    DO 83 I=K1,K3
0409                DO 83 J=1,K2
0410                    V0(I,J)=V(I,J)
0411          83        U0(I,J)=U(I,J)
0412                DO 84 I=2,M
0413                    U(I,N)=2.0*(3.*SF(I,N)-6.0*SF(I,N-1)+SF(I,N-2))/R1(N)
0414                    U(I,1)=SF(I,2)/ER6
0415          84        U(I,2)=2.0*(6.0*SF(I,3)-3.0*SF(I,2)-SF(I,4))/R1(2)
0416                DO 85 I=K1,P
0417                    U(I,N)=2.*(3*SF(I,N)-6*SF(I,N-1)+SF(I,N-2))/R1(N)/RO(I,N)
0418                    U(I,1)=SF(I,2)/ER6/RO(I,1)
0419          85        U(I,2)=2.*(6.*SF(I,3)-SF(I,4)-3.*SF(I,2))/R1(2)/RO(I,2)
0420                DO 86 I=2,M
0421                DO 86 J=3,K5
0422          86        U(I,J)=(SF(I,J-2)-8*SF(I,J-1)+8*SF(I,J+1)-SF(I,J+2))/R1(J)
0423                DO 89 I=K1,P
0424                DO 89 J=3,K5
0425          89        U(I,J)=(SF(I,J-2)-8*SF(I,J-1)+8*SF(I,J+1)-SF(I,J-2))/R1(J)
                     1  /RO(I,J)
0426                DO 90 J=2,N
0427                    V(M+2,J)=2.*(3.*SF(M+2,J)+SF(M+4,J)-6.*SF(M+3,J)+2*SF(M+1,J))
                     1  /R6(J)/RO(M+2,J)
0428                    V(P,J)=2.*(6.*SF(P-1,J)-3.*SF(P,J)-SF(P-2,J))/R6(J)/RO(P,J)
0429          90        VG(J)=2.*(SF(M+3,J)-8.*SF(M+2,J)+7.*SF(M+1,J))/R6(J)/RO(M+1,J
                     1  )
0430                DO 91 I=K6,K7
0431                DO 91 J=2,N
0432          91        V(I,J)=(SF(I+2,J)-8*SF(I+1,J)+8*SF(I-1,J)-SF(I-2,J))/R6(J)/RO
                     1  (I,J)
0433                DO 92 J=2,K2
```

```
0434          92        SF(M+1,J)=0.
0435                  DO 93 J=2,N
0436                    V(2,J)=2.0*(SF(4,J)-6.0*SF(3,J)+3.0*SF(2,J))/R2(J)
0437                    V(M,J)=2.0*(6.0*SF(M-1,J)-3.0*SF(M,J)-SF(M-2,J))/R2(J)
0438          93        V(M+1,J)=2.0*(8*SF(M,J)-SF(M-1,J))/R2(J)
0439                  DO 94 I=3,K8
0440                  DO 94 J=2,N
0441          94        V(I,J)=(SF(I+2,J)-8*SF(I+1,J)+8*SF(I-1,J)-SF(I-2,J))/R2(J)
0442                  IF(NT.LT.N1) GO TO 104
0443                  IF(NT.NE.NMAX) GO TO 95
0444                  PUNCH 204, A,PRESS,PO,X,NT,TIME,UU,DMBT,DMTT,((T(I,J),J=1,K2),
                     1I=1,K3),((SF(I,J),J=1,K2),I=1,K3)
0445                  GO TO 104
0446          95        NP1=TAU/(TAU1*N3)
0447                  IF(NP1.GE.1.) GO TO 104
0448                  GO TO 102
0449         104      IF(NT.LT.NC) GO TO 105
0450                     RR1=0
0451                  DO 96 I=2,M
0452                  DO 96 J=2,K2
0453                     RR2= ABS ((T(I,J)-TO(I,J))/(TO(I,J)+1.E-20))
0454          96      IF(RR1.LT.RR2) RR1=RR2
0455         105          NUG=0.
0456                      NUL=0.
0457                      RAL = 0.
0458                      RAG = 0.
0459                  DO 97 I=1,K1
0460                      HL(I)= ABS (KL*DTDRW(I)/A/(T(I,N+1)-T(I,1)))
0461                      RAL = RAL+DX*T(I,N+1)
0462          97          NUL = NUL+DX*HL(I)*A*X/AOVERB/KL
0463                      RAL = RAL*(X** 3)/(AOVERB** 4)
0464                  DO 98 I=K1,K3
0465                      J=I-M
0466                      HG(J)= ABS (KG*DTDRW(I)/A/(T(I,N+1)-T(I,1)))
0467                      RAG = RAG+DZ*T(I,N+1)
0468          98          NUG = NUG+DZ*HG(J)*A*(1-X)/AOVERB/KG
0469                      RAG = RAG * ((1-X)** 3) * BEITAG/RALPHA/RNEW/BEITA/
                     1      (AOVERB** 4)
0470                      CL = NUL/(RAL** 0.25)
0471                      CG = NUG/(RAG** 0.25)
0472                  UR=0.
0473                  DO 99 J=2,K2
0474          99          UR=(UR+U(I1,J)*R1(J))/12.0
0475                  DO 401 I=1,K3
0476                  DO 401 J=1,K2
0477         401      RT(I,J)=CONST3*T(I,J)
0478                  WRITE(6,210) NT,TIME,TAU,DT,UR,UU,PRESS,Z,X,DX,DME,DMT,DMB,DMBT,
                     1DM,DMTT,RQIN,DQIDT,DWDT,DQWDT,HFG,TSAT,TINIT
0479         210      FORMAT(1H1,'            NT=' I13,'          TIME=' E13.6,
                     1    '          TAU=' F13.6,      '          DT=' E13.6//
                     21X,'          UR='E13.6,      '          UU='E13.6,
                     3    '       PRESS=' F13.6,      '           Z=' F13.6//
                     41X,'           X=' F13.6,      '          DX=' F13.6,
                     5    '         DME=' E13.6,      '         DMT=' E13.6//
                     61X,'         DMB=' F13.6,      '        DMBT=' F13.6,
```

```
                7   '          DM=' E13.6,      '          DMTT=' E13.6//
               81X,'        RQIN=' E13.6,      '        DQIDT=' E13.6,
               9   '        DWDT=' F13.6,      '        DQWDT=' F13.6//
               11X,'         HFG=' F13.6,      '         TSAT=' F13.6
               2   '       TINIT=' F13.6///
               320X,'AXIAL VELOCITY COMPONENT---U(I,J)'//)
0480            DO 601 I=1,K3
0481      601   WRITE(6,211) I,(U(I,J),J=1,K2)
0482      211   FORMAT(1H0,I3,7(5X,E13.6)/4X,7(5X,E13.6)/4X,7(5X,E13.6))
0483            WRITE(6,212)
0484      212   FORMAT( //20X,'RADIAL VELOCITY COMPONENT---V(I,J)'//)
0485            DO 302 I=1,K3
0486      302   WRITE(6,211) I,(V(I,J),J=1,K2)
0487            WRITE(6,213)
0488      213   FORMAT( //20X,'NON DIMENSIONAL TEMPERATURE RISE---T(I,J)'//)
0489            DO 603 I=1,K3
0490      603   WRITE(6,211) I,(T(I,J),J=1,K2)
0491            WRITE(6,222)
0492      222   FORMAT(//20X,'REAL TEMPERATURE RISE---RT(I,J)'//)
0493            DO 608 I=1,K3
0494      608   WRITE(6,211) I,(RT(I,J),J=1,K2)
0495            WRITE(6,214)
0496      214   FORMAT(//20X,'STREAM FUNCTION---SF(I,J)'//)
0497            DO 304 I=1,K3
0498      304   WRITE(6,211) I,(SF(I,J),J=1,K2)
0499            WRITE(6,215)
0500      215   FORMAT(//20X,'RADIAL VAPOR VELOCITY COMPONENT AT INTERFACE---
              1VG(J)'//)
0501            WRITE(6,216) (VG(J),J=1,K2)
0502      216   FORMAT(4X,7(5X,E13.6)/4X,7(5X,E13.6)/4X,7(5X,E13.6))
0503            WRITE(6,217)
0504      217   FORMAT(//20X,'INTERFACE VELOCITY DUE TO INTERFACE CHANGE---UL(J)'
              1//)
0505            WRITE(6,216) (UL(J),J=1,K2)
0506            WRITE(6,218)
0507      218   FORMAT(//20X,'VAPOR STREAM FUNCTION AT INTERFACE---SFI(J)'//)
0508            WRITE(6,216) (SFI(J),J=1,K2)
0509            WRITE(6,219)
0510      219   FORMAT(//20X,'HEAT TRANSFER COEFFICIENT OF LIQUID---HL(J)'//)
0511            WRITE(6,216) (HL(J),J=1,K1)
0512            WRITE(6,220)
0513      220   FORMAT(//20X,'HEAT TRANSFER COEFFICIENT OF VAPOR---HG(J)'//)
0514            WRITE(6,223) (HG(J),J=1,11)
0515      223   FORMAT(4X,7(5X,E13.6)/4X,7(5X,E13.6))
0516            WRITE(6,221) NUL,NUG,RMAX,RR1,NE1,NE2,RAL,RAG,CL,CG,RP,DQILDT,
              1DQI,DQS,DQL
0517      221   FORMAT(1H0,'          NUL=' F13.6,'          NUG=' F13.6,
               1   '       RMAX='E13.6,      '         RR1='E13.6//
               21X,'         NE1=' I13,       '         NE2=' I13,
               3   '         RAL=' E13.6,     '         RAG=' E13.6//
               41X,'          CL=' F13.6,     '          CG='F13.6,
               5   '          RP=' F13.6,     '      DQILDT=' F13.6//
               61X,'         DQI=' E13.6,     '         DQS=' E13.6,
               7   '         DQL=' E13.6///)
0518            N3=N3+1
```

```
0519                NP2=TAU/(N4*TAU2)
0520                IF(NP2.GE.1.) N4=N4+1
0521                IF(NP2.GE.1.) WRITE(7,204) A,PRESS,PO,X,NT,TIME,UU,DMBT,DMTT,
                   1(((T(I,J),J=1,K2),I=1,K3),((SF(I,J),J=1,K2),I=1,K3)
0522                IF(NE1.GT.NE) GO TO 500
0523                IF(NT.EQ.NMAX) GO TO 101
0524                GO TO 102
0525          500   CALL SYSTEM
0526                END
```

APPENDIX C

LH_2 PROGRAM NOMENCLATURE

Symbols preceding the expression indicate the following:

* - Input data
** - Printout

Symbols following the expression indicate the following:

[0] - Integer
[1] - Dimensionless
[] - Units
() - Statement number in the source program of Appendix B

A			
*A	- [ft]	-	- Tank radius
*AOVERB	- [1] - A/B		
AOVERB2	- [1] - $(A/B)^2$	- (46)	
A5	- [1]	- (250)	
A6	- [1]	- (243)	
A1(J)	- [1]	- (48)	
A2(J)	- [1]	- (93)	
A3(J)	- [1]	- (94)	
A4(J)	- [1]	- (50)	
*ALPHA	- [ft^2/sec]	-	- Thermal diffusivity of liquid
*ALPHAW	- [ft^2/sec]	-	- Thermal diffusivity of wall
*ALPHAV	- [ft^2/sec]	-	- Thermal diffusivity of vapor
B			
BB		- (30,32,246)	- Temporary storage
B	- [ft]	- (19)	- Total tank height
BJ	- [1]	- (88)	
BJ1	- [1]	- (81)	
BO	- [1]	- (89,148,151)	
BOO	- [1]	- (147,150)	
*BEITA	- [$°F^{-1}$]	-	- Volumetric coefficient of expansion-liquid
BEITAG	- [$°F^{-1}$]	- (68)	- Volumetric coefficient of expansion-vapor
*B1		- (30,246)	- Pressure temperature relation
*B2		- (31,247)	- Pressure temperature relation
*B3		- (30,246)	- Pressure temperature relation
*B4		- (30,246)	- Pressure temperature relation
C			
C	- [1]	-	- Temporary storage
C1(1,J)	- [1]	- (202,340)	- Temporary storage
C2(J)	- [1]	- (49)	
C3(I,J)	- [1]	- (203,341,384)	- Temporary storage
C4(I,J)	- [1]	- (319,326)	- Temporary storage
**CL	- [1]	- (470)	- Coefficient of Rayleigh number correlation-liquid
**CG	- [1]	- (471)	- Coefficient of Rayleigh number correlation-vapor
*CP	- [Btu/lbm-°F]	-	- Specific heat-liquid
*CPV	- [Btu/lbm-°F]	-	- Specific heat-vapor-constant pressure
*CV	- [Btu/lbm-°F]	-	- Specific heat-vapor-constant volume
*CPW	- [Btu/lbm-°F]	-	- Specific heat-wall
CT	- [1]	- (70)	- Property term for vapor (=1 for ideal gas)

CT2 [8]	- [Btu]	- (315)	- Property term for wall
*CODE	- [0]	- (52,103,139)	- = 2 for a new run = 1 for continuation of prior run via READ FORMAT INPUT
**CONST	- [sec]	- (35)	- Conversion constant for dimensionless time
**CONST1	- [$°F^{-1}$]	- (36)	- Conversion constant for dimensionless temperature
**CONST2	- [sec^{-1}]	- (37)	- = 1/CONST
**CONST3	- [°F]	- (38)	- = 1/CONST1

D

D	- [1]	-	- Temporary storage
D1(J)	- [1]	- (95)	
D2(J)	- [1]	- (97)	
DI(J)	- [1]	- (388)	
DR1(J)	- [1]	- (191,321)	
DR2(J)	- [1]	- (192)	
DR3(J)	- [1]	- (193)	
DR4(J)	- [1]	- (194)	
DR5(J)	- [1]	- (196)	
DR6(J)	- [1]	- (197)	
DR7(J)	- [1]	- (198)	
DR8(J)	- [1]	- (199)	
DZX	- [1]	- (74)	
DZX1	- [1]	- (75)	
DZX2	- [1]	- (76)	
DZXH	- [1]	- (77)	
DR	- [1]	- (24)	- Radial grid space
D2R	- [1]	- (45)	- DR/2
DRZ	- [1]	- (79)	- $(DR/DZ)^2$
**DX	- [1]	- (71)	- Axial grid space-liquid
DX1	- [1]	- (163)	- DT/DX
DX2	- [1]	- (72)	- DX^2
DX3	- [1]	- (176)	
DX5	- [1]	- (180)	
DX7	- [1]	- (182)	
DX8	- [1]	- (183)	
DXR	- [1]	- (82)	- $(DX/DR)^2$
DRX	- [1]	- (83)	- 1/DXR
DYY	- [1]	- (27)	- $2(DR)^2$
DY1	- [1]	- (173)	
DY3	- [1]	- (172)	
DY5	- [1]	- (175)	
DY7	- [1]	- (174)	
DZ	- [1]	- (73)	- Axial grid space-vapor
DZ1	- [1]	- (164)	- DT/DZ
DZ2	- [1]	- (78)	- DZ^2
D2Z	- [1]	- (86)	- DZ/2
DZ3	- [1]	- (165)	
DZ5	- [1]	- (166)	
DZ7	- [1]	- (167)	
DZ8	- [1]	- (168)	
DZ88	- [1]	- (169)	
**DM	- [lbm]	- (241)	- Net phase change in time DT (minus sign for evaporation)
**DMB	- [lbm]	- (314,328)	- Phase change in time DT from energy balance on tank wall and liquid system (plus sign for evaporation)

**DME	- [lbm]	- (239)	- Phase change at L-V interface in time DT (minus sign for evaporation)
**DMT	- [lbm]	- (240)	- Cumulative total of DME (minus sign for evaporation)
**DMBT	- [lbm]	- (330)	- Cumulative total of DMB
**DMTT	- [lbm]	- (331)	- Cumulative total of DM (minus sign for evaporation)
*			
**DT	- [1]	-	- Time step interval
*DTS	- [°F]	- (311)	- Max. permissible liquid superheat at node adjacent to wall
*DTW	- [°F]	- (310)	- Max. permissible superheat of wall in contact with liquid
DTDRW(I)	- [1]	- (226,229)	- Temperature gradient in fluid at wall
DTDXG(J)	- [1]	- (220)	- Temperature gradient in vapor at liquid-vapor interface
DTDXL(J)	- [1]	- (219)	- Temperature gradient in liquid at liquid-vapor interface
DQIL	- [1]	- (231,233)	- Mean temperature gradient in liquid at L-V interface
DQILDT	- [Btu/sec]	- (237)	- Heat transfer rate in liquid at L-V interface (plus for heat transfer to liquid)
**DQIDT	- [Btu/sec]	- (238)	- Heat transfer rate in vapor at L-V interface (plus for heat transfer out of vapor)
**DQWDT	- [Btu/sec]	- (235)	- Heat transfer rate to vapor from wall (plus for heat transfer to vapor)
**DWDT	- [Btu/sec]	- (333)	- Work rate by vapor control volume
DQI	- [Btu]	- (327)	- Sum of heat transfer to wall in contact with liquid and to liquid at L-V interface in DT (plus for heat transfer in)
DQL	- [Btu]	- (313,325)	- Enthalpy rise of liquid in DT
DQS	- [Btu]	- (312,318)	- Enthalpy rise of wall in contact with liquid in DT
*DELTA	- [ft]	-	- Wall thickness
E			
EJ(J)	- [1]	- (90,102)	
EJ1(J)	- [1]	- (91,98)	
*EPSLON	- [1]	- (308,400)	- Maximum fractional change in stream function between iterations before iteration is terminated
E1	- [1]	- (185)	
E2	- [1]	- (186)	
E3	- [1]	- (187)	
EI	- [1]	- (190)	
ER1	- [1]	- (181)	
ER2	- [1]	- (25)	
ER3	- [1]	- (177)	
ER4	- [1]	- (178)	
ER5	- [1]	- (179)	
ER6	- [1]	- (28)	
ER7	- [1]	- (184)	
F			
F	-	-	- Temporary storage
F(J)	- [1]	- (295,298,389)	- Temporary storage
FI	- [1]	- (189,364)	- Temporary storage

F1	- [1]	- (84)	
F2	- [1]	- (85)	
F3	- [1]	- (80)	
*FHHFG	- [Joule/gram mole]	- (62)	- Input function value of HFG in the subroutine ATSM
G			
*G	- [ft/sec^2]	-	- Acceleration corresponding to effective body force acting on container
GAM	- [1]	- (26)	- Ratio of specific heats-vapor
H			
H	- [0]	- (300)	- Index
**HFG	- [Btu/lbm]	- (64)	- Latent heat of vaporization corresponding to TSAT
HGFJ	- [Joule/gram mole]	- (63,64)	- HFG in Joule/gram mole corresponding to TSAT obtained by subroutine ATSM
**HG(I)	- [Btu/sec-ft^2-°F]	- (466)	- Local heat transfer coefficient of vapor based on ΔT between wall and centerline
**HL(I)	- [Btu/sec-ft^2-°F]	- (460)	- Local heat transfer coefficient of liquid based on ΔT between wall and centerline
HHFG	- [Joule/gram mole]	- (62,63)	- Function value of HFG in given table-HFG vs. TSAT appearing subroutine ALI and ATSM
I			
I	- [0]	-	- Axial nodal index number
I1	- [0]	- (17)	- Mid-vertical height of liquid
IER	- [0]	- (63)	- Error parameter for subroutine ALI
J			
J	- [0]	-	- Radial nodal index number
K			
*KG	- [Btu/sec-ft-°F]	-	- Thermal conductivity-vapor
*KL	- [Btu/sec-ft-°F]	-	- Thermal conductivity-liquid
K1	-	- (8)	- (M + 1)
K2	-	- (9)	- (N + 1)
K3	-	- (10)	- (P + 1)
K4	-	- (11)	- (M + 2)
K5	-	- (12)	- (N - 1)
K6	-	- (13)	- (M + 3)
K7	-	- (14)	- (P - 1)
K8	-	- (15)	- (M - 1)
M			
*M	- [0]	-	- Number of vertical divisions in liquid (M + 1 = L-V interface)
M1	- [1]	- (40)	- Liquid-wall property
M2	- [1]	- (41)	- Liquid-wall property
M3	- [1]	- (42)	- Vapor-wall property
M4	- [1]	- (69)	- Vapor property
M5	- [1]	- (44)	- Initial temperature
M6	- [1]	- (244)	- Pressure rise ratio in DT
M7	- [1]	- (43)	- Vapor-wall property
M11	- [1]	- (170)	
M23	- [1]	- (171)	

N

*N	- [0]	-	- Number of radial divisions (N + 1 = wall)
*N1	- [1]	- (442)	- Minimum number of time steps before punch is permitted
N3	- [0]	- (57,518)	- Control number for establishing time steps between printouts
N4	- [0]	- (58,520)	- Control number for establishing time steps between punchouts
*NC	- [0]	- (449)	- Minimum number of time steps NT before fractional temperature changes between time steps is computed
*NE	- [0]	- (381)	- Maximum number of iterations permitted in computations of stream function
**NE1	- [0]	- (287,288,289)	- Counter on iterations on stream function-liquid
**NE2	- [0]	- (379,380,381)	- Counter on iterations on stream function-vapor
NP1	- [1]	- (446,447)	- Control for printout instruction
NP2	- [1]	- (519)	
*NR	- [0]	- (396,397)	- Index steps of grid spaces for which fractional change in stream function with iterations is computed
**NT	- [0]	- (60,523)	- Time step number
*NMAX	-	- (523)	- Maximum number of time steps NT permitted before program is terminated
*NEW	- [ft^2/sec]	-	- Kinematic viscosity-liquid
*NEWV	- [ft^2/sec]	-	- Kinematic viscosity-vapor
**NUG	- [1]	- (455,468)	- Mean Nusselt number-vapor
**NUL	- [1]	- (456,462)	- Mean Nusselt number-liquid
*NDIM	- [0]	- (62,63)	- Number of points which must be selected out of given table (ZTT,FHHFG)

P

*P	- [0]	-	- Total number of vertical divisions
*PO	- [lbf/$in.^2$]	-	- Initial system pressure
P1	- [lbf/$in.^2$]	- (59,245)	- Pressure at previous time step
**PRESS	- [lbf/$in.^2$]	- (29,242)	- Current system pressure
**PR	- [1]	- (20)	- Prandtl number-liquid
**PRV	- [1]	- (21)	- Prandtl number-vapor

Q

QI	- [1]	- (230,234)	- Mean temperature gradient in vapor at L-V interface
QW	- [1]	- (227,229)	- Mean temperature gradient in vapor at wall
*QSURFG	- [Btu/sec-ft^2]	-	- Imposed heat flux on container exterior on vapor portion
*QSURFL	- [Btu/sec-ft^2]	-	- Imposed heat flux on container exterior on liquid portion

R

**RR1	- [1]	- (450,454)	- Maximum value of R2
RR2	- [1]	- (453,454)	- Fractional change in temperature between time steps
RR3	- [1]	- (306,307,398, 399)	- Fractional change in stream function with iteration
R1(J)	- [1]	- (51)	
R2(J)	- [1]	- (96)	

R3(J)	- [1]	- (195)	
R4(J)	- [1]	- (99)	
R5(J)	- [1]	- (100)	
R6(J)	- [1]	- (101)	
RO(I,J)	- [lbm/ft^3]	- (113,217)	- Local vapor density
*ROL	- [lbm/ft^3]	-	- Liquid density
*ROW	- [lbm/ft^3]	-	- Wall density
**RP	- [1]	- (65)	- Ratio of current pressure to initial
**RMAX	- [1]	- (303,307)	- Maximum value of change in stream function with iteration-liquid
RMAXX	- [1]	- (395,399,400)	- Maximum value of change in stream function with iteration-vapor
**RAG	- [1]	- (458,467,469)	- Mean Rayleigh number-vapor
**RAL	- [1]	- (457,461,463)	- Mean Rayleigh number-liquid
*RGAS	- [ft-lbf/lbm-°R]	-	- Gas constant-vapor
**RQIN	- [1]	- (236)	- Fraction of total heat transfer rate to vapor part of tank going into vapor
RALPHA	- [1]	- (23)	- Ratio-thermal diffusivity of vapor to liquid
RNEW	- [1]	- (22)	- Ratio-kinematic viscosity of vapor to liquid
RT(I,J)	- [°F or °R]	- (477)	- Real temperature rise
S			
S	- [1]	- (144,154,155, 157,158)	- Stability criteria
SMAX	- [1]	- (155,158)	- Maximum value of S
**SF(I,J)	- [1]	-	- Stream function
**SFI(J)	- [1]	- (376)	- Vapor stream function at L-V interface
T			
**T(I,J)	- [1]	-	- Current temperature
TO(I,J)	- [1]	- (56)	- Temperature of prior time step
**TAU	- [sec]	- (161)	- Current time
*TAU1	- [sec]	- (446)	- Basic multiple of time for which printout occurs
*TAU2	- [sec]	- (519)	- Basic multiple of time for which punch-out occurs
**TIME	- [1]	- (160)	- Current time
TINIT	- [°R]	- (34)	- Initial saturation temperature corresponding to initial pressure
TSAT	- [°R]	- (33,249)	- Current saturation temperature corresponding to current pressure
TSATK	- [°K]	- (61,62,63)	- Saturation temperature in °K in subroutine ALI and ASTM
TT	- [°K]	- (62,63)	- Argument value for temperature in the subroutine ALI
U			
**U(I,J)	- [1]	-	- Axial component of velocity
**UU	- [1]	- (224,332)	- Mean velocity of liquid-vapor interface
UG	- [1]	- (116,334)	- Mean velocity of vapor at liquid-vapor interface
**UL(J)	- [1]	- (221)	- Local L-V interface velocity due to interface phase change
UO(I,J)	- [1]	- (411)	- Temporary storage of U(I,J)
**UR	- [1]	- (472,474)	- Mean axial velocity at mid-point of liquid (serves as check on continuity)

V			
**V(I,J)	- [1]	-	- Radial component of velocity
VO(I,J)	- [1]	- (410)	- Temporary storage of V(I,J)
**VG(J)	- [1]	- (128,429)	- Radial velocity of vapor at L-V at interface
W			
W(I,J)	- [1]	-	- Vorticity
WO(I,J)	- [1]	- (213)	- Vorticity of prior time step
X			
**X	- [1]	- (162)	- Liquid fraction in container
Y			
Y	- [1]	- (18)	- A/B
Z			
**Z	- [1]	-	- Compressibility factor, Z = 1 for ideal gas
ZOVR2	- [1]	- (87)	- = Z/2, = 0.5 for ideal gas
*ZTT	- [°K]	- (62)	- Input argument value of temperature in the subroutine ATSM

APPENDIX D

LH_2 PROGRAM—DATA INPUTS

CODE	[0]	= 2 for a new run = 1 for continuation of prior run via format input
DT	[1]	Initial estimate of dimensionless time step
EPSLON	[1]	Maximum fractional change in stream function between iterations before iteration is terminated
M	[0]	Number of vertical grid spaces in liquid
N	[0]	Number of radial grid spaces
NC	[0]	Minimum number of time steps NT before fractional temperature changes between time steps is computed
NDIM	[0]	Number of points which must be selected out of given table (ZTT,FHHFG)
NE	[0]	Maximum number of iterations permitted in computations of stream function
NMAX	[0]	Maximum number of time steps NT permitted before program is terminated
NR	[0]	Multiple of index steps of grid spaces for which fractional change in stream function with iterations is computed
N1	[0]	Minimum number of time steps NT before punchout format is executed
P	[lbf/in.^{2}]	Total number of vertical grid spaces
TAU1	[sec]	Basic multiple of real time for which printout is executed
TAU2	[sec]	Basic multiple of real time for which punchout is executed
A	[ft]	Tank radius
ALPHA	[ft^2/sec]	Thermal diffusivity of liquid

ALPHAV	[ft^2/sec]	Thermal diffusivity of vapor
ALPHAW	[ft^2/sec]	Thermal diffusivity of tank wall
AOVERB	[1]	Ratio of tank radius to height
BEITA	[$°F^{-1}$]	Volumetric coefficient of expansion of liquid
B1,B2,B3, and B4		Coefficients in pressure and temperature relation
CP	[Btu/lbm-°F]	Specific heat of liquid
CPV	[Btu/lbm-°F]	Specific heat of vapor, constant pressure
CPW	[Btu/lbm-°F]	Specific heat of tank wall
CV	[Btu/lbm-°F]	Specific heat of vapor, constant volume
DELTA	[ft]	Tank wall thickness
DTS	[°R]	Imposed maximum permissible temperature difference between liquid nodes adjacent to tank wall and saturation
DTW	[°R]	Imposed maximum permissible temperature difference between tank wall and saturation
FHHFG	(Joule/gram mole]	Input function values of heat of vaporization in table between temperature and heat of vaporization
G	[ft/sec^2]	Acceleration corresponding to effective body force acting on tank
KG	[Btu/sec-ft-°F]	Thermal conductivity of vapor
KL	[Btu/sec-ft-°F]	Thermal conductivity of liquid
NEW	[ft^2/sec]	Kinematic viscosity of liquid
NEWV	[ft^2/sec]	Kinematic viscosity of vapor
PO	[$lbf/in.^2$]	Initial system pressure

QSURFG	[Btu/sec-ft^2]	Imposed heat flux on tank exterior on vapor portion
QSURFL	[Btu/sec-ft^2]	Imposed heat flux on tank exterior on liquid portion
RGAS	[lbf-ft/lbm-°R]	Gas constant of vapor
ROL	[lbm/ft^3]	Liquid density
ROW	[lbm/ft^3]	Density of tank wall
X	[1]	Initial fraction of liquid in tank
Z	[1]	Compressibility factor
ZTT	[°K]	Input argument values of temperature in table between temperature and heat of vaporization

APPENDIX E

LH_2 PROGRAM—TYPICAL OUTPUT (RUN B-H 47)

```
$RUN  CYLIGH**SSP                5=*SOURCE* 6=*SINK* 7=*PUNCH*
EXECUTION BEGINS
&DATA1
A=  11.000000    ,AOVERB= 0.37699997    ,P=         30,M=         20,N=         20,X= 0.32299995    ,CODE=          2,DT=
 0.99999943E-06,NMAX=       1644,PO=  12.400000    ,G= 0.55000000E-02,QSURFG= 0.43199994E-02,QSURFL= 0.45999996E-01,DTW=
  1.0000000    ,DTS=  1.0000000    ,ALPHA= 0.16599997E-05,NEW= 0.20649995E-05,KL= 0.18899998E-04,BEITA= 0.86199977E-02,ROL=
  4.3899994    ,CP=  2.5999994    ,ALPHAV= 0.10600000E-04,NEWV= 0.84999992E-05,KG= 0.24999999E-05,CPV=  2.8599997    ,CV=
  1.4919996    ,RGAS=  766.39990    ,ALPHAW= 0.19849995E-05,CPW= 0.34999996    ,ROW=  10.000000    ,DELTA= 0.59099998E-01,TAU1=
       200,N1=         1,NE=       160,EPSLON= 0.99999979E-02,NC=         5,NR=         4,B1=  3.1679363    ,B2=
 -90.174744    ,B3=  1.8079195    ,B4= 0.97138286E-02,Z=  1.0000000    ,ZTT=  18.000000    ,  19.000000    ,  20.000000    ,
  21.000000    ,  22.000000    ,  23.000000    ,  24.000000    ,  25.000000    ,  26.000000    ,  27.000000    ,  28.000000    ,
  29.000000    ,FHHFG=  911.59985    ,  907.29980    ,  900.19995    ,  898.29980    ,  890.59985    ,  877.29980    ,
  860.50000    ,  839.69995    ,  814.59985    ,  784.59985    ,  704.29980    ,  651.29980    ,NDIM=          5,TAU2=       1500
&END
&DATA2
CONST=  72891568.    ,CONST2= 0.13719006E-07,CONST1= 0.69400207E 10,CONST3= 0.14409178E-09,PR=  1.2439756    ,PRV= 0.80188674
&END
```

NT= 1644 TIME= 0.646461E-04 TAU= 4712.152344 DT= 0.287711E-07

UR= 0.168978E 04 UU=-0.414617E 02 PRESS= 18.574661 Z= 1.000000

X= 0.320767 DX= 0.016038 DME=-0.234399E-03 DMT=-0.439927E 00

DMB= 0.057820 DMBT= 106.511505 DM=-0.568196E-01 DMTT=-0.106951E 03

RQIN= 0.120051E 00 DQIDT= 0.395722E-02 DWDT= 0.021672 DQWDT= 0.710023

HFG= 193.040054 TSAT= 37.956543 TINIT= 35.468872

AXIAL VELOCITY COMPONENT---U(I,J)

1	0.0	0.0	0.0	0.0	0.0	0.0	0.0
	0.0	0.0	0.0	0.0	0.0	0.0	0.0
	0.0	0.0	0.0	0.0	0.0	0.0	0.0
2	-0.378249E 05	-0.380702E 05	-0.391893E 05	-0.404994E 05	-0.419683E 05	-0.433900E 05	-0.445103E 05
	-0.450434E 05	-0.446796E 05	-0.430679E 05	-0.397489E 05	-0.339494E 05	-0.234420E 05	0.124573E 04
	0.249151E 05	0.320525E 05	0.299789E 05	0.178306E 05	-0.258490E 05	0.920880E 04	0.0
3	-0.742263E 05	-0.746481E 05	-0.767244E 05	-0.791901E 05	-0.819737E 05	-0.846552E 05	-0.867292E 05
	-0.876438E 05	-0.868214E 05	-0.836477E 05	-0.774085E 05	-0.671303E 05	-0.512657E 05	-0.278801E 05
	-0.137634E 04	0.211788E 05	0.354701E 05	0.351857E 05	0.256945E 04	0.833868E 05	0.0
4	-0.108251E 06	-0.108802E 06	-0.111703E 06	-0.115181E 06	-0.119112E 06	-0.122863E 06	-0.125696E 06
	-0.126825E 06	-0.125466E 06	-0.120843E 06	-0.112164E 06	-0.985822E 05	-0.792690E 05	-0.540331E 05
	-0.251982E 05	0.418896E 04	0.310598E 05	0.497999E 05	0.380904E 05	0.160392E 06	0.0
5	-0.139174E 06	-0.139825E 06	-0.143438E 06	-0.147793E 06	-0.152700E 06	-0.157329E 06	-0.160730E 06
	-0.161927E 06	-0.159983E 06	-0.154029E 06	-0.143267E 06	-0.126975E 06	-0.104651E 06	-0.764362E 05
	-0.436535E 05	-0.802578E 04	0.286538E 05	0.629300E 05	0.681690E 05	0.226372E 06	0.0
6	-0.166405E 06	-0.167137E 06	-0.171362E 06	-0.176464E 06	-0.182183E 06	-0.187509E 06	-0.191316E 06
	-0.192470E 06	-0.189926E 06	-0.182759E 06	-0.170171E 06	-0.151485E 06	-0.126261E 06	-0.945881E 05
	-0.572845E 05	-0.154527E 05	0.296418E 05	0.754031E 05	0.907488E 05	0.278579E 06	0.0
7	-0.189459E 06	-0.190259E 06	-0.195001E 06	-0.200727E 06	-0.207106E 06	-0.212978E 06	-0.217065E 06
	-0.218114E 06	-0.214996E 06	-0.206752E 06	-0.192565E 06	-0.171725E 06	-0.143716E 06	-0.108483E 06
	-0.666256E 05	-0.189586E 05	0.334080E 05	0.876415E 05	0.106495E 06	0.316748E 06	0.0
8	-0.207944E 06	-0.208801E 06	-0.213971E 06	-0.220204E 06	-0.227111E 06	-0.233407E 06	-0.237694E 06
	-0.238625E 06	-0.235010E 06	-0.225859E 06	-0.210322E 06	-0.187602E 06	-0.157025E 06	-0.118379E 06
	-0.722409E 05	-0.193060E 05	0.395220E 05	0.101129E 06	0.119459E 06	0.341486E 06	0.0
9	-0.221545E 06	-0.222450E 06	-0.227961E 06	-0.234596E 06	-0.241919E 06	-0.248548E 06	-0.252997E 06
	-0.253844E 06	-0.249859E 06	-0.240025E 06	-0.223439E 06	-0.199191E 06	-0.166413E 06	-0.124718E 06
	-0.747902E 05	-0.173435E 05	0.472957E 05	0.115206E 06	0.165537E 06	0.373586E 06	0.0
10	-0.230026E 06	-0.230968E 06	-0.236737E 06	-0.243676E 06	-0.251318E 06	-0.258218E 06	-0.262824E 06
	-0.263668E 06	-0.259487E 06	-0.249241E 06	-0.231977E 06	-0.206663E 06	-0.172231E 06	-0.128098E 06
	-0.750733E 05	-0.141911E 05	0.551203E 05	0.128615E 06	0.210632E 06	0.396591E 06	0.0
11	-0.233216E 06	-0.234184E 06	-0.240128E 06	-0.247277E 06	-0.255155E 06	-0.262280E 06	-0.267067E 06
	-0.268019E 06	-0.263853E 06	-0.253514E 06	-0.236010E 06	-0.210212E 06	-0.174879E 06	-0.129230E 06
	-0.740239E 05	-0.110449E 05	0.611046E 05	0.138815E 06	0.241424E 06	0.406940E 06	0.0

12	-0.231018E 06	-0.231999E 06	-0.238031E 06	-0.245295E 06	-0.253326E 06	-0.260639E 06	-0.265642E 06
	-0.266830E 06	-0.262913E 06	-0.252830E 06	-0.235576E 06	-0.209981E 06	-0.174701E 06	-0.128785E 06
	-0.727905E 05	-0.879692E 04	0.642831E 05	0.145318E 06	0.260186E 06	0.406961E 06	0.0
13	-0.223407E 06	-0.224382E 06	-0.230407E 06	-0.237683E 06	-0.245776E 06	-0.253233E 06	-0.258486E 06
	-0.260037E 06	-0.256600E 06	-0.247125E 06	-0.230634E 06	-0.205998E 06	-0.171870E 06	-0.127151E 06
	-0.719883E 05	-0.804719E 04	0.650273E 05	0.148934E 06	0.270015E 06	0.398148E 06	0.0
14	-0.210444E 06	-0.211389E 06	-0.217295E 06	-0.224459E 06	-0.232501E 06	-0.240035E 06	-0.245543E 06
	-0.247561E 06	-0.244816E 06	-0.236275E 06	-0.221029E 06	-0.198064E 06	-0.166135E 06	-0.124034E 06
	-0.713168E 05	-0.867249E 04	0.639010E 05	0.149782E 06	0.271190E 06	0.380439E 06	0.0
15	-0.192282E 06	-0.193172E 06	-0.198824E 06	-0.205721E 06	-0.213556E 06	-0.221048E 06	-0.226771E 06
	-0.229314E 06	-0.227430E 06	-0.220107E 06	-0.206506E 06	-0.185769E 06	-0.156835E 06	-0.118478E 06
	-0.696769E 05	-0.995604E 04	0.609483E 05	0.146487E 06	0.262142E 06	0.353475E 06	0.0
16	-0.169193E 06	-0.169999E 06	-0.175233E 06	-0.181666E 06	-0.189079E 06	-0.196339E 06	-0.202155E 06
	-0.205210E 06	-0.204300E 06	-0.198428E 06	-0.186800E 06	-0.168694E 06	-0.143266E 06	-0.109405E 06
	-0.657874E 05	-0.110870E 05	0.555987E 05	0.136862E 06	0.241363E 06	0.317529E 06	0.0
17	-0.141586E 06	-0.142279E 06	-0.146895E 06	-0.152620E 06	-0.159323E 06	-0.166065E 06	-0.171740E 06
	-0.175183E 06	-0.175276E 06	-0.171046E 06	-0.161711E 06	-0.146619E 06	-0.125110E 06	-0.963173E 05
	-0.590221E 05	-0.116766E 05	0.471807E 05	0.119321E 06	0.208787E 06	0.273584E 06	0.0
18	-0.110028E 06	-0.110579E 06	-0.114355E 06	-0.119080E 06	-0.124710E 06	-0.130533E 06	-0.135686E 06
	-0.139228E 06	-0.140203E 06	-0.137726E 06	-0.131030E 06	-0.119480E 06	-0.102514E 06	-0.795191E 05
	-0.496762E 05	-0.118285E 05	0.355629E 05	0.939395E 05	0.166076E 06	0.222615E 06	0.0
19	-0.752670E 05	-0.756488E 05	-0.783513E 05	-0.817629E 05	-0.858976E 05	-0.902924E 05	-0.943748E 05
	-0.974974E 05	-0.989738E 05	-0.981205E 05	-0.942951E 05	-0.869155E 05	-0.754593E 05	-0.594378E 05
	-0.383527E 05	-0.116376E 05	0.216426E 05	0.626972E 05	0.115757E 06	0.164136E 06	0.0
20	-0.382286E 05	-0.384237E 05	-0.398423E 05	-0.416467E 05	-0.438651E 05	-0.462792E 05	-0.486167E 05
	-0.505647E 05	-0.517847E 05	-0.519273E 05	-0.506445E 05	-0.475917E 05	-0.424193E 05	-0.347498E 05
	-0.241396E 05	-0.100477E 05	0.779323E 04	0.293539E 05	0.598911E 05	0.938967E 05	0.0
21	0.193843E 04	0.193843E 04	0.258457E 04	0.258456E 04	0.258457E 04	0.258457E 04	0.258457E 04
	0.258457E 04	0.258456E 04	0.258457E 04	0.258457E 04	0.258456E 04	0.258456E 04	0.258457E 04
	0.258457E 04	0.258457E 04	0.258457E 04	0.258457E 04	0.258457E 04	-0.486306E 04	0.0
22	-0.159402E 05	-0.160391E 05	-0.212446E 05	-0.208778E 05	-0.200921E 05	-0.188664E 05	-0.172390E 05
	-0.152463E 05	-0.129036E 05	-0.102357E 05	-0.733035E 04	-0.437785E 04	-0.164662E 04	0.576461E 03
	0.206247E 04	0.274983E 04	0.274792E 04	0.230538E 04	0.106085E 04	0.841988E 04	0.0
23	-0.248086E 05	-0.249588E 05	-0.328232E 05	-0.320338E 05	-0.306350E 05	-0.287478E 05	-0.265189E 05
	-0.239716E 05	-0.209989E 05	-0.174561E 05	-0.133068E 05	-0.879422E 04	-0.447141E 04	-0.866002E 03
	0.181775E 04	0.363547E 04	0.483024E 04	0.582175E 04	0.717641E 04	0.165147E 05	0.0
24	-0.292020E 05	-0.293514E 05	-0.382687E 05	-0.370698E 05	-0.352583E 05	-0.331318E 05	-0.308863E 05
	-0.284369E 05	-0.254752E 05	-0.216146E 05	-0.166001E 05	-0.107241E 05	-0.524845E 04	-0.153346E 04
	0.353595E 03	0.940382E 03	0.585448E 03	-0.470401E 03	0.277533E 04	0.261061E 05	0.0
25	-0.293643E 05	-0.294727E 05	-0.381314E 05	-0.367213E 05	-0.348349E 05	-0.328590E 05	-0.309343E 05
	-0.288352E 05	-0.260930E 05	-0.221233E 05	-0.163870E 05	-0.897955E 04	-0.200731E 04	0.139059E 04
	0.135566E 04	-0.147450E 02	-0.166852E 04	-0.224883E 04	0.176393E 05	0.499934E 05	0.0
26	-0.266108E 05	-0.266729E 05	-0.343586E 05	-0.330222E 05	-0.314089E 05	-0.299191E 05	-0.286445E 05
	-0.273334E 05	-0.255464E 05	-0.227475E 05	-0.183438E 05	-0.118901E 05	-0.404674E 04	0.135375E 04
	0.148553E 04	-0.154596E 04	-0.503945E 04	-0.993001E 04	0.136690E 05	0.580305E 05	0.0

27	-0.219390E 05	-0.219704E 05	-0.282592E 05	-0.271770E 05	-0.260119E 05	-0.251662E 05	-0.247391E 05
	-0.245462E 05	-0.242886E 05	-0.236244E 05	-0.221435E 05	-0.193415E 05	-0.146756E 05	-0.829942E 04
	-0.217990E 04	0.104445E 04	0.551476E 03	-0.355625E 04	0.255971E 05	0.754558E 05	0.0
28	-0.159101E 05	-0.159282E 05	-0.204646E 05	-0.196851E 05	-0.189631E 05	-0.186988E 05	-0.190286E 05
	-0.198592E 05	-0.210311E 05	-0.223734E 05	-0.236417E 05	-0.244164E 05	-0.239926E 05	-0.213062E 05
	-0.151160E 05	-0.581411E 04	0.174822E 04	0.196837E 04	0.367004E 05	0.926055E 05	0.0
29	-0.916709E 04	-0.918605E 04	-0.117330E 05	-0.112039E 05	-0.107697E 05	-0.108103E 05	-0.115089E 05
	-0.128655E 05	-0.148534E 05	-0.174769E 05	-0.206947E 05	-0.242600E 05	-0.274680E 05	-0.287678E 05
	-0.253508E 05	-0.138005E 05	0.206008E 04	0.142887E 05	0.484380E 05	0.896615E 05	0.0
30	-0.305114E 04	-0.307754E 04	-0.383036E 04	-0.349811E 04	-0.316710E 04	-0.311867E 04	-0.354270E 04
	-0.450334E 04	-0.608132E 04	-0.848049E 04	-0.120195E 05	-0.170502E 05	-0.237582E 05	-0.316400E 05
	-0.382690E 05	-0.370678E 05	-0.162548E 05	0.278840E 05	0.827401E 05	0.946931E 05	0.0
31	0.0	0.0	0.0	0.0	0.0	0.0	0.0
	0.0	0.0	0.0	0.0	0.0	0.0	0.0
	0.0	0.0	0.0	0.0	0.0	0.0	0.0

RADIAL VELOCITY COMPONENT---V(I,J)

1	0.0	0.0	0.0	0.0	0.0	0.0	0.0
	0.0	0.0	0.0	0.0	0.0	0.0	0.0
	0.0	0.0	0.0	0.0	0.0	0.0	0.0
2	0.0	0.580980E 05	0.118038E 06	0.180370E 06	0.245641E 06	0.313909E 06	0.384613E 06
	0.456505E 06	0.527607E 06	0.595182E 06	0.655663E 06	0.704512E 06	0.736225E 06	0.746371E 06
	0.740046E 06	0.698334E 06	0.622899E 06	0.532254E 06	0.450417E 06	0.370143E 06	0.0
3	0.0	0.551072E 05	0.111727E 06	0.170441E 06	0.231770E 06	0.295730E 06	0.361734E 06
	0.428558E 06	0.494364E 06	0.556763E 06	0.612943E 06	0.660017E 06	0.696284E 06	0.726273E 06
	0.770528E 06	0.792753E 06	0.772561E 06	0.704808E 06	0.584055E 06	0.385621E 06	0.0
4	0.0	0.507899E 05	0.102844E 06	0.156727E 06	0.212884E 06	0.271262E 06	0.331246E 06
	0.391671E 06	0.450886E 06	0.506893E 06	0.557544E 06	0.600915E 06	0.636013E 06	0.663743E 06
	0.685231E 06	0.695978E 06	0.684144E 06	0.632312E 06	0.520394E 06	0.343039E 06	0.0
5	0.0	0.454628E 05	0.919959E 05	0.140112E 06	0.190160E 06	0.242019E 06	0.295078E 06
	0.348259E 06	0.400123E 06	0.449008E 06	0.493215E 06	0.531218E 06	0.561885E 06	0.584488E 06
	0.597606E 06	0.596811E 06	0.576109E 06	0.525721E 06	0.432455E 06	0.292583E 06	0.0
6	0.0	0.393049E 05	0.795144E 05	0.121071E 06	0.164230E 06	0.208830E 06	0.254293E 06
	0.299660E 06	0.343698E 06	0.385031E 06	0.422267E 06	0.454040E 06	0.478984E 06	0.495549E 06
	0.501562E 06	0.493639E 06	0.467473E 06	0.418374E 06	0.342170E 06	0.241974E 06	0.0
7	0.0	0.324664E 05	0.656883E 05	0.100032E 06	0.135675E 06	0.172450E 06	0.209838E 06
	0.247026E 06	0.282988E 06	0.316598E 06	0.346697E 06	0.372027E 06	0.391076E 06	0.401916E 06
	0.402232E 06	0.389489E 06	0.360569E 06	0.313055E 06	0.248934E 06	0.193300E 06	0.0
8	0.0	0.250792E 05	0.507754E 05	0.773803E 05	0.105018E 06	0.133540E 06	0.162523E 06
	0.191313E 06	0.219100E 06	0.245000E 06	0.268062E 06	0.287150E 06	0.300733E 06	0.306756E 06
	0.302934E 06	0.287403E 06	0.257506E 06	0.209716E 06	0.141394E 06	0.304166E 05	0.0
9	0.0	0.172632E 05	0.350117E 05	0.534668E 05	0.727231E 05	0.926764E 05	0.113024E 06
	0.133295E 06	0.152901E 06	0.171198E 06	0.187463E 06	0.200737E 06	0.209617E 06	0.212113E 06
	0.206038E 06	0.190046E 06	0.162196E 06	0.116806E 06	0.448642E 05	-0.132024E 06	0.0

10	0.0	-0.913023E 04	0.186163E 05	0.286144E 05	0.392074E 05	0.503617E 05	0.619099E 05
	0.735813E 05	0.850262E 05	0.958500E 05	0.105585E 06	0.113550E 06	0.118641E 06	0.119165E 06
	0.113145E 06	0.993865E 05	0.780261E 05	0.428929E 05	-0.129807E 05	-0.142009E 06	0.0
11	0.0	0.788995E 03	0.180007E 04	0.312769E 04	0.485966E 04	0.703918E 04	0.965693E 04
	0.126528E 05	0.159284E 05	0.193587E 05	0.227718E 05	0.258634E 05	0.280262E 05	0.281813E 05
	0.248135E 05	0.165972E 05	0.449105E 04	-0.149826E 05	-0.505563E 05	-0.121663E 06	0.0
12	0.0	-0.764898E 04	-0.152286E 05	-0.226948E 05	-0.299531E 05	-0.368751E 05	-0.433037E 05
	-0.490769E 05	-0.540396E 05	-0.580389E 05	-0.609069E 05	-0.624696E 05	-0.626230E 05	-0.615613E 05
	-0.601114E 05	-0.599016E 05	-0.619000E 05	-0.663316E 05	-0.859498E 05	-0.114918E 06	0.0
13	0.0	-0.160628E 05	-0.322376E 05	-0.485272E 05	-0.648398E 05	-0.809563E 05	-0.965553E 05
	-0.111245E 06	-0.124614E 06	-0.136230E 06	-0.145586E 06	-0.151976E 06	-0.154506E 06	-0.152362E 06
	-0.145633E 06	-0.136367E 06	-0.127978E 06	-0.120899E 06	-0.125648E 06	-0.119552E 06	0.0
14	0.0	-0.243142E 05	-0.489550E 05	-0.739879E 05	-0.993396E 05	-0.124718E 06	-0.149634E 06
	-0.173464E 06	-0.195529E 06	-0.215121E 06	-0.231428E 06	-0.243327E 06	-0.249274E 06	-0.247559E 06
	-0.237426E 06	-0.220775E 06	-0.202301E 06	-0.184010E 06	-0.169496E 06	-0.127044E 06	0.0
15	0.0	-0.322381E 05	-0.650610E 05	-0.986206E 05	-0.132898E 06	-0.167554E 06	-0.201946E 06
	-0.235208E 06	-0.266368E 06	-0.294426E 06	-0.318313E 06	-0.336674E 06	-0.347617E 06	-0.348840E 06
	-0.338603E 06	-0.317485E 06	-0.289095E 06	-0.255828E 06	-0.214306E 06	-0.132979E 06	0.0
16	0.0	-0.396383E 05	-0.801669E 05	-0.121862E 06	-0.164807E 06	-0.208661E 06	-0.252659E 06
	-0.295692E 06	-0.336446E 06	-0.373561E 06	-0.405673E 06	-0.431270E 06	-0.448389E 06	-0.454463E 06
	-0.446738E 06	-0.423481E 06	-0.384910E 06	-0.331649E 06	-0.256733E 06	-0.137448E 06	0.0
17	0.0	-0.462824E 05	-0.938063E 05	-0.143011E 06	-0.194146E 06	-0.246942E 06	-0.300577E 06
	-0.353724E 06	-0.404691E 06	-0.451618E 06	-0.492651E 06	-0.525943E 06	-0.549424E 06	-0.560436E 06
	-0.555472E 06	-0.530447E 06	-0.481446E 06	-0.405686E 06	-0.296154E 06	-0.143988E 06	0.0
18	0.0	-0.519046E 05	-0.105427E 06	-0.161209E 06	-0.219732E 06	-0.280901E 06	-0.343953E 06
	-0.407443E 06	-0.469335E 06	-0.527171E 06	-0.578312E 06	-0.620101E 06	-0.649862E 06	-0.664621E 06
	-0.660576E 06	-0.632498E 06	-0.573643E 06	-0.477403E 06	-0.337847E 06	-0.159002E 06	0.0
19	0.0	-0.562210E 05	-0.114420E 06	-0.175460E 06	-0.240109E 06	-0.308553E 06	-0.380251E 06
	-0.453860E 06	-0.527219E 06	-0.597423E 06	-0.660980E 06	-0.714005E 06	-0.752403E 06	-0.771927E 06
	-0.768079E 06	-0.735771E 06	-0.668787E 06	-0.558515E 06	-0.397027E 06	-0.192796E 06	0.0
20	0.0	-0.589438E 05	-0.120138E 06	-0.184631E 06	-0.253461E 06	-0.327121E 06	-0.405410E 06
	-0.487313E 06	-0.570927E 06	-0.653426E 06	-0.731102E 06	-0.799455E 06	-0.853314E 06	-0.886986E 06
	-0.894412E 06	-0.869262E 06	-0.804718E 06	-0.691506E 06	-0.518302E 06	-0.276474E 06	0.0
21	0.0	-0.598984E 05	-0.122163E 06	-0.187933E 06	-0.258389E 06	-0.334212E 06	-0.415452E 06
	-0.501406E 06	-0.590540E 06	-0.680434E 06	-0.767769E 06	-0.848323E 06	-0.916938E 06	-0.967446E 06
	-0.992490E 06	-0.983263E 06	-0.929443E 06	-0.821014E 06	-0.645659E 06	-0.368457E 06	0.0
22	0.0	0.467443E 04	0.935100E 04	0.139241E 05	0.182466E 05	0.221991E 05	0.257266E 05
	0.288060E 05	0.313929E 05	0.333909E 05	0.346604E 05	0.350756E 05	0.346133E 05	0.333555E 05
	0.313733E 05	0.288956E 05	0.260754E 05	0.229291E 05	0.193269E 05	0.149716E 05	0.0
23	0.0	0.228546E 04	0.451225E 04	0.659273E 04	0.843916E 04	0.100630E 05	0.115626E 05
	0.130337E 05	0.144952E 05	0.158549E 05	0.169070E 05	0.173907E 05	0.171932E 05	0.165840E 05
	0.159137E 05	0.153022E 05	0.148307E 05	0.145305E 05	0.146069E 05	0.130583E 05	0.0
24	0.0	0.790798E 03	0.149089E 04	0.205333E 04	0.246332E 04	0.281558E 04	0.323943E 04
	0.380467E 04	0.448264E 04	0.513748E 04	0.550582E 04	0.519705E 04	0.395016E 04	0.244511E 04
	0.187154E 04	0.236931E 04	0.378307E 04	0.592993E 04	0.793501E 04	-0.899199E 03	0.0

25	0.0	-0.548076E 03	-0.116432E 04	-0.184137E 04	-0.252326E 04	-0.309082E 04	-0.344759E 04
	-0.355721E 04	-0.342558E 04	-0.308300E 04	-0.260716E 04	-0.220913E 04	-0.237271E 04	-0.355645E 04
	-0.453780E 04	-0.411855E 04	-0.245991E 04	-0.157682E 03	0.341742E 04	-0.865826E 04	0.0
26	0.0	-0.141509E 04	-0.284495E 04	-0.424541E 04	-0.552814E 04	-0.658674E 04	-0.734017E 04
	-0.771755E 04	-0.761345E 04	-0.685280E 04	-0.518400E 04	-0.235238E 04	0.152208E 04	0.498464E 04
	0.612787E 04	0.534374E 04	0.404517E 04	0.327125E 04	0.456913E 04	0.572612E 03	0.0
27	0.0	-0.200739E 04	-0.398759E 04	-0.588695E 04	-0.762434E 04	-0.912031E 04	-0.103005E 05
	-0.110678E 05	-0.112649E 05	-0.106464E 05	-0.886509E 04	-0.549556E 04	-0.167799E 03	0.681389E 04
	0.127739E 05	0.148507E 05	0.127010E 05	0.858729E 04	0.421363E 04	-0.916628E 04	0.0
28	0.0	-0.241257E 04	-0.478004E 04	-0.705769E 04	-0.919408E 04	-0.111552E 05	-0.128988E 05
	-0.143474E 05	-0.153668E 05	-0.157467E 05	-0.151913E 05	-0.133328E 05	-0.978833E 04	-0.428612E 04
	0.272959E 04	0.865678E 04	0.941495E 04	0.576475E 04	-0.107744E 04	-0.546366E 04	0.0
29	0.0	-0.248330E 04	-0.491659E 04	-0.726901E 04	-0.953624E 04	-0.117664E 05	-0.139989E 05
	-0.162341E 05	-0.184242E 05	-0.204414E 05	-0.220243E 05	-0.227136E 05	-0.217853E 05	-0.182345E 05
	-0.109512E 05	0.339951E 03	0.113410E 05	0.115575E 05	-0.484662E 04	-0.139205E 05	0.0
30	0.0	-0.183686E 04	-0.362919E 04	-0.533200E 04	-0.693180E 04	-0.852488E 04	-0.102637E 05
	-0.122940E 05	-0.147379E 05	-0.176945E 05	-0.212177E 05	-0.252576E 05	-0.295504E 05	-0.334603E 05
	-0.358219E 05	-0.349684E 05	-0.295000E 05	-0.248009E 05	-0.287082E 05	-0.185867E 05	0.0
31	0.0	0.0	0.0	0.0	0.0	0.0	0.0
	0.0	0.0	0.0	0.0	0.0	0.0	0.0
	0.0	0.0	0.0	0.0	0.0	0.0	0.0

NON DIMENSIONAL TEMPERATURE RISE---T(I,J)

1	0.661023E 09	0.466617E 09	0.472951E 09	0.481880E 09	0.492565E 09	0.504777E 09	0.518218E 09
	0.532434E 09	0.546878E 09	0.560891E 09	0.573748E 09	0.584547E 09	0.591854E 09	0.588784E 09
	0.534301E 09	0.468383E 09	0.407998E 09	0.372266E 09	0.720757E 09	0.242045E 11	0.242045E 11
2	0.164309E 11	0.165230E 11	0.166530E 11	0.168174E 11	0.170136E 11	0.172374E 11	0.174828E 11
	0.177416E 11	0.180037E 11	0.182574E 11	0.184893E 11	0.186836E 11	0.188123E 11	0.186966E 11
	0.169536E 11	0.148741E 11	0.129712E 11	0.117627E 11	0.126854E 11	0.136863E 11	0.242045E 11
3	0.165675E 11	0.167038E 11	0.169105E 11	0.171800E 11	0.175050E 11	0.178759E 11	0.182792E 11
	0.186979E 11	0.191123E 11	0.195019E 11	0.198468E 11	0.201290E 11	0.203305E 11	0.204284E 11
	0.204139E 11	0.199698E 11	0.190766E 11	0.180741E 11	0.179770E 11	0.163518E 11	0.242045E 11
4	0.166351E 11	0.168033E 11	0.170725E 11	0.174294E 11	0.178611E 11	0.183509E 11	0.188767E 11
	0.194119E 11	0.199271E 11	0.203936E 11	0.207878E 11	0.210940E 11	0.213063E 11	0.214278E 11
	0.214683E 11	0.214185E 11	0.211081E 11	0.204905E 11	0.199998E 11	0.179135E 11	0.242045E 11
5	0.166814E 11	0.168746E 11	0.171969E 11	0.176287E 11	0.181507E 11	0.187385E 11	0.193612E 11
	0.199817E 11	0.205610E 11	0.210629E 11	0.214610E 11	0.217437E 11	0.219163E 11	0.219995E 11
	0.220216E 11	0.220034E 11	0.218596E 11	0.214659E 11	0.209588E 11	0.188709E 11	0.242045E 11
6	0.167174E 11	0.169306E 11	0.172982E 11	0.177939E 11	0.183921E 11	0.190605E 11	0.197591E 11
	0.204409E 11	0.210571E 11	0.215649E 11	0.219358E 11	0.221625E 11	0.222617E 11	0.222696E 11
	0.222343E 11	0.221981E 11	0.221141E 11	0.218569E 11	0.214254E 11	0.194856E 11	0.242045E 11
7	0.167475E 11	0.169767E 11	0.173821E 11	0.179314E 11	0.185925E 11	0.193260E 11	0.200831E 11
	0.208074E 11	0.214413E 11	0.219356E 11	0.222605E 11	0.224138E 11	0.224222E 11	0.223363E 11
	0.222233E 11	0.221548E 11	0.221117E 11	0.219660E 11	0.216300E 11	0.198911E 11	0.242045E 11

8	0.167740E 11	0.170156E 11	0.174516E 11	0.180442E 11	0.187556E 11	0.195401E 11	0.203410E 11
	0.210936E 11	0.217323E 11	0.222026E 11	0.224743E 11	0.225497E 11	0.224646E 11	0.222808E 11
	0.220804E 11	0.219706E 11	0.219747E 11	0.219394E 11	0.216845E 11	0.199997E 11	0.242045E 11
9	0.167980E 11	0.170489E 11	0.175083E 11	0.181337E 11	0.188832E 11	0.197055E 11	0.205377E 11
	0.213082E 11	0.219447E 11	0.223886E 11	0.226092E 11	0.226136E 11	0.224445E 11	0.221708E 11
	0.218811E 11	0.217093E 11	0.217844E 11	0.218681E 11	0.216713E 11	0.242045E 11	0.242045E 11
10	0.168206E 11	0.170776E 11	0.175529E 11	0.182008E 11	0.189762E 11	0.198240E 11	0.206768E 11
	0.214577E 11	0.220897E 11	0.225110E 11	0.226911E 11	0.226403E 11	0.224066E 11	0.220621E 11
	0.216931E 11	0.213992E 11	0.216004E 11	0.218065E 11	0.216970E 11	0.242045E 11	0.242045E 11
11	0.168423E 11	0.171026E 11	0.175860E 11	0.182458E 11	0.190349E 11	0.198965E 11	0.207603E 11
	0.215466E 11	0.221755E 11	0.225832E 11	0.227391E 11	0.226558E 11	0.223843E 11	0.219989E 11
	0.215826E 11	0.210996E 11	0.215071E 11	0.217721E 11	0.218353E 11	0.242045E 11	0.242045E 11
12	0.168638E 11	0.171242E 11	0.176081E 11	0.182687E 11	0.190594E 11	0.199230E 11	0.207891E 11
	0.215772E 11	0.222067E 11	0.226130E 11	0.227653E 11	0.226765E 11	0.223992E 11	0.220112E 11
	0.216067E 11	0.213311E 11	0.215099E 11	0.217764E 11	0.220448E 11	0.242045E 11	0.242045E 11
13	0.168854E 11	0.171407E 11	0.176155E 11	0.182656E 11	0.190464E 11	0.199029E 11	0.207668E 11
	0.215589E 11	0.221990E 11	0.226216E 11	0.227940E 11	0.227269E 11	0.224728E 11	0.221127E 11
	0.217498E 11	0.215227E 11	0.215971E 11	0.218595E 11	0.223091E 11	0.242045E 11	0.242045E 11
14	0.169078E 11	0.171520E 11	0.176080E 11	0.182355E 11	0.189943E 11	0.198341E 11	0.206912E 11
	0.214903E 11	0.221527E 11	0.226115E 11	0.228294E 11	0.228115E 11	0.226060E 11	0.222920E 11
	0.219679E 11	0.217526E 11	0.217846E 11	0.220475E 11	0.226102E 11	0.242045E 11	0.242045E 11
15	0.169315E 11	0.171589E 11	0.175857E 11	0.181776E 11	0.189007E 11	0.197121E 11	0.205554E 11
	0.213617E 11	0.220557E 11	0.225691E 11	0.228581E 11	0.229179E 11	0.227875E 11	0.225403E 11
	0.222689E 11	0.220779E 11	0.220873E 11	0.223409E 11	0.229263E 11	0.242045E 11	0.242045E 11
16	0.169575E 11	0.171619E 11	0.175487E 11	0.180907E 11	0.187622E 11	0.195297E 11	0.203472E 11
	0.211552E 11	0.218848E 11	0.224679E 11	0.228528E 11	0.230208E 11	0.229953E 11	0.228393E 11
	0.226392E 11	0.224896E 11	0.224897E 11	0.227117E 11	0.232360E 11	0.242045E 11	0.242045E 11
17	0.169870E 11	0.171624E 11	0.174977E 11	0.179737E 11	0.185741E 11	0.192764E 11	0.200479E 11
	0.208424E 11	0.216013E 11	0.222607E 11	0.227627E 11	0.230714E 11	0.231871E 11	0.231520E 11
	0.230415E 11	0.229441E 11	0.229433E 11	0.231145E 11	0.235224E 11	0.242045E 11	0.242045E 11
18	0.170223E 11	0.171626E 11	0.174342E 11	0.178260E 11	0.183309E 11	0.189386E 11	0.196311E 11
	0.203794E 11	0.211416E 11	0.218649E 11	0.224921E 11	0.229724E 11	0.232766E 11	0.234104E 11
	0.234207E 11	0.233859E 11	0.233892E 11	0.235027E 11	0.237735E 11	0.242045E 11	0.242045E 11
19	0.170677E 11	0.171668E 11	0.173621E 11	0.176487E 11	0.180275E 11	0.184988E 11	0.190595E 11
	0.196998E 11	0.204006E 11	0.211312E 11	0.218503E 11	0.225079E 11	0.230534E 11	0.234457E 11
	0.236695E 11	0.237532E 11	0.237726E 11	0.238346E 11	0.239787E 11	0.242045E 11	0.242045E 11
20	0.171340E 11	0.171863E 11	0.172915E 11	0.174490E 11	0.176631E 11	0.179395E 11	0.182849E 11
	0.187047E 11	0.192026E 11	0.197779E 11	0.204245E 11	0.211283E 11	0.218650E 11	0.225963E 11
	0.232653E 11	0.237877E 11	0.240409E 11	0.240686E 11	0.241224E 11	0.242045E 11	0.242045E 11
21	0.172645E 11	0.172645E 11	0.172645E 11	0.172645E 11	0.172645E 11	0.172645E 11	0.172645E 11
	0.172645E 11	0.172645E 11	0.172645E 11	0.172645E 11	0.172645E 11	0.172645E 11	0.172645E 11
	0.172645E 11	0.172645E 11	0.172645E 11	0.172645E 11	0.172645E 11	0.172645E 11	0.242045E 11
22	0.524194E 11	0.524321E 11	0.525597E 11	0.528040E 11	0.531766E 11	0.536431E 11	0.541533E 11
	0.546561E 11	0.550979E 11	0.554163E 11	0.555424E 11	0.554259E 11	0.550748E 11	0.544148E 11
	0.529387E 11	0.512971E 11	0.499698E 11	0.492551E 11	0.499503E 11	0.457376E 11	0.627079E 12

23	0.524838E 11	0.525239E 11	0.528017E 11	0.533697E 11	0.542231E 11	0.552655E 11	0.564037E 11
	0.575785E 11	0.587358E 11	0.597806E 11	0.605382E 11	0.607638E 11	0.602887E 11	0.592548E 11
	0.579581E 11	0.565832E 11	0.552950E 11	0.542200E 11	0.535507E 11	0.533541E 11	0.626661E 12
24	0.524863E 11	0.525649E 11	0.529955E 11	0.538544E 11	0.550866E 11	0.565287E 11	0.580792E 11
	0.597250E 11	0.614751E 11	0.632770E 11	0.649181E 11	0.658951E 11	0.654815E 11	0.637272E 11
	0.618248E 11	0.600371E 11	0.586812E 11	0.577409E 11	0.566563E 11	0.777804E 11	0.628014E 12
25	0.524882E 11	0.526128E 11	0.531619E 11	0.542179E 11	0.556464E 11	0.572429E 11	0.589339E 11
	0.607687E 11	0.628220E 11	0.651103E 11	0.674853E 11	0.693341E 11	0.689915E 11	0.653653E 11
	0.619521E 11	0.596992E 11	0.583481E 11	0.575148E 11	0.574693E 11	0.185211E 12	0.640984E 12
26	0.524892E 11	0.526541E 11	0.532594E 11	0.543754E 11	0.558016E 11	0.573337E 11	0.589356E 11
	0.606935E 11	0.627098E 11	0.650407E 11	0.676514E 11	0.703075E 11	0.722931E 11	0.706154E 11
	0.666151E 11	0.638168E 11	0.637058E 11	0.652118E 11	0.598762E 11	0.183505E 12	0.645059E 12
27	0.524892E 11	0.526674E 11	0.532577E 11	0.543145E 11	0.556091E 11	0.569478E 11	0.583154E 11
	0.598126E 11	0.615512E 11	0.636098E 11	0.660255E 11	0.687762E 11	0.717285E 11	0.742801E 11
	0.745533E 11	0.726387E 11	0.705033E 11	0.703622E 11	0.621772E 11	0.249747E 12	0.652953E 12
28	0.524880E 11	0.526507E 11	0.531647E 11	0.540734E 11	0.551532E 11	0.562239E 11	0.572788E 11
	0.584282E 11	0.598023E 11	0.615197E 11	0.637013E 11	0.664805E 11	0.699825E 11	0.742669E 11
	0.790552E 11	0.818495E 11	0.800908E 11	0.774857E 11	0.702299E 11	0.278469E 12	0.657959E 12
29	0.524857E 11	0.526035E 11	0.529838E 11	0.536657E 11	0.544680E 11	0.552258E 11	0.559258E 11
	0.566785E 11	0.576276E 11	0.589216E 11	0.607450E 11	0.633640E 11	0.671743E 11	0.727257E 11
	0.806019E 11	0.905571E 11	0.888037E 11	0.832229E 11	0.104113E 12	0.344073E 12	0.664486E 12
30	0.524825E 11	0.525324E 11	0.527252E 11	0.531005E 11	0.535634E 11	0.539804E 11	0.543067E 11
	0.546163E 11	0.550264E 11	0.556539E 11	0.566487E 11	0.582675E 11	0.610019E 11	0.658400E 11
	0.748008E 11	0.917672E 11	0.121424E 12	0.148368E 12	0.202377E 12	0.410694E 12	0.668951E 12
31	0.524807E 11	0.524783E 11	0.524789E 11	0.524808E 11	0.524843E 11	0.524894E 11	0.524957E 11
	0.525035E 11	0.525135E 11	0.525277E 11	0.525489E 11	0.525828E 11	0.526397E 11	0.527393E 11
	0.529179E 11	0.532291E 11	0.536918E 11	0.541513E 11	0.577342E 11	0.105846E 12	0.631431E 12

REAL TEMPERATURE RISE---RT(I,J)

1	0.952480E-01	0.672356E-01	0.681483E-01	0.694349E-01	0.709746E-01	0.727341E-01	0.746710E-01
	0.767193E-01	0.788006E-01	0.808197E-01	0.826724E-01	0.842285E-01	0.852812E-01	0.848389E-01
	0.769884E-01	0.674901E-01	0.587891E-01	0.536405E-01	0.103855E 00	0.348767E 01	0.348767E 01
2	0.236756E 01	0.238082E 01	0.239956E 01	0.242325E 01	0.245151E 01	0.248376E 01	0.251912E 01
	0.255642E 01	0.259419E 01	0.263074E 01	0.266416E 01	0.269215E 01	0.271070E 01	0.269403E 01
	0.244288E 01	0.214323E 01	0.186905E 01	0.169491E 01	0.182787E 01	0.197208E 01	0.348767E 01
3	0.238724E 01	0.240688E 01	0.243667E 01	0.247549E 01	0.252233E 01	0.257577E 01	0.263389E 01
	0.269422E 01	0.275393E 01	0.281006E 01	0.285976E 01	0.290042E 01	0.292945E 01	0.294357E 01
	0.294147E 01	0.287749E 01	0.274878E 01	0.260432E 01	0.259034E 01	0.235615E 01	0.348767E 01
4	0.239698E 01	0.242122E 01	0.246001E 01	0.251143E 01	0.257364E 01	0.264421E 01	0.271998E 01
	0.279710E 01	0.287133E 01	0.293856E 01	0.299535E 01	0.303947E 01	0.307006E 01	0.308756E 01
	0.309340E 01	0.308623E 01	0.304151E 01	0.295252E 01	0.288181E 01	0.258119E 01	0.348767E 01
5	0.240366E 01	0.243150E 01	0.247794E 01	0.254015E 01	0.261537E 01	0.270007E 01	0.278979E 01
	0.287920E 01	0.296267E 01	0.303500E 01	0.309236E 01	0.313308E 01	0.315795E 01	0.316995E 01
	0.317313E 01	0.317051E 01	0.314979E 01	0.309306E 01	0.301999E 01	0.271914E 01	0.348767E 01

6	0.240884E 01	0.243956E 01	0.249253E 01	0.256395E 01	0.265014E 01	0.274646E 01	0.284712E 01
	0.294536E 01	0.303416E 01	0.310733E 01	0.316076E 01	0.319344E 01	0.320772E 01	0.320887E 01
	0.320378E 01	0.319857E 01	0.318646E 01	0.314939E 01	0.308722E 01	0.280772E 01	0.348767E 01
7	0.241318E 01	0.244620E 01	0.250462E 01	0.258377E 01	0.267903E 01	0.278472E 01	0.289381E 01
	0.299818E 01	0.308952E 01	0.316073E 01	0.320755E 01	0.322964E 01	0.323085E 01	0.321848E 01
	0.320220E 01	0.319232E 01	0.318611E 01	0.316513E 01	0.311671E 01	0.286614E 01	0.348767E 01
8	0.241699E 01	0.245180E 01	0.251464E 01	0.260002E 01	0.270253E 01	0.281556E 01	0.293097E 01
	0.303941E 01	0.313145E 01	0.319922E 01	0.323836E 01	0.324922E 01	0.323697E 01	0.321048E 01
	0.318161E 01	0.316578E 01	0.316637E 01	0.316128E 01	0.312456E 01	0.288179E 01	0.348767E 01
9	0.242046E 01	0.245660E 01	0.252279E 01	0.261292E 01	0.272092E 01	0.283940E 01	0.295932E 01
	0.307033E 01	0.316205E 01	0.322601E 01	0.325780E 01	0.325843E 01	0.323407E 01	0.319463E 01
	0.315289E 01	0.312813E 01	0.313895E 01	0.315101E 01	0.312265E 01	0.348767E 01	0.348767E 01
10	0.242371E 01	0.246075E 01	0.252923E 01	0.262259E 01	0.273432E 01	0.285648E 01	0.297936E 01
	0.309188E 01	0.318295E 01	0.324366E 01	0.326960E 01	0.326228E 01	0.322860E 01	0.317897E 01
	0.312580E 01	0.308345E 01	0.311244E 01	0.314214E 01	0.312635E 01	0.348767E 01	0.348767E 01
11	0.242684E 01	0.246434E 01	0.253400E 01	0.262906E 01	0.274278E 01	0.286692E 01	0.299139E 01
	0.310469E 01	0.319531E 01	0.325405E 01	0.327652E 01	0.326451E 01	0.322539E 01	0.316986E 01
	0.310987E 01	0.304027E 01	0.309900E 01	0.313718E 01	0.314629E 01	0.348767E 01	0.348767E 01
12	0.242993E 01	0.246746E 01	0.253718E 01	0.263237E 01	0.274630E 01	0.287074E 01	0.299554E 01
	0.310910E 01	0.319981E 01	0.325835E 01	0.328029E 01	0.326749E 01	0.322755E 01	0.317164E 01
	0.311335E 01	0.307363E 01	0.309940E 01	0.313780E 01	0.317648E 01	0.348767E 01	0.348767E 01
13	0.243305E 01	0.246983E 01	0.253825E 01	0.263192E 01	0.274443E 01	0.286784E 01	0.299232E 01
	0.310646E 01	0.319870E 01	0.325959E 01	0.328443E 01	0.327476E 01	0.323814E 01	0.318625E 01
	0.313397E 01	0.310125E 01	0.311197E 01	0.314977E 01	0.321456E 01	0.348767E 01	0.348767E 01
14	0.243627E 01	0.247147E 01	0.253717E 01	0.262759E 01	0.273692E 01	0.285792E 01	0.298143E 01
	0.309658E 01	0.319203E 01	0.325813E 01	0.328952E 01	0.328695E 01	0.325734E 01	0.321210E 01
	0.316539E 01	0.313437E 01	0.313898E 01	0.317686E 01	0.325795E 01	0.348767E 01	0.348767E 01
15	0.243969E 01	0.247245E 01	0.253395E 01	0.261924E 01	0.272344E 01	0.284035E 01	0.296186E 01
	0.307805E 01	0.317804E 01	0.325202E 01	0.329366E 01	0.330228E 01	0.328349E 01	0.324788E 01
	0.320876E 01	0.318124E 01	0.318260E 01	0.321914E 01	0.330349E 01	0.348767E 01	0.348767E 01
16	0.244344E 01	0.247289E 01	0.252863E 01	0.260672E 01	0.270348E 01	0.281406E 01	0.293186E 01
	0.304829E 01	0.315343E 01	0.323744E 01	0.329290E 01	0.331710E 01	0.331344E 01	0.329096E 01
	0.326212E 01	0.324057E 01	0.324058E 01	0.327257E 01	0.334811E 01	0.348767E 01	0.348767E 01
17	0.244769E 01	0.247296E 01	0.252128E 01	0.258986E 01	0.267637E 01	0.277758E 01	0.288874E 01
	0.300322E 01	0.311258E 01	0.320759E 01	0.327992E 01	0.332439E 01	0.334106E 01	0.333601E 01
	0.332009E 01	0.330605E 01	0.330594E 01	0.333060E 01	0.338938E 01	0.348767E 01	0.348767E 01
18	0.245277E 01	0.247298E 01	0.251213E 01	0.256858E 01	0.264133E 01	0.272889E 01	0.282868E 01
	0.293650E 01	0.304633E 01	0.315055E 01	0.324092E 01	0.331013E 01	0.335396E 01	0.337324E 01
	0.337473E 01	0.336972E 01	0.337020E 01	0.338654E 01	0.342556E 01	0.348767E 01	0.348767E 01
19	0.245931E 01	0.247360E 01	0.250173E 01	0.254303E 01	0.259762E 01	0.266552E 01	0.274631E 01
	0.283858E 01	0.293955E 01	0.304484E 01	0.314844E 01	0.324321E 01	0.332180E 01	0.337834E 01
	0.341063E 01	0.342263E 01	0.342544E 01	0.343437E 01	0.345514E 01	0.348767E 01	0.348767E 01
20	0.246886E 01	0.247641E 01	0.249157E 01	0.251426E 01	0.254510E 01	0.258494E 01	0.263470E 01
	0.269520E 01	0.276694E 01	0.284984E 01	0.294301E 01	0.304442E 01	0.315057E 01	0.325595E 01
	0.335233E 01	0.342762E 01	0.346410E 01	0.346809E 01	0.347583E 01	0.348767E 01	0.348767E 01

21	0.248767E 01	0.248767E 01	0.248767E 01	0.248767E 01	0.248767E 01	0.248767E 01	0.248767E 01
	0.248767E 01	0.248767E 01	0.248767E 01	0.248767E 01	0.248767E 01	0.248767E 01	0.248767E 01
	0.248767E 01	0.248767E 01	0.248767E 01	0.248767E 01	0.248767E 01	0.248767E 01	0.348767E 01
22	0.755321E 01	0.755504E 01	0.757342E 01	0.760862E 01	0.766231E 01	0.772954E 01	0.780305E 01
	0.787549E 01	0.793915E 01	0.798503E 01	0.800321E 01	0.798641E 01	0.793583E 01	0.784072E 01
	0.762804E 01	0.739148E 01	0.720024E 01	0.709725E 01	0.719743E 01	0.659041E 01	0.903569E 02
23	0.756248E 01	0.756827E 01	0.760829E 01	0.769013E 01	0.781310E 01	0.796330E 01	0.812731E 01
	0.829659E 01	0.846334E 01	0.861390E 01	0.872306E 01	0.875556E 01	0.868710E 01	0.853813E 01
	0.835128E 01	0.815317E 01	0.796755E 01	0.781266E 01	0.771622E 01	0.768788E 01	0.902966E 02
24	0.756284E 01	0.757417E 01	0.763621E 01	0.775997E 01	0.793752E 01	0.814532E 01	0.836874E 01
	0.860588E 01	0.885806E 01	0.911770E 01	0.935416E 01	0.949495E 01	0.943535E 01	0.918257E 01
	0.890844E 01	0.865085E 01	0.845547E 01	0.831999E 01	0.816371E 01	0.112075E 02	0.904917E 02
25	0.756312E 01	0.758107E 01	0.766019E 01	0.781236E 01	0.801819E 01	0.824823E 01	0.849189E 01
	0.875627E 01	0.905213E 01	0.938186E 01	0.972407E 01	0.999047E 01	0.994110E 01	0.941860E 01
	0.892679E 01	0.860217E 01	0.840748E 01	0.828741E 01	0.828085E 01	0.266873E 02	0.923605E 02
26	0.756327E 01	0.758702E 01	0.767424E 01	0.783505E 01	0.804054E 01	0.826131E 01	0.849214E 01
	0.874543E 01	0.903597E 01	0.937183E 01	0.974802E 01	0.101307E 02	0.104168E 02	0.101751E 02
	0.959869E 01	0.919547E 01	0.917949E 01	0.939648E 01	0.862766E 01	0.264415E 02	0.929478E 02
27	0.756326E 01	0.758894E 01	0.767399E 01	0.782628E 01	0.801281E 01	0.820570E 01	0.840277E 01
	0.861850E 01	0.886902E 01	0.916564E 01	0.951373E 01	0.991008E 01	0.103355E 02	0.107031E 02
	0.107425E 02	0.104666E 02	0.101589E 02	0.101386E 02	0.895923E 01	0.359865E 02	0.940851E 02
28	0.756309E 01	0.758653E 01	0.766060E 01	0.779153E 01	0.794713E 01	0.810140E 01	0.825340E 01
	0.841903E 01	0.861702E 01	0.886448E 01	0.917883E 01	0.957929E 01	0.100839E 02	0.107013E 02
	0.113912E 02	0.117938E 02	0.115404E 02	0.111651E 02	0.101195E 02	0.401252E 02	0.948065E 02
29	0.756276E 01	0.757974E 01	0.763453E 01	0.773279E 01	0.784840E 01	0.795759E 01	0.805845E 01
	0.816691E 01	0.830366E 01	0.849012E 01	0.875286E 01	0.913023E 01	0.967926E 01	0.104792E 02
	0.116141E 02	0.130485E 02	0.127959E 02	0.119917E 02	0.150018E 02	0.495781E 02	0.957470E 02
30	0.756230E 01	0.756948E 01	0.759727E 01	0.765134E 01	0.771805E 01	0.777814E 01	0.782515E 01
	0.786976E 01	0.792885E 01	0.801926E 01	0.816262E 01	0.839587E 01	0.878987E 01	0.948700E 01
	0.107782E 02	0.132229E 02	0.174962E 02	0.213786E 02	0.291608E 02	0.591776E 02	0.963903E 02
31	0.756204E 01	0.756169E 01	0.756177E 01	0.756206E 01	0.756255E 01	0.756329E 01	0.756420E 01
	0.756532E 01	0.756676E 01	0.756881E 01	0.757186E 01	0.757675E 01	0.758495E 01	0.759930E 01
	0.762503E 01	0.766987E 01	0.773655E 01	0.780275E 01	0.831902E 01	0.152516E 02	0.909840E 02

STREAM FUNCTION---SF(I,J)

1	0.0	0.0	0.0	0.0	0.0	0.0	0.0
	0.0	0.0	0.0	0.0	0.0	0.0	0.0
	0.0	0.0	0.0	0.0	0.0	0.0	0.0
2	0.0	-0.472812E 02	-0.192401E 03	-0.441511E 03	-0.802481E 03	-0.128298E 04	-0.188792E 04
	-0.261654E 04	-0.345911E 04	-0.439334E 04	-0.537925E 04	-0.634936E 04	-0.718259E 04	-0.761678E 04
	-0.707948E 04	-0.601032E 04	-0.479529E 04	-0.376682E 04	-0.352133E 04	-0.491221E 04	0.0
3	0.0	-0.927829E 02	-0.377087E 03	-0.864449E 03	-0.156986E 04	-0.250784E 04	-0.368735E 04
	-0.510607E 04	-0.674444E 04	-0.855941E 04	-0.104769E 05	-0.123812E 05	-0.140959E 05	-0.153585E 05
	-0.158399E 05	-0.154597E 05	-0.143275E 05	-0.127896E 05	-0.115051E 05	-0.108253E 05	0.0

4	0.0	-0.135314E 03	-0.549429E 03	-0.125860E 04	-0.228407E 04	-0.364620E 04	-0.535686E 04
	-0.741142E 04	-0.978061E 04	-0.124029E 05	-0.151766E 05	-0.179514E 05	-0.205196E 05	-0.226153E 05
	-0.239506E 05	-0.243264E 05	-0.236257E 05	-0.219012E 05	-0.194573E 05	-0.163768E 05	0.0
5	0.0	-0.173968E 03	-0.705910E 03	-0.161618E 04	-0.293142E 04	-0.467665E 04	-0.686567E 04
	-0.949087E 04	-0.125137E 05	-0.158565E 05	-0.193947E 05	-0.229512E 05	-0.262918E 05	-0.291314E 05
	-0.311615E 05	-0.320984E 05	-0.316932E 05	-0.297740E 05	-0.263205E 05	-0.212110E 05	0.0
6	0.0	-0.208006E 03	-0.843644E 03	-0.193079E 04	-0.350057E 04	-0.558170E 04	-0.818896E 04
	-0.113115E 05	-0.149023E 05	-0.188693E 05	-0.230691E 05	-0.273010E 05	-0.313049E 05	-0.347661E 05
	-0.373357E 05	-0.386585E 05	-0.383843E 05	-0.362011E 05	-0.319048E 05	-0.252775E 05	0.0
7	0.0	-0.236824E 03	-0.960245E 03	-0.219711E 04	-0.398219E 04	-0.634702E 04	-0.930682E 04
	-0.128475E 05	-0.169144E 05	-0.214034E 05	-0.261547E 05	-0.309470E 05	-0.354937E 05	-0.394461E 05
	-0.424100E 05	-0.439690E 05	-0.436938E 05	-0.411854E 05	-0.361774E 05	-0.285353E 05	0.0
8	0.0	-0.259929E 03	-0.105377E 04	-0.241080E 04	-0.436872E 04	-0.696120E 04	-0.102036E 05
	-0.140790E 05	-0.185263E 05	-0.234315E 05	-0.286211E 05	-0.338557E 05	-0.388233E 05	-0.431400E 05
	-0.463668E 05	-0.480365E 05	-0.476540E 05	-0.447498E 05	-0.390437E 05	-0.307296E 05	0.0
9	0.0	-0.276932E 03	-0.112266E 04	-0.256841E 04	-0.465416E 04	-0.741527E 04	-0.108673E 05
	-0.149910E 05	-0.197205E 05	-0.249344E 05	-0.304485E 05	-0.360082E 05	-0.412787E 05	-0.458432E 05
	-0.492204E 05	-0.509017E 05	-0.503344E 05	-0.469505E 05	-0.403129E 05	-0.294849E 05	0.0
10	0.0	-0.287532E 03	-0.116574E 04	-0.266730E 04	-0.483395E 04	-0.770244E 04	-0.112887E 05
	-0.155723E 05	-0.204845E 05	-0.258988E 05	-0.316242E 05	-0.373946E 05	-0.428577E 05	-0.475679E 05
	-0.510074E 05	-0.526347E 05	-0.518614E 05	-0.480137E 05	-0.404971E 05	-0.273134E 05	0.0
11	0.0	-0.291520E 03	-0.118215E 04	-0.270558E 04	-0.490480E 04	-0.781778E 04	-0.114612E 05
	-0.158148E 05	-0.208088E 05	-0.263152E 05	-0.321393E 05	-0.380098E 05	-0.435629E 05	-0.483340E 05
	-0.517770E 05	-0.533224E 05	-0.523800E 05	-0.481882E 05	-0.400333E 05	-0.253446E 05	0.0
12	0.0	-0.288772E 03	-0.117140E 04	-0.268209E 04	-0.486464E 04	-0.775810E 04	-0.113805E 05
	-0.157128E 05	-0.206870E 05	-0.261761E 05	-0.319870E 05	-0.378488E 05	-0.433966E 05	-0.481590E 05
	-0.515758E 05	-0.530566E 05	-0.520051E 05	-0.476345E 05	-0.390554E 05	-0.235713E 05	0.0
13	0.0	-0.279259E 03	-0.113332E 04	-0.259638E 04	-0.471257E 04	-0.752186E 04	-0.110440E 05
	-0.152630E 05	-0.201142E 05	-0.254755E 05	-0.311598E 05	-0.369042E 05	-0.423536E 05	-0.470464E 05
	-0.504242E 05	-0.518806E 05	-0.507921E 05	-0.463680E 05	-0.375365E 05	-0.217930E 05	0.0
14	0.0	-0.263054E 03	-0.106815E 04	-0.244891E 04	-0.444910E 04	-0.710935E 04	-0.104516E 05
	-0.144639E 05	-0.190874E 05	-0.242080E 05	-0.296490E 05	-0.351625E 05	-0.404141E 05	-0.449679E 05
	-0.482838E 05	-0.497463E 05	-0.486885E 05	-0.443031E 05	-0.354106E 05	-0.199116E 05	0.0
15	0.0	-0.240352E 03	-0.976617E 03	-0.224107E 04	-0.407631E 04	-0.652300E 04	-0.960539E 04
	-0.133165E 05	-0.176057E 05	-0.223694E 05	-0.274455E 05	-0.326059E 05	-0.375454E 05	-0.418654E 05
	-0.450610E 05	-0.465243E 05	-0.455522E 05	-0.413146E 05	-0.326388E 05	-0.179260E 05	0.0
16	0.0	-0.211491E 03	-0.859999E 03	-0.197553E 04	-0.359831E 04	-0.576808E 04	-0.851095E 04
	-0.118257E 05	-0.156715E 05	-0.199587E 05	-0.245427E 05	-0.292193E 05	-0.337165E 05	-0.376806E 05
	-0.406569E 05	-0.420741E 05	-0.412342E 05	-0.373102E 05	-0.292330E 05	-0.158639E 05	0.0
17	0.0	-0.176982E 03	-0.720259E 03	-0.165642E 04	-0.302180E 04	-0.485357E 04	-0.717867E 04
	-0.100016E 05	-0.132930E 05	-0.169801E 05	-0.209403E 05	-0.249969E 05	-0.289142E 05	-0.323876E 05
	-0.350264E 05	-0.363306E 05	-0.356693E 05	-0.322761E 05	-0.252367E 05	-0.137243E 05	0.0
18	0.0	-0.137536E 03	-0.560183E 03	-0.128981E 04	-0.235686E 04	-0.379369E 04	-0.562598E 04
	-0.786293E 04	-0.104873E 05	-0.134465E 05	-0.166455E 05	-0.199421E 05	-0.231430E 05	-0.259985E 05
	-0.281924E 05	-0.293248E 05	-0.288892E 05	-0.262499E 05	-0.206635E 05	-0.114287E 05	0.0

19	0.0	-0.940838E 02	-0.383487E 03	-0.883937E 03	-0.161775E 04	-0.260952E 04	-0.388044E 04
	-0.544157E 04	-0.728670E 04	-0.938519E 04	-0.116757E 05	-0.140608E 05	-0.164027E 05	-0.185194E 05
	-0.201799E 05	-0.210976E 05	-0.209195E 05	-0.191992E 05	-0.153817E 05	-0.877068E 04	0.0
20	0.0	-0.477858E 02	-0.194883E 03	-0.449583E 03	-0.823839E 03	-0.133123E 04	-0.198427E 04
	-0.279116E 04	-0.375223E 04	-0.485630E 04	-0.607713E 04	-0.736996E 04	-0.866813E 04	-0.987912E 04
	-0.108794E 05	-0.115078E 05	-0.115590E 05	-0.107943E 05	-0.891256E 04	-0.530682E 04	0.0
21	0.0	0.0	0.0	0.0	0.0	0.0	0.0
	0.0	0.0	0.0	0.0	0.0	0.0	0.0
	0.0	0.0	0.0	0.0	0.0	0.0	0.0
22	0.0	-0.161620E 01	-0.648283E 01	-0.145343E 02	-0.255100E 02	-0.389190E 02	-0.540869E 02
	-0.702003E 02	-0.863095E 02	-0.101322E 03	-0.114053E 03	-0.123389E 03	-0.128556E 03	-0.129347E 03
	-0.126291E 03	-0.120579E 03	-0.113698E 03	-0.107096E 03	-0.101650E 03	-0.101239E 03	0.0
23	0.0	-0.251484E 01	-0.100598E 02	-0.224574E 02	-0.391991E 02	-0.595081E 02	-0.825094E 02
	-0.107271E 03	-0.132685E 03	-0.157313E 03	-0.179325E 03	-0.196720E 03	-0.207952E 03	-0.212623E 03
	-0.211300E 03	-0.205023E 03	-0.194940E 03	-0.181739E 03	-0.165017E 03	-0.142596E 03	0.0
24	0.0	-0.296017E 01	-0.117952E 02	-0.261963E 02	-0.454610E 02	-0.687162E 02	-0.951675E 02
	-0.124038E 03	-0.154272E 03	-0.184207E 03	-0.211369E 03	-0.232673E 03	-0.245703E 03	-0.251028E 03
	-0.251545E 03	-0.249568E 03	-0.247362E 03	-0.246778E 03	-0.249751E 03	-0.231795E 03	0.0
25	0.0	-0.297661E 01	-0.118138E 02	-0.261165E 02	-0.451228E 02	-0.680476E 02	-0.943034E 02
	-0.123299E 03	-0.154031E 03	-0.184657E 03	-0.212126E 03	-0.232108E 03	-0.240560E 03	-0.239050E 03
	-0.235290E 03	-0.233456E 03	-0.235356E 03	-0.241418E 03	-0.246790E 03	-0.146445E 03	0.0
26	0.0	-0.269748E 01	-0.106768E 02	-0.235410E 02	-0.406145E 02	-0.613285E 02	-0.853810E 02
	-0.112490E 03	-0.142011E 03	-0.172583E 03	-0.201757E 03	-0.225671E 03	-0.239291E 03	-0.239520E 03
	-0.234245E 03	-0.233481E 03	-0.241040E 03	-0.257115E 03	-0.290281E 03	-0.184096E 03	0.0
27	0.0	-0.222391E 01	-0.879139E 01	-0.193674E 02	-0.334348E 02	-0.506817E 02	-0.711376E 02
	-0.949571E 02	-0.122138E 03	-0.152306E 03	-0.184475E 03	-0.216724E 03	-0.245827E 03	-0.267036E 03
	-0.276405E 03	-0.275678E 03	-0.271941E 03	-0.273147E 03	-0.289289E 03	-0.137430E 03	0.0
28	0.0	-0.161278E 01	-0.637245E 01	-0.140315E 02	-0.242367E 02	-0.368946E 02	-0.523173E 02
	-0.710663E 02	-0.937673E 02	-0.121008E 03	-0.153204E 03	-0.190300E 03	-0.231223E 03	-0.273009E 03
	-0.309729E 03	-0.332108E 03	-0.333877E 03	-0.324322E 03	-0.324487E 03	-0.134681E 03	0.0
29	0.0	-0.929260E 00	-0.366853E 01	-0.805360E 01	-0.138499E 02	-0.210678E 02	-0.301379E 02
	-0.418282E 02	-0.571459E 02	-0.773525E 02	-0.103970E 03	-0.138592E 03	-0.182272E 03	-0.234131E 03
	-0.288783E 03	-0.332775E 03	-0.344618E 03	-0.323838E 03	-0.277640E 03	-0.977782E 02	0.0
30	0.0	-0.309295E 00	-0.121800E 01	-0.263711E 01	-0.440286E 01	-0.647581E 01	-0.912129E 01
	-0.129008E 02	-0.186398E 02	-0.275709E 02	-0.416069E 02	-0.636206E 02	-0.975596E 02	-0.147917E 03
	-0.217290E 03	-0.299517E 03	-0.366720E 03	-0.363773E 03	-0.257598E 03	-0.622091E 02	0.0
31	0.0	0.0	0.0	0.0	0.0	0.0	0.0
	0.0	0.0	0.0	0.0	0.0	0.0	0.0
	0.0	0.0	0.0	0.0	0.0	0.0	0.0

RADIAL VAPOR VELOCITY COMPONENT AT INTERFACE--- VG(J)

0.0	0.639192E 04	0.128222E 05	0.191908E 05	0.253334E 05	0.310494E 05	0.361499E 05
0.404735E 05	0.438784E 05	0.462381E 05	0.474575E 05	0.475127E 05	0.464876E 05	0.445805E 05
0.421198E 05	0.395183E 05	0.371608E 05	0.353467E 05	0.342054E 05	0.345637E 05	0.0

INTERFACE VELOCITY DUE TO INTERFACE CHANGE---UL(J)

-0.315153E-01	-0.324650E-01	-0.344721E-01	-0.375375E-01	-0.418359E-01	-0.475946E-01	-0.550976E-01
-0.646890E-01	-0.767604E-01	-0.917355E-01	-0.110030E 00	-0.131936E 00	-0.157361E 00	-0.185205E 00
-0.212332E 00	-0.235093E 00	-0.246334E 00	-0.246364E 00	-0.248436E 00	-0.246463E 00	0.0

VAPOR STREAM FUNCTION AT INTERFACE---SFI(J)

0.0	0.222756E 00	0.891026E 00	0.200481E 01	0.356410E 01	0.556891E 01	0.801923E 01
0.109151E 02	0.142564E 02	0.180433E 02	0.222756E 02	0.269535E 02	0.320769E 02	0.376458E 02
0.436602E 02	0.501202E 02	0.570256E 02	0.643766E 02	0.721731E 02	0.804151E 02	0.0

HEAT TRANSFER COEFFICIENT OF LIQUID---HL(J)

0.102777E-01	0.312332E-01	0.317858E-01	0.320641E-01	0.322575E-01	0.324098E-01	0.325391E-01
0.326549E-01	0.327387E-01	0.328460E-01	0.329434E-01	0.330402E-01	0.331384E-01	0.332403E-01
0.333490E-01	0.334686E-01	0.336055E-01	0.337706E-01	0.339765E-01	0.339523E-01	0.142478E-01

HEAT TRANSFER COEFFICIENT OF VAPOR---HG(J)

0.188462E-02	0.847101E-05	0.832100E-05	0.777129E-05	0.530393E-05	0.537205E-05	0.391993E-05
0.338347E-05	0.233831E-05	0.183483E-05	0.713526E-05			

NUL= 5158.742188 NUG= 1043.777588 RMAX= 0.101707E-03 RR1= 0.993754E 00

NE1= 1 NE2= 1 RAL= 0.133192E 11 RAG= 0.665264E 12

CL= 15.185343 CG= 1.155738 RP= 1.497664 DQILDT= -0.017565

DQI= 0.623343E 02 DQS= 0.171359E 00 DQL= 0.510014E 02

EXECUTION TERMINATED

REFERENCES

1. Clark, J. A. and Barakat, H. Z. Transient Laminar Free-Convection Heat and Mass Transfer in Closed Partially Filled Liquid Containers: Technical Report 04268-6-T, Office of Research Administration, University of Michigan, Ann Arbor, Michigan, Contract NAS-8-825, Marshall Space Flight Center, January 1964.

2. Barakat, H. Z. and Clark, J. A. Transient Natural Convection Flows in Closed Containers: Technical Report 04268-10-T, Office of Research Administration, University of Michigan, Ann Arbor, Michigan, Contract NAS-8-825, Marshall Space Flight Center, August 1965.

3. Merte, H., Clark, J. A., and Barakat, H. Z. Finite Difference Solution of Stratification and Pressure Rise in Containers: Technical Report 07461-30-T, Office of Research Administration, University of Michigan, Ann Arbor, Michigan, Contract NAS-8-20228, Marshall Space Flight Center, January 1968.

4. Coeling, K. J. Incipient Boiling of Cryogenic Liquid: Ph.D. Thesis, University of Michigan, December 1967.

5. Clark, J. A. A Review of Pressurization, Stratification and Interfacial Phenomena: International Advances in Cryogenic Engineering, Vol. 10, pp. 259-284, 1966.

6. Thomas, P. D. and Morse, F. H. Analytical Solution for the Phase Change in a Suddenly Pressurized Liquid-Vapor System: Advances in Cryogenic Engineering, Vol. 8, pp. 550-562, 1964.

7. Knuth, E. L. Evaporation and Condensation of One Component Systems: Journal of the American Rocket Society, Vol. 32, pp. 1424-1426, 1962.

8. Yang, W. J. Phase Change of One-Component System in a Container: AIChE Paper No. 63-A48, presented at the 6th National Heat Transfer Conference, Boston, Mass., August 1963.

9. Yang, W. J. and Clark, J. A. On the Application of the Source Theory on Problems Involving Phase Change—Part 2: J. Heat Transfer, Trans. ASME, Ser. C. Vol. 86, pp. 443, 1964.

10. Yang, W. J., Larsen, P. S., and Clark, J. A. Interfacial Heat and Mass Transfer in a Suddenly Pressurized, Binary Liquid-Vapor System: Trans. ASME, J. Eng. for Ind., Vol. 87, pp. 413, 1965.

11. Epstein, M., Georgius, H. K., and Anderson, R. E. Generalized Propellant Tank Pressurization Analysis: International Advances in Cryogenic Engineering, Vol. 10, 1966.

12. Huntley, S. C. Temperature-Pressure-Time Relations in a Closed Cryogenic Container: Advances in Cryogenic Engineering, Vol. 3, p. 342, 1960.

13. Leibenberg, D. H. and Edescuty, F. J. Pressurization Analysis of a Large Scale Hydrogen Dewar: International Advances in Cryogenic Engineering, Vol. 10, 1966.

14. Jacob, M. Heat Transfer: Vol. 1, John Wiley and Sons, Inc. Chapter 29.

15. Swim, R. T. Temperature Distribution in Liquid and Vapor Phases of Helium in Cylindrical Dewars: Advances in Cryogenic Engineering, Vol. 5, 1960.

16. Brenteri, E. G., Giarratano, P. J., and Smith, R. V. Boiling Heat Transfer for Oxygen, Nitrogen, Hydrogen and Helium: NBS Technical Note No. 317, September 1965.

17. Evaluation of AS-203 Low Gravity Orbital Experiments: Technical Report HSM-R421-67, Contract NAS-8-4016, Space Div., Chrysler Corporation, Huntsville Operation, January 1967.

18. A Compendium of the Properties of Materials at Low Temperature—Phase I, Part 1, Properties of Fluids (WADD Tech. Report 60-56, Part 1), Nat. Bureau of Std., V. J. Johnson, General Editor, July 1960.

19. Barron, R. Cryogenic Systems: McGraw Hill, 1966.

20. Weber, L. A., Diller, D. E., Rader, H. M., and Goodwin, R. D. The Vapour Pressure of 20°K Equilibrium Hydrogen, R-236, NBS, March 1962.

21. Roder, H. M., Weber, L. A., and Goodwin, R. D. Thermodynamic and Related Properties of Parahydrogen from the Triple Point to 100°K at Pressure to 340 Atmospheres: NBS Monograph 94, NBS, 1965.

22. Personal communication from Marshall Space Flight Center.